学位論文

Numerical Models of the Progenitor Star of SN 1987A Based on the Stellar Merger Scenario

(恒星合体シナリオを基にした SN 1987A の親星の数値モデル)

平成 29 年 12 月博士（理学）申請

東京大学大学院理学系研究科天文学専攻

漆畑　貴樹

Abstract

SN 1987A is a core collapse supernova (CCSN), which occurred in the Large Magellanic Cloud. Thanks to its proximate, we succeeded in observing multi-wavelength variation of the SN, from the onset. The observations contained several mysteries, e.g. the red to blue evolution, ring like nebula, chemical anomalies in the ejecta and nebula, and its post-blue lifetime. Based on these mysteries, the progenitor of the SN is thought to have undergone a peculiar evolution.

Many authors have been trying to solve these mysteries. There are two major dues as to the cause of the red to blue evolution; the increasing helium abundance in the envelope and the decreasing core-total mass ratio, $q \equiv M_{\rm core}/M_{\rm tot}$. Saio *et al.* (1988b) suggested that the helium abundance enhancement was caused by rotational mixing. This leads to decreasing envelope opacity, and to increasing stellar luminosity. As a result, the star contracts to remain in energy equilibrium. Podsiadlowski *et al.* (1992) suggested that the decreasing q helps to understand the evolution, in a binary scenario. The mass can increase due to binary interactions, such as mass accretion and stellar merger, increasing gravity in the envelope. This leads to contraction. Despite this relative understanding, present models are unable to quantitatively account for all of the observational constraints.

Studies of CCSNe progenitors are useful for numerical simulations of SNe, their light curves, and origins of progenitors of CCSNe. There are many observational constraints for the progenitor of SN 1987A. Therefore, constructing a more complete model is possible and can be utilized for the above studies. To achieve this purpose, I first begin to verify both effects for the red to blue evolution suggested by previous works, with the stellar evolutionary code described by Takahashi *et al.* (2014). I construct a model in which surface matter accretion is parametrized. In this model, I use a RSG, whose initial mass is 14.0 $M_\odot$, in two phases; one having a He core and another having a CO core. The main differences between these are the stages of development of convection in the envelope and core. Physical quantities of surfaces of evolved stars are adopted for accreted matter. For the He core case, the RSG becomes a blue progenitor, if 5.0 $M_\odot$ or more is accreted. In the CO core case, the RSG never transitions to blue even if 12.0 $M_\odot$ is accreted. This indicates that the decreasing q is informative, and that physical structure of accreted matter must be considered. To verify the effect of helium enhancement, I construct a

model in which helium abundance in the whole envelope is modified with a RSG having a CO core of initial mass 16.0 $M_{\odot}$. In this model, the RSG becomes a blue progenitor if the helium abundance is 0.625 or more by mass fraction. The value is, however, very high within realistic parameters. As a final verification, I construct a model in which both effects are included with a RSG having a CO core. The procedure is such that the helium enhancement model proceeds after the increasing mass model. The results show that a blue progenitor is produced, but that such an outcome is difficult within realistic parameters.

Using parameters, I construct an evolutionary model for the progenitor based on the stellar merger scenario (Podsiadlowski *et al.*, 1992; Ivanova *et al.*, 2002). The scenario is as follows; there are two stars in a close binary system. The primary star has a mass of about 15.0 $M_{\odot}$, and the secondary star about 7.0 $M_{\odot}$. If drastic mass transfer occurs between them, the system enters into a common envelope phase. When the secondary spirals inward due to friction between it and the envelope, its orbital angular momentum is transfered to the surrounding matter. After the secondary has reached about 10.0 $R_{\odot}$, it starts to dissolve. The matter moves toward the core, and interaction between them occurs. It is expected that this interaction leads to mixing, and matter in the deep inner region is dredged up to the surface. The model can be described with two parts; injection of orbital angular momentum and dissolution of the secondary. My best model, in which the primary is a RSG having a CO core, succeeds in quantitatively explaining the red to blue evolution, the post-blue lifetime, the chemical anomalies, the envelope mass, and the position on the Hertzsprung-Russell diagram. In this case, the initial mass of the primary is 14.0 $M_{\odot}$ and the mass of the secondary 7.7 $M_{\odot}$. The difference between the merger and the increasing mass models is the structure of the merged object while/after the mass is accreted. Therefore, the decreasing q and the physical quantities of the accreted matter are important for the red to blue evolution. From analysis of the modeled spiral-in phase, it is implied that mass loss with a more effective loss of angular momentum, such as disk- like mass loss, is required instead of wind mass loss assumed in the code. Large scale mixing due to interaction would not affect the evolution. Matching the chemical anomalies however is important.

Contents

List of Figures

List of Tables

Chapter 1

Introduction

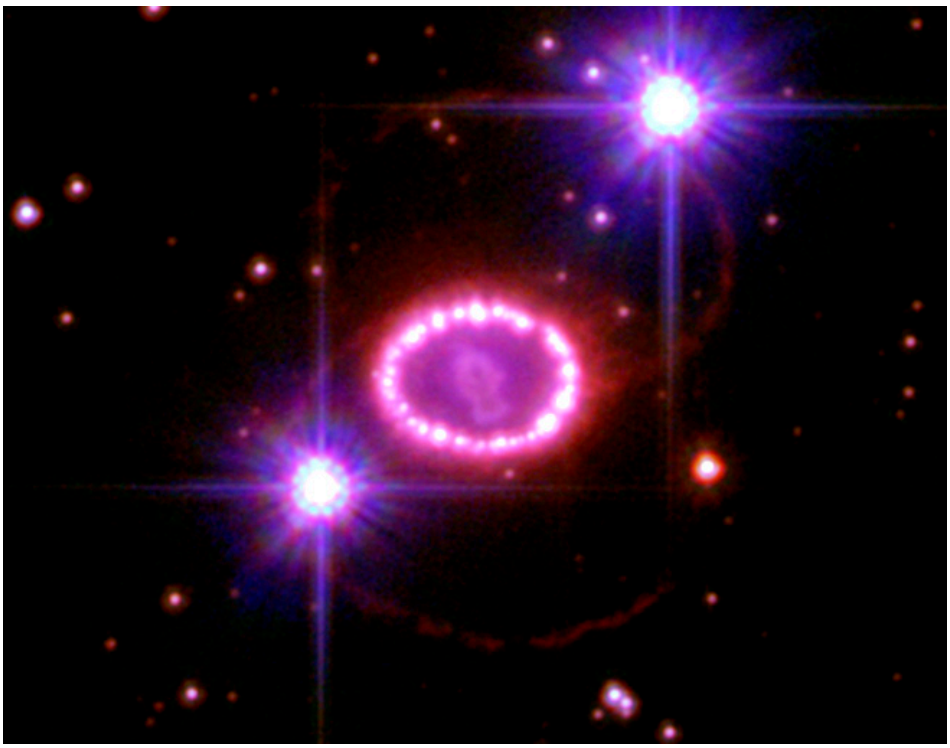

Figure 1.1. An image of SN 1987A taken in February 21st 2007 (credit: NASA, ESA, P.Challis and R.Kirshner)

A supernova (SN), occurred in the Large Magellanic Could (LMC), was observed on February 23rd 1987. It was named SN 1987A and has brought a lot of knowledge to us until now. This was a very peculiar SN. Multi-wavelength observations, since the beginning of the explosion, were possible because the LMC is the nearest galaxy from the Earth. In this chapter, I describe history of these observations and previous studies, the background knowledge, and the goal of this thesis.

1.1 Observations

1.1.1 Blue progenitor

Kamiokande II detected neutrinos originating from the SN before it began to shine (Hirata *et al.*, 1987). The emission of neutrinos was expected by the theory of stellar evolution, and the detection confirmed the final stage of evolution. Unexpectedly, the SN became 6.4 magnitude in about 3.0 hr after the detection, which was shorter than predicted by the theory. In addition, the peak luminosity was fainter. A relation between the time and luminosity can be understood as follows; For a core collapse supernova (CCSN), after infalling matter from the stellar envelope reaches the surface of the core, the matter is rebounded by the core, and it moves toward the stellar surface with a shockwave. At almost the same time, neutrinos are emitted. While the shockwave is proceeding, the kinetic energy is converted to thermal and radiative forms. When the shock breaks through the envelope, luminosity of a SN starts to shine. Therefore, the breakthrough time-scale determines the beginning of the increasing post-collapse luminosity. Since the reaction cross section of a neutrino is very small, it reaches the surface almost without any interaction with matter. Thus, if an observer measures the deviation between the time of the detection and the increasing luminosity, we can find the diffusion time of a photon, by which the stellar size can be roughly estimated. If the progenitor was a RSG, the deviation would be a few days, which is obviously longer than the observation. Therefore, it was expected that the progenitor was a blue supergiant (BSG) whose typical radius is about 10.0 $R_{\odot}$. This was confirmed by direct observation of the progenitor. It was SK -69∘202, which was the first case of a prior identification of a CCSN progenitor. In this way, the progenitor was identified as a BSG from observational facts.

1.1.2 Ring like nebula

There is a ring like nebula around the position of the explosion. The nebula can be described as one equatorial ring (ER) and two outer rings (ORs) which can also further separated into north-OR (NOR) and south-OR (SOR).

Wampler & Richichi (1989) presented the first evidence of the ER from spectra of emission lines of [O III], which were detected 310 days after the explosion, taken by the European Southern Observatory Cassegrain echelle spectrograph on the 3.6 meter telescope. Crotts & Heathcote (1991) investigated velocity structure of the ER, which was about 10.0 km sec^{-1}. They assumed that the origin of the ER was due to an interaction between stellar winds of the RSG and BSG, meaning the occurrence of the transition from red to blue due to some mechanisms. Time at the beginning of the transition was

estimated to be about 2.0×10^4 yr before the explosion from the velocity and size of the ER.

On the other hand, studies about the ORs have been fewer than that of the ER because its faintness has made spectral observations difficult. Existences of the ORs were first implied by Wampler *et al.* (1990) as loop like structures. The geometries were clearly confirmed by Burrows *et al.* (1995) with the Hubble Space Telescope (HST). They estimated that the SOR was about 2".5 south and the NOR about 2" north from the position of the explosion, implying that material of the rings was ejected by asymmetric mass loss.

The masses of the rings are summarized in Table 1.1. The mass range of the ER is 0.34 $M_\odot$ – 1.7 $M_\odot$(Crotts & Heathcote, 1991; Sugerman *et al.*, 2005), and the masses of the ORs are 0.045 $M_\odot$(Lundqvist & Fransson, 1996), indicating that the ER is about 10.0 – 1.0×10^2 times as massive as the ORs are. Therefore, most of the mass of the ring system is concentrated in the ER.

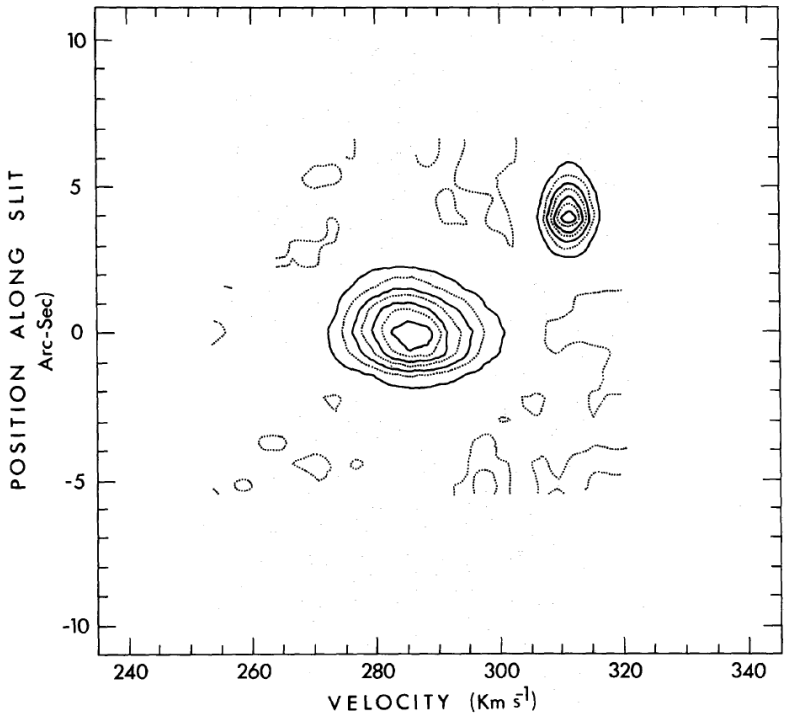

Figure 1.2. Structure of [O III] λ5007 taken in March 26th 1988 (Wampler & Richichi, 1989).

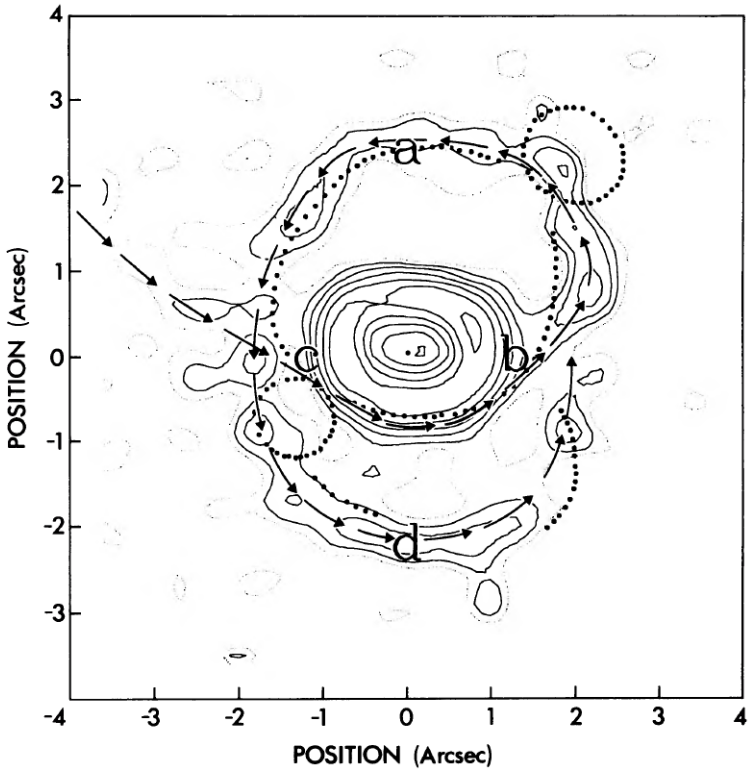

Figure 1.3. A contour map of the deconvolved [O III] λ5008 together with sketch (dot) given by Crotts *et al.* (1989) (Wampler *et al.*, 1990)

1.1.3 Chemical anomalies

Chemical anomalies in the ring system have been confirmed (see e.g. Fransson *et al.* (1989)). Lundqvist & Fransson (1996) measured chemical anomalies in the ER; N/C = 5.0 ± 2.0, N/O = 1.1 ± 0.4, and He/H = 0.25 ± 0.05, by number. Here, N is nitrogen, O oxygen, He helium, and H hydrogen. These imply that the progenitor experienced a RSG stage with a large convective envelope, which dredged up the CNO elements to the surface, reinforcing the scenario that the progenitor became a BSG from a RSG 2.0×10^4 yr before the explosion. Mattila *et al.* (2010) also presented the enhancement; N/O = 1.5 ± 0.7 and He/H = 0.17 ± 0.06, and so on. The He/H ratio is lower than the previous study. Panagia *et al.* (1996) found that the CNO elements in the ORs were about 3.0

Ring masses		
	The ER [$M_\odot$]	The ORs [$M_\odot$]
Lundqvist & Fransson (1996)	-	0.045
Crotts & Heathcote (1991)	0.34	-
Sugerman *et al.* (2005)	1.7	-

Table 1.1. Masses of the triple rings in the observations. The ER is the equatorial ring and the ORs are the outer rings.

times lower than in the ER, but Maran *et al.* (2000) suggested that the abundances of the CNO elements were the same in the NOR and the ER. In either case, the material would be ejected in the phase during which the progenitor was a RSG with a CO core.

1.1.4 Light curves

Multi-wavelength light curves (LCs) of SN1987A were taken since the beginning of the explosion. The shape of the LC was very interesting. As mentioned above, the brightness due to the breakout at the peak was, however, fainter than expected. In addition, there was no plateau phase after the peak. Instead, the luminosity decreased until about 10.0 days from the beginning. Amazingly, it started to increase again after this. It lasted until about 1.0×10^2 days with plateau like shape. Therefore, there were two peaks in the LCs. Such a LC has been classified as a Type II-pec.

1.2 Theoretical studies

As seen above, there are observational constraints about the evolution of the progenitor; the transition from red to blue, timing of the transition before the explosion, formation of the three rings, and the chemical anomalies. Many authors have proposed numerical models for explaining the observations with various scenarios and methods as described in the followings.

1.2.1 Single star models

Making blue progenitor stars is easy under a specific condition; the low metallicity region (e.g., Brunish & Truran, 1982). Because the radiation pressure does not work efficiently, the stars are harder to expand. Therefore, the stars can become BSGs at their ends, but they never enter a RSG phase. To explain that the progenitor was a BSG, this condition was very reasonable and natural. The models would be, however, inconsistent

with observations of star population in the LMC where there are many RSGs. In addition, these cannot explain the evolutionary history.

To produce blue progenitor stars, there are mechanisms by which convection can be restricted. If the Ledoux criterion is adopted instead of the Schwarzaschld one, semiconvection near the surface of the core is suppressed. Woosley (1988) proposed models in which 15.0 and 20.0 $M_\odot$ stars with the metallicity of the LMC ended their lives as BSGs after they first moved redder and climbed up along the Hayashi line although the stars with solar metallicity ended their lives as RSGs. In their models, the notable point is that convective overshooting and semiconvection are not allowed under the Ledoux criterion. Under the same conditions, a 25.0 $M_\odot$ star, however, became a red progenitor. Therefore, they could not conclude whether the restricting convection was important for the transition or not. However, this remains as one important possibility for consideration.

Saio *et al.* (1988b) suggested that increasing helium abundance in the envelope was the critical factor, and investigated this effect with a stellar evolution code. Since massive stars have high initial surface velocities generally, they thought that the rotation could cause strong matter mixing of the interior, while the helium layer of the core was reduced (Saio *et al.*, 1988a). Due to the mechanism, the increasing helium abundance is achieved because He-rich matters of the layer of the core have been dredged-up toward the surface. In general, opacity in the envelope of massive stars can be described by electron scattering as follows in cgs units;

$$\kappa_{\rm el} = 0.2 \times (1 + X) \tag{1.1}$$

where $\kappa_{\rm el}$ is the opacity of electron scattering and X is the mass fraction of hydrogen. Therefore, it is expected that increasing helium abundance leads to a decreasing $\kappa_{\rm el}$, and photons can go through the envelope more easily than with lower helium abundance. This leads to increasing luminosity. As a result, the surface contracts to maintain energy equilibrium. Because their code could not treat the rotation effects, they set the mass-loss rate, metallicity, and helium abundance in the envelope as free parameters at the start of the calculation. As conditions for making a blue progenitor in their models, they required higher mass-loss rate, higher helium abundance, and lower metallicity. Their scenario can be summarized as follows; The star was born in a very low metallicity region, and the stellar mass at ZAMS was about 20.0 $M_\odot$. During a RSG phase, the star was evolving toward the right in the HRD with high mass-loss rate. Before reaching the Hayashi line, much of the envelope was lost, which was at least more than 5.0 $M_\odot$. H-rich matter around the surface was lost and He-rich matter was dredged up due to inner mixing enhanced by the rotation, meaning that helium abundance in the envelope was enhanced. As a result, the star moved bluer, and a BSG exploded.

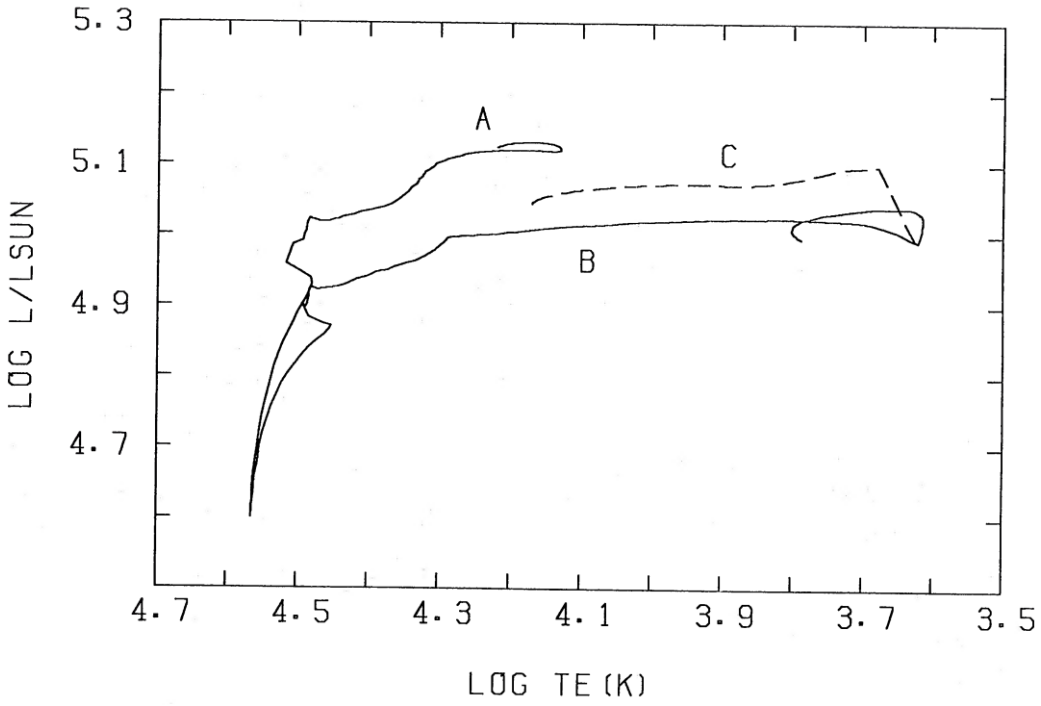

Figure 1.4. Results from Saio *et al.* (1988b). Each evolutionary track was calculated until the central carbon ignition. "A, B, and C" correspond to models Z_0M_0, $Z_0M_2Y_0$, $Z_0M_2Y_2$, respectively. Here, Z is the metallicity, Y the given helium abundance, and M_2 a free parameter which times the empirical formula of the mass-loss suggested by de Jager *et al.* (1988). Z_0 indicates $Z = 0.005$, $Y_0 = 0.25$ and $Y_2 = 0.4$, and M_2 5.0 times the mass-loss rate.

1.2.2 Binary models

When a binary system evolves, roughly, there are two remarkable phenomena; a mass transfer and a merger. To understand these, concepts of the effective potential and Roche lobe are important. The effective potential, $\phi_{\rm eff}$, is defined by the sum of gravitational and centrifugal potentials, $\phi_{\rm g}$ and $\phi_{\rm c}$ as follows;

$$\phi_{\rm eff} = \phi_{\rm g} + \phi_{\rm c} \tag{1.2}$$

$$= -\frac{G(M_1 + M_2)}{|\vec{r_1} - \vec{r_2}|} + |\vec{\Omega} \times \vec{r}|^2 \tag{1.3}$$

where M_1 is the mass at point 1, $\vec{r_1}$ the position vector at point 1, M_2 the mass at point 2, $\vec{r_2}$ the position vector at point 2, Ω the angular velocity vector, and $\vec{r}$ the relative vector between them. There is a saddle point L_1 between the two mass points. The effective potential passing L_1 is like a lobe, so the region is called the Roche lobe. In the inner region of the Roche lobe, gravity generated by each point is dominant. Thus, if any matter drops into the inner region, it becomes trapped there. As stars evolve, the size of a more massive star increases more rapidly, through expansion of its envelope, than that of a lighter star. Therefore, the bigger star can overflow from its own Roche lobe, such that matter originating from it flows toward the lighter star. In extreme cases, the stars will merge. In the case that the bigger star has a convective envelope and the lighter star a radiative one, in a close binary system, the mass transfer becomes unstable when the bigger star enters into RSG phase. This occurs because the thermal time-scale of the bigger star is shorter than that of the lighter star. As a result, matter originating from the bigger star also overflows from the Roche lobe of the lighter star. After this unstable phase is completed, the system enters into a common envelope phase, in which the core of the bigger star and the lighter star are immersed by matter originating from the envelope of the bigger star. Classification of the mass-transfer depends on the main composition of the core. If the composition is helium, it is called a late case B transfer, and if the compositions are C and O, it is called a late case C transfer. In the system, the lighter star spirals inward due to friction between it and the envelope because of transfer of its orbital angular momentum to the surrounding matter, which accelerates ejection of the envelope. When the lighter star approaches the center, mass-transfer between it and the core occurs. As a result, the lighter star is dissolved into the system: a merger occurs.

Podsiadlowski *et al.* (1992) investigated progenitor stars of CCSNe originating from a binary evolution with a stellar evolution code and estimated the fates of binary scenarios quantitatively. In their merger models, which were based on the above scenario, they introduced that the gravitational constant, G, was transfered to a function of the radius and mass coordinate as an effect of the motion of the secondary during the spiral-in phase;

$$\acute{G}(r) = \begin{cases} \mathrm{G} & (r < r(m_{\rm p})) \\ \mathrm{G}(m(r) + M_2)/m(r) & (r > r(m_{\rm p})) \end{cases} \tag{1.4}$$

where $\acute{G}$ is the transfered gravitational constant, $m_{\rm p}$ the portion of the primary's mass within the orbit of the secondary, $r(m_{\rm p})$ a distance which corresponds to $m_{\rm p}$, $m(r)$ the

primary's mass enclosed in a sphere of radius r. The radius of the secondary, which is estimated by $R = (M/M_{\odot})^{0.8}$, is compared with its Roche-radius, $R_{\rm L}$, in each time step, where it was estimated as follows;

$$R_{\rm L} = \frac{0.49 q_{\rm L}^{0.49}}{0.6 q_{\rm L}^{2/3} + \ln(1 + q_{\rm L}^{1/3})} a \tag{1.5}$$

where $q_{\rm L}$ is the mass ratio of the primary and secondary and a the separation between the core and the secondary. This equation can represent the mentioned above mechanism clearly. When the secondary moves to the inner region, the Roche-radius decreases because a becomes smaller. If the radius of the secondary becomes larger than the Roche-radius, the secondary's radius becomes the Roche-radius. At this time, there is no portion of the secondary enclosed by a sphere of the Roche-radius. This extra matter of the secondary is added to the local mass shell in which the secondary is located in their model. They showed a model which was consistent with the progenitor on the HRD and the mass of the progenitor was 18.6 $M_{\odot}$ (see Fig 1.5). Because their code could not treat stellar rotation, they did not discuss rotational effects on the evolutionary history quantitatively.

Ivanova *et al.* (2002) presented detailed two-dimensional hydrodynamical simulations of the interaction between a stream from the Roche lobe of the secondary and the core of the primary in the system in which the mass of the primary is 20.0 $M_{\odot}$ and that of the secondary is 1.0 – 5.0 $M_{\odot}$. This corresponds to the late phase in the merger scenario. In this situation, the typical mass-loss rate is 10^{-2} – 10 $M_{\odot}$ yr^{-1} (Podsiadlowski, 2001). The penetration depth depends on the initial properties of the stream, which are its entropy, its angular momentum, and its width. The depth also depends on the density and rotation of the primary's core. They found that the depth is 1.0 – 3.0 $\times 10^{10}$ cm as a typical value. Because the stream is composed of H-rich material, nuclear burning occurs at the impact region. In most cases, the burning dose not affect the structure and motion of the stream because the characteristic time-scale of the burning is generally longer than the dynamical time-scale of the stream. However, in the special condition where the core rotates relatively fast and has a very steep density gradient, a strong shockwave is generated. It causes heating of the ambient matter, leading to a nuclear runaway. Hence, a detonation wave induced by it occurs. The wave propagates toward the surface of the merged object, and leads to an expansion of the envelope. If a long time calculation of their study were carried out, matter from near the surface of the core to the stellar surface may be mixed due to the established convection.

Recently, Menon & Heger (2017) advanced this study with presenting the evolutionary models based on the merger scenario. The melting, the stellar rotation, and the erosion were taken into account as parameters in their models. They succeeded in quantitatively explaining many evolutionary properties, such as the transition, the position on the HRD,

and chemical anomalies. The spiral-in phase was, however, not modeled. Thus a discussion about the mass loss, during the spiral-in phase and after the merger, was incomplete. In addition, the lifetime and N/C were a bit in excess of the observational constraints in their best model.

1.2.3 Simulations for the rings

Initial models for formation of the rings were presented from the perspective of how the ER was created. Blondin & Lundqvist (1993) presented two-dimensional time-dependent hydrodynamic calculations of the scenario that fast wind from the SN interacted with a slow wind from a progenitor RSG, which enhanced the density contrast in the ER. Luo & McCray (1991) had suggested this scenario previously, and had ruled out one of the possibilities that the ring was the protostellar disk which was formed when the progenitor was born.

The above scenario was, however, excluded by discovery of the ORs because it was required that the three rings was formed at the same time. Meyer (1997) proposed a model for the triple rings based on the scenario that heating of matter originating from the RSG due to ionization from the wind interaction which in-turn induced by hydrodynamic motions, creating the rings. Unfortunately, the observation could not be explained with realistic parameters. The problem was solved naturally if it was considered that the progenitor resulted from binary evolution. Morris & Podsiadlowski (2006) investigated the mass loss from a common envelope in which the companion spirals toward the center rapidly where the total mass is 20.0 $M_\odot$ and the orbital period, P, about 10 yr with three-dimensional smoothed particle hydrodynamics (SPH) calculations. Their model proposed that the mass loss enhanced at mid-latitudes the distorted system, and that the wind interaction led to formation of the ORs. In one of the more remarkable results, if the deposited energy was less than about one-third of binding energy of the envelope, the mass loss at the equatorial plane was suppressed completely. Morris & Podsiadlowski (2007) presented a model which succeeded in explaining evolutionary history from the beginning of the merger to formation of the triple rings consistently. Especially, properties of geometry of the rings were well reproduced as seen in Fig 1.6. They estimated that the mass of the ejected matter during the transition was several $M_\odot$ for typical parameters. In their best model, the ER contains 0.4 $M_\odot$ and the ORs do 0.02 $M_\odot$ each. It may use constraint on the lower limit of total mass of the ejected matter during the phase of the merger although the observational constraints for the mass has been uncertain.

1.2.4 Models for the light curves

SNe are classified by their LC shapes and their spectra. There are two classes; Type I and II. The difference between them is whether H line (emission or absorption) emerges or not in the spectra. Type II events are also classified into subclasses. Most of Type II SNe are Type II-P. The envelope of a progenitor of Type II-P starts to expand after the shock goes through it. Thanks to the expansion, temperature of the envelope decreases to about 6.0×10^3 K from about 10^5 K. At this time, ionized hydrogen due to the shock heating starts recombination. As a result, the region at about 6.0×10^3 K becomes a photosphere. With the expansion, the photosphere extends to the inner region in the mass coordinate, but is fixed in the radial coordinate. Since the luminosity of a SN, $L_{\rm SN}$, can be represented as blackbody radiation, it is described as follows;

$$L_{\rm SN} \sim 4\pi R_{\rm ph}^2 \sigma_{\rm B} T_{\rm ph}^4 \tag{1.6}$$

where $R_{\rm ph}$ and $T_{\rm ph}$ are the radius and temperature of a photosphere and $\sigma_{\rm B}$ is the Stefan-Boltzmann constant. Therefore, there is a phase of constant luminosity in LCs of Type II-P, which is called a "plateau". The phase continues until about 1.0×10^2 days since the explosion. LCs of SN 1987A are peculiar comparing with these of Type II-P. Thus, LCs like SN 1987A are called Type II-pec. This type is a very rare event whose rate is 1 – 3 % of all CCSNe.

LCs of SNe can provide us with a lot of information about the state of the envelope of the progenitor, the ejecta mass, the explosion energy, and the mechanism of SNe. There are three sources of its brightness. The first is due to matter heating driven by propagation of the shockwave, which is mentioned above. The second is due to radioactive decay of ^{56}Ni which is created at the explosion. ^{56}Ni β-decays to ^{56}Co. This ^{56}Co γ-decays to ^{56}Fe, as γ-rays and positive electrons are emitted by stellar matter. The third is due to the rotational energy of a pulsar. Accelerated particles due to the wind of a pulsar collide with the ejected matter. In the case of SN 1987A, the increasing brightness after the first peak was due to radioactive decay. This contribution could be identified thanks to its faintness. After the second peak, the decay rates of the LCs corresponded to a half-life of ^{56}Ni.

A lot of information has been brought out by modeling the LCs by many authors. Shigeyama *et al.* (1988) presented hydrodynamical calculations in which the propagation of the shockwave, the expansion of the progenitor, and the optical LC were included. Parameters of their models were the ejecta mass $M_{\rm eje}$, the explosion energy $E_{\rm exp}$, and the compositions of the surface, and they assumed the matter mixing due to the Rayleigh-Taylor instability as a parameter. The rate of explosion energy and the envelope mass

$M_{\rm env}$, $E_{\rm exp}/M_{\rm env}$, is a indicator for the lower limit from the initial steep rising and the plateau around the second peak and for the upper limit from the slow expansion velocity of the inner layers. The best value of $E_{\rm exp}/M_{\rm env}$ was $1.5 \pm 0.5 \times 10^{50}$ erg ${\rm M}_\odot{}^{-1}$. In details, $E_{\rm exp}$ was 1.0 ± 10^{51} erg and $M_{\rm env}$ 6.7 $\rm M_\odot$. Shigeyama & Nomoto (1990) refined this study because new observational data had been collected on the abundance distribution in the ejecta. The updated $E_{\rm exp}/M_{\rm env}$ was $1.1 \pm 0.3 \times 10^{50}$ erg ${\rm M}_\odot{}^{-1}$. The propagation time, $\tau_{\rm prop}$, was approximated by the stellar radius R_0, $M_{\rm eje}$, and $E_{\rm exp}$ (Shigeyama *et al.*, 1987);

$$\tau_{\rm prop} \sim 2{\rm hr}\frac{R_0}{3\times10^{12}{\rm cm}}\left(\frac{M_{\rm eje}}{10M_\odot}\frac{E_{\rm exp}}{1\times10^{51}{\rm erg}}\right)^{1/2} \tag{1.7}$$

The detections of neutrinos ruled out $\tau_{\rm prop} < 3$ hr, so the radius has been limited. According to their model, the radius of the progenitor larger than 4.5×10^{12} cm did not agree with the observation.

1.3 Goal and aim of this thesis

A goal of this study is to construct the evolutionary model which succeeds in quantitatively explaining all of the observational constraints to reveal the amazing evolutionary history of the progenitor and to understand properties of progenitors of Type II SNe.

Towards this aim, I have been constructing the evolutionary model with a binary merger scenario until now (Urushibata *et al.*, 2017, 2018). The scenario has been mentioned in Sec 1.1.2 and is split into two parts in my model. Firstly, angular momentum is injected to the convective region for modeling spiral motion of the secondary due to friction. Secondly, mass is added near the core of the primary for modeling dissolution of the secondary in the inner region. After these, the calculation has been carried out until the Fe core is formed. In this thesis, I refine my previous models and present a more variable model than previously suggested by many authors. I also discuss the evolutionary mechanism and properties.

The previous three models are summarized in Table 1.2. The models of Saio *et al.* (1988b) and Podsiadlowski *et al.* (1992) explained the position on the HRD, the mass of the envelope in a progenitor phase, and lifetime from the transition to the end, but did not present the ejected mass for the triple rings and the chemical anomalies quantitatively. These models probably use an older opacity treatment than the OPAL, which considerably affects stellar evolution. Therefore, the results are uncertain if the OPAL is included. The model of Menon & Heger (2017) was nearly able to provide constraints. However, the lifetime was not explained when the chemical anomalies were matched, and the anomalies were not matched when the lifetime was explained. Their model is similar to mine although

their work was carried out independently. A crucial difference between my work and theirs is whether a model for the spiral-in phase is included or not because their model only included a phase of the melting of the secondary. It is expected that enhancement of the mass loss induced by transfer of angular momentum significantly affect stellar evolution. The mass of the ring system can be discussed using the ejected mass due to the enhancement. Therefore, a model including the spiral-in phase is very important.

This thesis is constructed as follows: Understanding history of SN 1987A respect to observations and theory is important to construct a refined model. This overview is summarized in Chapter 1. Since a stellar evolution code has been run in my work, it is useful that its description is described. In order to approach the goal, verifying a mechanism for transition from the red to blue suggested by the previous studies is important. Therefore, I construct three parametric models, in which effects of increasing helium abundance in the stellar envelope, adding matter to the envelope, and a combination of both effects are verified. After this, the progenitor model based on the merger scenario is constructed. Details of the computational code and numerical models are given in Chapter 2. In Chapter 3, calculation results of the three parametric and merger models are summarized. I use the results to bring out variable knowledge for the aim in Chapter 4. Finally, I conclude this thesis in Chapter 5.

Previous models for the progenitor			
	SA88	PO92	ME17
	Rotation	Merger	Merger
The HRD	Yes	Yes	Yes
Envelope mass	Yes	Yes	Yes
Ring mass	?	?	?
Chemical anomalies	?	?	Yes or No^{*1}
Lifetime	Yes	Yes	Yes or No^{*1}

Table 1.2: The previous studies. SA88 is Saio *et al.* (1988b), PO92 Podsiadlowski *et al.* (1992), and ME17 Menon & Heger (2017), respectively. "Lifetime" means that the transition occurred about 2.0×10^4 yr before the explosion. The others are in the literature. "?" indicates uncertain about whether the observational value is met or not. "Yes or No^{*1}" means that there is a much in one or the other, but not both.

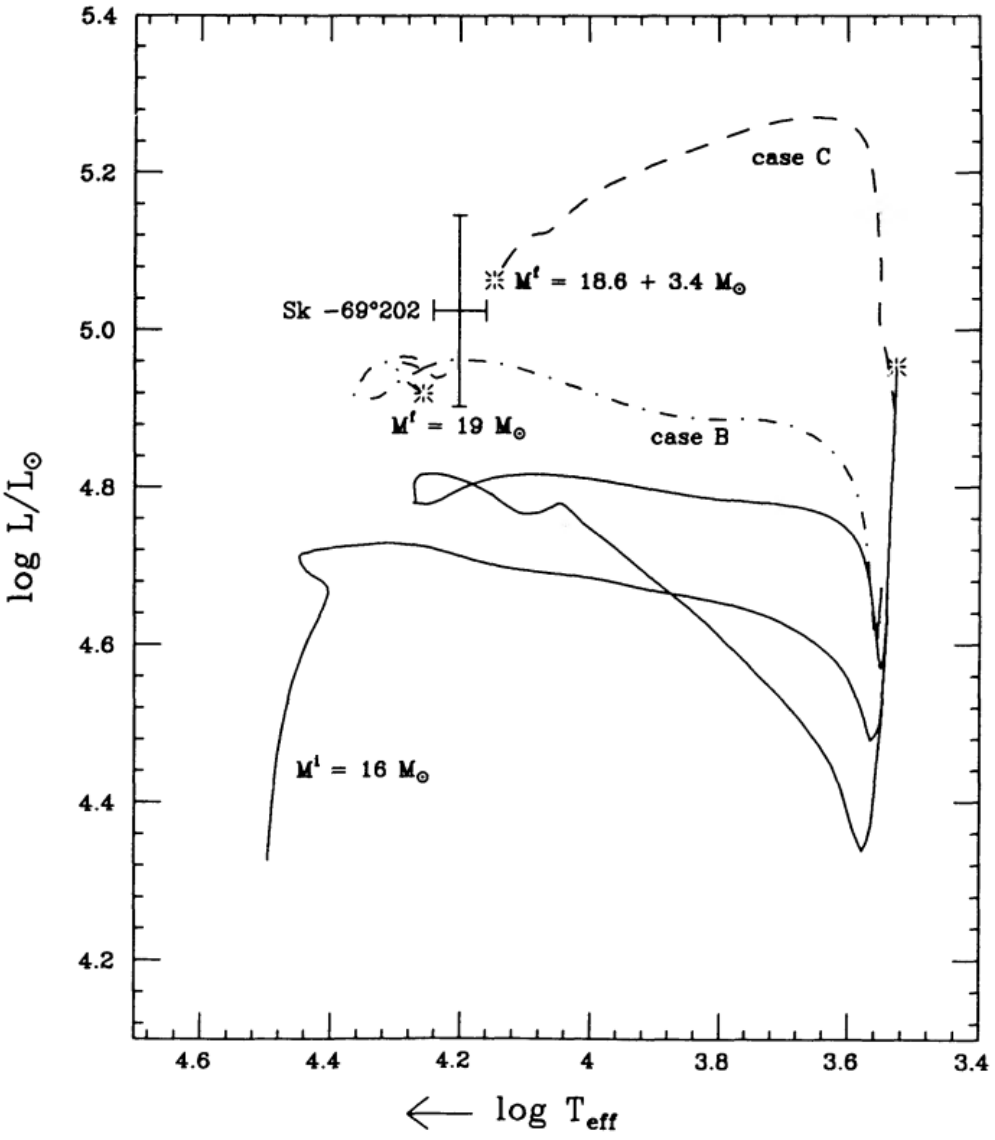

Figure 1.5. The results of the merger calculation in Podsiadlowski *et al.* (1992). The initial mass of the primary is 16.0 $M_\odot$. "case B" indicates the binary system in which the primary is a RSG having a He core and the secondary 3.0 $M_\odot$. "case C" is also the binary system, but the primary is a RSG having a CO core and the secondary 6.0 $M_\odot$. In this case, the secondary does not dissolve completely, and the added mass is 2.6 $M_\odot$.

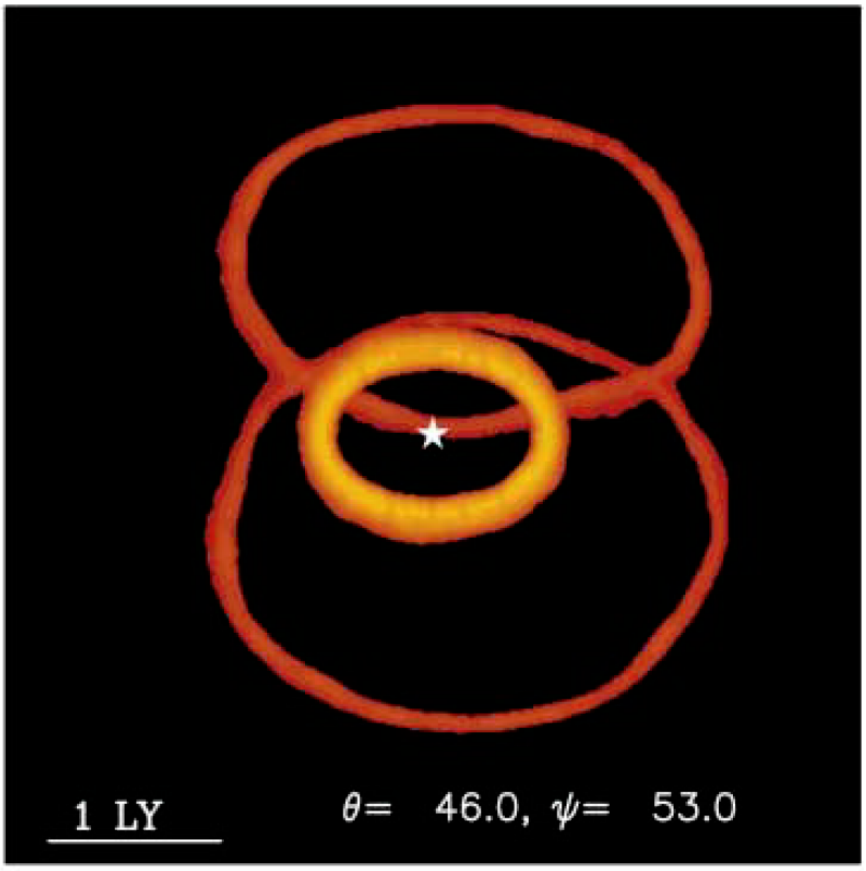

Figure 1.6. Simulation of emission at about 2.0×10^3 days after the SN in the 656 nm Hα line in Morris & Podsiadlowski (2007).

Chapter 2

Numerical Models

I describe overviews about the stellar evolution code used in this study and verify two effects for the red to blue transition suggested by the previous studies with three parametric models. I also construct a model for the slow merger scenario in which the two effects can be introduced naturally. The model includes effects of transfer of the orbital angular momentum and of melting of the secondary.

2.1 Overview of our stellar evolution code

I use the one-dimensional stellar evolution code described by Takahashi *et al.* (2014). In general, stellar evolution codes have been posed by an assumption of a spherical symmetric. Then, basic equations for the structure are

$$\frac{\partial r}{\partial M_r} = \frac{1}{4\pi r^2 \rho} \tag{2.1}$$

$$\frac{\partial p}{\partial M_r} = -\frac{GM}{4\pi r^4} + \frac{1}{4\pi r^2}\frac{\partial v}{\partial t} \tag{2.2}$$

$$\frac{\partial U}{\partial t} = -p\frac{\partial (1/\rho)}{\partial t} - \frac{\partial L}{\partial M_r} + \epsilon \tag{2.3}$$

$$L = L_{\rm rad} + L_{\rm conv} \tag{2.4}$$

where r is the radius, ρ the density, p the pressure, G the gravitational constant, M the total mass, v the velocity, U the internal energy, L the total luminosity, ϵ the energy generation, $L_{\rm rad}$ the luminosity due to radiation, and $L_{\rm conv}$ the luminosity due to convection.

Stars rotate generally. For massive stars, some effects induced by the rotation on their evolution can be serious. Here, four effects are incorporated in the code; deformation of a stellar configuration due to centrifugal force, matter mixing due to some circulation induced by the rotational instabilities, enhancement of the mass loss due to centrifugal force, and transfer of angular momentum inside a star. A pseudo spherical symmetric is

posed as an assumption for rotationally stellar configuration although the rotation is multi-dimensional phenomenon in nature. Besides, the shellular rotation, which originates from the strong horizontal turbulence, is assumed as the rotational profile (Zahn, 1992). The turbulence produces constant angular velocity, ω, on the isobaric shells, so the rotation profile is represented as follows;

$$\omega(r,\theta) = \bar{\omega}(r) + \omega_2(r)\mathrm{P}_2(cos\theta) \tag{2.5}$$

P_2 is the second Legendre polynomial, here.

This idea is extended to formalization for the equations for the structure and any physical quantities. Any value is evaluated on the isobaric shells with its volume $V_p \equiv 4\pi r_p^3/3$. Here, r_p is the effective radius of the shell. Since the configuration is generally a spheroid due to centrifugal force, with the approximation by Denissenkov & VandenBerg (2003) the radius depending on angle is

$$r(cos\theta) = a_{\mathrm{sc}}\{1 - \epsilon\mathrm{P}_2(\mathrm{cos}\theta)\} \tag{2.6}$$

where a_{sc} is the scaling radius and ϵ degree of the rotation. These parameters are defined as

$$r_p = a_{\mathrm{sc}}\left(1 + \frac{3}{5}\epsilon^2 - \frac{2}{35}\epsilon^3\right)^{1/3} \tag{2.7}$$

$$\epsilon = \frac{\omega_p^2 r_p^3}{3\mathrm{G}M_p}\left(\frac{a_{\mathrm{sc}}}{r_p}\right)^3 \tag{2.8}$$

where ω_p is the angular velocity on the shells and M_p the mass coordinate corresponding to r_p. None of the quantities are not constant over the shells, so their mean values are used in the calculation, which are defined by

$$\langle q \rangle \equiv \frac{1}{S_p}\int_{\mathrm{isobar}} q\mathrm{d}\sigma \tag{2.9}$$

where S_p is the total surface area and $\mathrm{d}\sigma$ its element. With these, the equations for the continuity and hydrostatic equilibrium can be expressed as follows:

$$\frac{\partial r_p}{\partial M_p} = \frac{1}{4\pi r_p^2 \rho} \tag{2.10}$$

$$\frac{\partial p}{\partial M_p} = -\frac{GM_p}{4\pi r_p^4} f_p \tag{2.11}$$

with

$$f_p = \frac{4\pi r_p^4}{GM_pS_p}\frac{1}{\langle g_{\rm eff}^{-1}\rangle} \tag{2.12}$$

where f_p is a modification coefficient due to the rotation and $\langle g_{\rm eff}\rangle$ a mean value of the effective gravity whose components are

$$g_{\rm eff,r} = \frac{\partial\Phi}{\partial r} + \Omega^2 r{\rm sin}\theta \tag{2.13}$$

$$g_{{\rm eff},\theta} = \frac{1}{r}\frac{\partial\Phi}{\partial\theta} + \Omega^2 r{\rm sin}\theta{\rm cos}\theta \tag{2.14}$$

where $g_{\rm eff,r}$ is the radial component and $g_{{\rm eff},\theta}$ the angular one.

To express the opacity of stellar matter, the Rossland mean opacity, κ

$$\frac{1}{\kappa} = \int_0^\infty \frac{1}{\kappa_\nu + \sigma_\nu}\frac{{\rm d}B_\nu}{{\rm d}T}d\nu \left(\int_0^\infty \frac{{\rm d}B_\nu}{{\rm d}T}d\nu\right)^{-1} \tag{2.15}$$

is adopted because it is a complicated function of photon's frequency, where κ_ν is the absorption coefficient depending on the frequency, σ_ν the scattering coefficient depending on the frequency, and B_ν the Planck's function, respectively. Using this mean opacity, the radiative luminosity can be expressed by

$$L_{\rm rad} = \frac{4aT^4}{3p}\frac{4\pi cGM_p}{\kappa}\frac{d{\rm log}T}{d{\rm log}p}\frac{f_p}{f_T} \tag{2.16}$$

with

$$f_T = \left(\frac{4\pi r_p^2}{S_p}\right)^2 \frac{1}{\langle g_{eff}\rangle\langle g_{eff}^{-1}\rangle} \tag{2.17}$$

Where f_T is a modification coefficient due to the rotation.

A criterion for convection is adopted the Ledoux one;

$$\nabla_{\rm rad} > \nabla_{\rm ad} + \frac{\phi}{\delta}\nabla_\mu \tag{2.18}$$

where $\phi \equiv \partial{\rm ln}\rho/\partial{\rm ln}\mu$ and $\delta \equiv -\partial{\rm ln}\rho/\partial{\rm ln}T$ are thermodynamic functions, and $\nabla_{\rm rad}$ and $\nabla_{\rm ad}$ the radiative and adiabatic temperature gradients, and $\nabla_\mu \equiv d{\rm log}\mu/d{\rm log}p$ is the μ gradient. Our understanding of convection in a star has been uncertain, so its luminosity is calculated with the mixing length theory (Böhm-Vitense, 1958).

As mentioned above, several instabilities caused by the rotation are included in the code: the Eddington-Sweet circulation, the Goldreich-Schubert-Fricke instability, the Solberg-Hoiland instability, the dynamical instability, the secular shear instability, and the Tayler-Spruit dynamo. Although the effects are incorporated as diffusion coefficients, these except

for the Tayler-Spruit dynamo are introduced as viscosities. The corresponding expressions are $\nu_{\rm ES}$, $\nu_{\rm GSF}$, $\nu_{\rm SH}$, $\nu_{\rm dyn}$, and $\nu_{\rm shear}$. The Tayler-Spruit dynamo is directly incorporated as a diffusion coefficient, $D_{\rm TS}$. The total diffusion coefficient is the sum of a certain free parameter, $f_{\rm c}$, times the viscosities and $D_{\rm TS}$. Therefore, the final expression, $D_{\rm inst}$, can be expressed by

$$D_{\rm inst} = f_{\rm c} \times (\nu_{\rm ES} + \nu_{\rm GSF} + \nu_{\rm SH} + \nu_{\rm dyn} + \nu_{\rm shear}) + D_{\rm TS}. \tag{2.19}$$

The values calculated by Heger *et al.* (2000) are adopted as the parameters mentioned here.

The equation for transfer of the angular momentum is expressed as a diffusion one;

$$\frac{\partial \omega}{\partial t} = \frac{1}{I}\frac{\partial}{\partial M}\left((4\pi r^2\rho)^2 I \nu_{\rm eff}\frac{\partial \omega}{\partial M}\right) - \frac{\omega}{r}\frac{\partial r}{\partial t}\frac{\partial {\rm ln}I}{\partial {\rm ln}r} \tag{2.20}$$

with

$$\nu_{\rm eff} = \nu_{\rm ES} + \nu_{\rm GSF} + \nu_{\rm SH} + \nu_{\rm dyn} + \nu_{\rm shear} + \nu_{\rm TS} \tag{2.21}$$

where I is the specific moment of inertia, $\nu_{\rm eff}$ the effective viscosity, and $\nu_{\rm TS}$ the viscosity due to the Tayler-Spruit dynamo, respectively. The first term in the right hand shows the transfer caused by the matter mixing and the second does the conservation of local angular momentum.

The mass loss is enhanced due to the rotation (Langer, 1998). This is represented as follows:

$$\dot{M} = -{\rm min}\left\{|\dot{M}(v_{\rm s,rot}=0)| \times \left(1 - \frac{v_{\rm s,rot}}{v_{\rm crit}}\right)^{-0.43}, 0.3\frac{M}{\tau_{\rm KH}}\right\} \tag{2.22}$$

with

$$v_{\rm crit} = \sqrt{\frac{GM}{R}\left(1 - \frac{L}{L_{\rm Edd}}\right)} \tag{2.23}$$

where $\dot{M}$ is the mass loss rate, $v_{\rm s,rot}$ the surface velocity of a star, $v_{\rm crit}$ the critical surface velocity of a star, $L_{\rm Edd}$ the Eddington luminosity, and $\tau_{\rm KH}$ the Kelvin-Helmholtz timescale, respectively.

2.2 Changed star

In this study, the stellar structure is changed by some processes. Especially, the changed star is called a primary star and its companion a secondary one in a binary system. The

primary is more massive than the secondary.

One of the conditions for the changed star is to have the mass of the core in which nuclear synthesis can proceed until Fe is formed because the star has to explode at its death. In addition, since a constraint for the mass of the envelope at the progenitor phase is 4.0 $M_\odot$ – 14.0 $M_\odot$, the initial mass may be about 20.0 $M_\odot$. In a merger scenario, the mass of the secondary is added to the envelope of the primary. Therefore, I select the range of the initial mass of the changed star from 14.0 $M_\odot$ – 16.0 $M_\odot$ to meet the constraint and a condition for creating a common envelope. I also test various initial velocities of the surface, $v_{\rm ini}$. It affects the mass of the core and envelope and chemical compositions in the envelope. Since the explosion occurred in the LMC, the metallicity of the LMC, whose value is set to be 1/3 $Z_\odot$, is adopted in all models.

Informations of the changed stars are summarized in Table 2.1. $\tau_{\rm rest}$ is rest time until the explosion, so it should be close to about 2.0×10^4 yr to match the transition time from a red to blue star. "Stage" indicates when the drastic mass transfer takes place for forming a common envelope. In the merger model, P14b, P15a, and P16b are adopted as the primary. On the other hand, P14a and P16a are used in the verification models.

P14: $M_{\rm ini}$ = 14 $M_\odot$ with $v_{\rm ini}$ = 102.7 km/s				
Name	$M_{\rm tot}$ [$M_\odot$]	$M_{\rm core}$ [$M_\odot$]	$\tau_{\rm rest}$ [$\times 10^4$ yr]	Stage
P14a	12.93	4.27	72.15	case B
P14b	12.01	4.84	2.065	case C
P15: $M_{\rm ini}$ = 15 $M_\odot$ with $v_{\rm ini}$ = 111.6 km/s				
P15a	12.33	5.47	2.059	case C
P16: $M_{\rm ini}$ = 16 $M_\odot$ with $v_{\rm ini}$ = 162.3 km/s				
P16a	12.51	6.23	5.753	case C
P16b	12.38	6.27	1.981	case C

Table 2.1. The changed stars in my models. $M_{\rm core}$ is the mass of the core. "Stage" represents a classification of the drastic mass-transfer for forming a common envelope.

2.3 Parametric models for the red to blue evolution

One of the mysteries is what causes the red to blue evolution about 2.0×10^4 yr before the explosion. Many researchers made an effort to unravel the mechanism of the evolution as seen in Introduction. It turned out that two important factors are as follows:

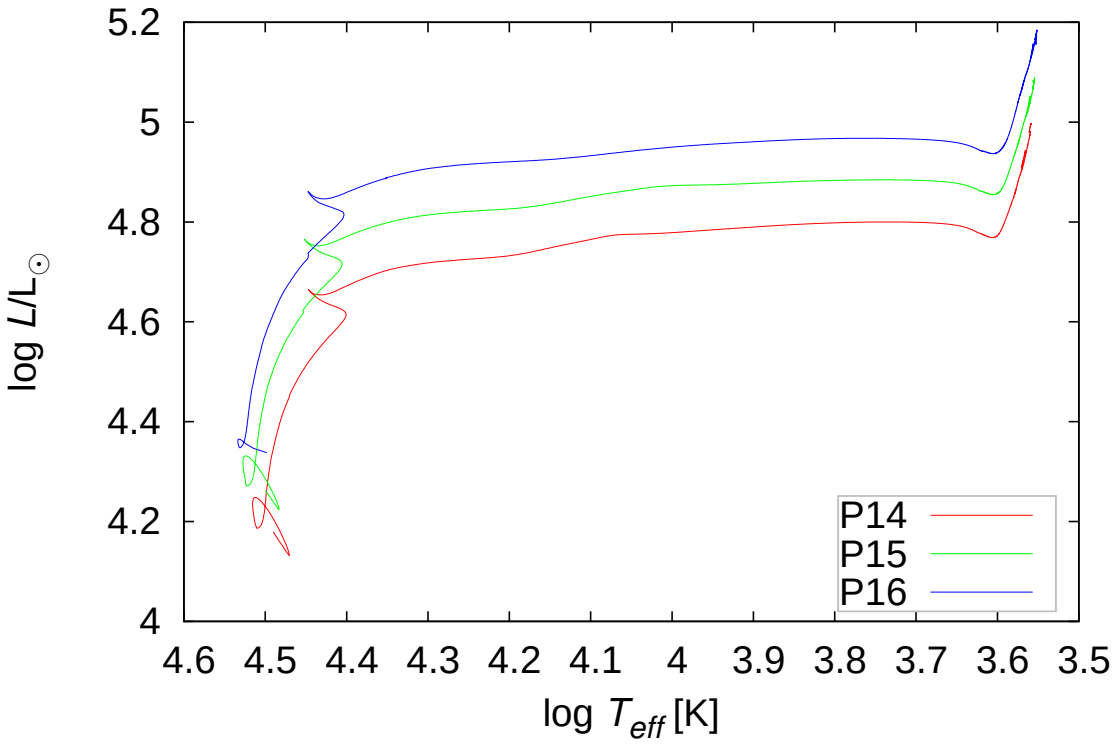

Figure 2.1. The HRDs of the changed stars. The initial masses of P14, P15, and P16 are 14.0 $M_\odot$, 15.0 $M_\odot$, and 16.0 $M_\odot$, respectively. The initial velocities of P14, P15, and P16 are 102.7 km/s, 111.6 km/s, and 162.3 km/s, respectively.

- Smaller core-to-total mass ratio, $q \equiv M_{\rm core}/M_{\rm tot}$
- Larger helium abundance in the envelope

To verify these effects, I construct three parametric models.

2.3.1 Increasing mass model: roles of decreasing the mass ratio

For single stars, their masses are always lost via their stellar wind. Typically, massive stars at the ZAMS have high initial rotations and the surface rotation velocity which is represented as follows under a spherical assumption;

$$v_{\rm s,rot} = M R_{\rm surf} \omega_{\rm s,rot} \tag{2.24}$$

where $R_{\rm surf}$ is the radius of the surface and $\omega_{\rm s,rot}$ the angular frequency of the surface. According to (2.22), the mass loss is enhanced in the case of rotation. Therefore, $M_{\rm tot}$ becomes smaller.

Also, the rotation can affect the mass of the core during the main-sequence (MS) phase.

Mixing caused by the rotation brings hydrogen into the core. Thus, new fuel is supplied into the core while nuclear synthesize is proceeding in the central region. As a result, the core mass of the rotating models becomes larger than for non-rotating models.

Therefore, effects of the rotation on $M_{\rm tot}$ and $M_{\rm core}$ lead to a larger q. This means that the rotation prevents the red to blue evolution.

On the other hand, the situation changes for a close binary system. Stars interact with each other in the system due to their gravity, leading to the mass transfer or stellar merger. These mean that there is a way to increase the mass of the stellar envelope, which never occurs for single stars. Therefore, q can decrease for the close binary.

I construct a parametric model which simulates the increasing mass. The procedures in this model are as follows: I add matter whose mass is $M_{\rm add}$ to the primary from its surface in a certain time, $\tau_{\rm add}$. Since this model supposes a binary interaction, especially a stellar merger, $\tau_{\rm add}$ is set to be 1.0×10^2 yr which matches to the order of time-scale of a common envelope (Meyer & Meyer-Hofmeister, 1979).

The rate of the mass loss, $\dot{M}_{\rm add}$, is set to be constant and is defined by

$$\dot{M}_{\rm add} \equiv \frac{M_{\rm add}}{\tau_{\rm add}} \tag{2.25}$$

Therefore, the added mass in every step, $M_{\rm add,1step}$, is

$$M_{\rm add,1step} = dtime \times \dot{M}_{\rm add}. \tag{2.26}$$

where $dtime$ is the time between the proximate time steps.

To model the increasing mass, the original rate of the mass loss is replaced with $\dot{M}_{\rm add}$, and $M_{\rm add,1step}$ is added to $M_{\rm tot}$ just before the structure equations are solved. Given information of the secondary is only its mass. The physical structure of the secondary, such as the density, entropy, pressure, temperature, chemical abundance and so on, is not considered. Instead, the physical quantities of the surface of the primary are taken to be those of the secondary. A sample of the changed chemical profile is described in Fig 2.2.

The used parameters are summarized in Table 2.2. Since a convective region in the envelope and the core develop for the case C more than for the case B, I use P14a and P14b as the changed stars to investigate effects of different structures of the changed stars on the evolution. $M_{\rm add}$ is 5.0 $M_\odot$ – 7.0 $M_\odot$ for P14a, and 9.0 $M_\odot$ and 10.0 $M_\odot$ for P14b.

2.3.2 Helium enhanced model: roles of helium enhancement in the envelope

I construct a model to verify the effect of helium enhancement. In this model, helium abundance in the envelope is artificially altered using some parameters. Firstly, the altered region is designated by two parameters, $M_{\rm He,bottom}$ and $M_{\rm surf}$. $M_{\rm He,bottom}$ indicates

The changed star	$M_{\rm add}$ [$M_\odot$]
P14a	5.0 – 7.0
P14b	9.0, 12.0

Table 2.2. Parameters in the increasing mass model. "The changed star" represents the stellar model added mass, whose information is included in Table 2.1. $M_{\rm add}$ is the mass to be added.

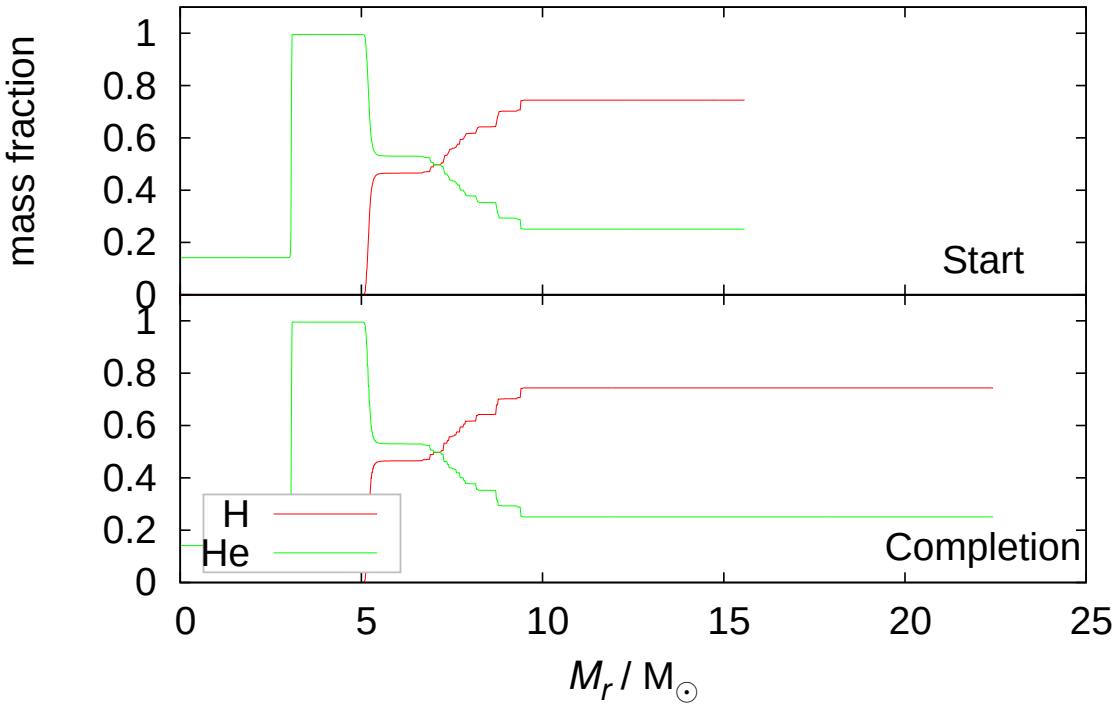

Figure 2.2. Profiles of hydrogen and helium in the increasing mass model. The top panel represents the profiles of the changed star at the start of this calculation. The bottom panel is same as the top, but at the end of the mass addition.

a certain mass coordinate in the changed star and $M_{\rm surf}$ does the surface. Therefore, chemical profiles in the mass region surrounded from $M_{\rm He,bottom}$ to $M_{\rm surf}$ are altered. Secondly, helium mass fraction in the region is replaced with an arbitrary value, $Y_{\rm He}$, whose value is given as the mass fraction. To avoid unconvergence of the calculation due to a drastic change of abundance, the value is changed gradually. As the original helium abundance is represented by $Y_{\rm original}$, the increasing amount, ΔY, is

$$\Delta Y = Y_{\rm He} - Y_{\rm original} \tag{2.27}$$

Thus, the changed rate, $\Delta\dot{Y}_{\rm He}$, is determined by

$$\Delta\dot{Y}_{\rm He} \equiv \frac{\Delta Y_{\rm He}}{\tau_{\rm He}} \tag{2.28}$$

where $\tau_{\rm He}$ is time for the change, which is set to be 10.0 yr in all the models, so helium abundance at a certain time, $\tau_{\rm cert}$ ($< \tau_{\rm He}$), $\tilde{Y}_{He}$, is

$$\tilde{Y}_{\rm He} = Y_{\rm original} + \int_0^{\tau_{\rm cert}} \Delta\dot{Y}_{\rm He}{\rm dt} \tag{2.29}$$

Therefore, $Y_{\rm original}$ has been replaced with $Y_{\rm He}$ in $\tau_{\rm He}$. Since the main composition in the envelope is hydrogen at the start of the calculation, this value also has to be modified. Here, the new hydrogen abundance is set to be $1.0 - \tilde{Y}_{\rm He}$, and mass fractions of the rest isotopes are not modified artificially. Strictly speaking, there is contradiction because the sum of the mass fractions exceeds 1.0 in this way. This may be, however, no problem because the sum of the mass fractions except for the new hydrogen and helium is much less than 1.0. After this, the calculation has been carried out for 1.0×10^7 yr with stopping change of the chemical abundance due to nuclear synthesis in the central region and of the mass loss. These mean that this model investigates only evolution of the envelope.

The setting time of the calculation, 1.0×10^7 yr, is much longer than the Kelvin Helmholtz time-scale in the envelope. Therefore, it is expected that the envelope reaches thermal equilibrium within the setting time efficiently. If the original equilibrium breaks in the envelope of a RSG, the star would become a BSG to keep the equilibrium.

A sample of the change is described in Fig 2.3. The parameters are summarized in Table 2.3. $M_{\rm He,bottom}$ is set to be 5.8 $M_\odot$in all the models.

The changed star	$Y_{\rm He}$
P16a	0.55 – 0.65

Table 2.3. Parameters in the helium enhanced model. $Y_{\rm He}$, which is given by mass fraction, is the new helium mass fraction in the region from $M_{\rm He,bottom}$ to $M_{\rm surf}$.

2.3.3 Combination model: roles of combining the increasing mass with the helium enhancement

I construct a model to verify combining the two effects. The procedures are combining the ways of the increasing mass and helium enhanced models. Firstly, the mass is added to the envelope with the ways of the increasing mass model. The added mass range is 4.73 $M_\odot$ – less than 20.0 $M_\odot$. τ_{add} is set to be within 50.0 yr. The time is different in each model, but it is not important for the evolution because the added time is much less than

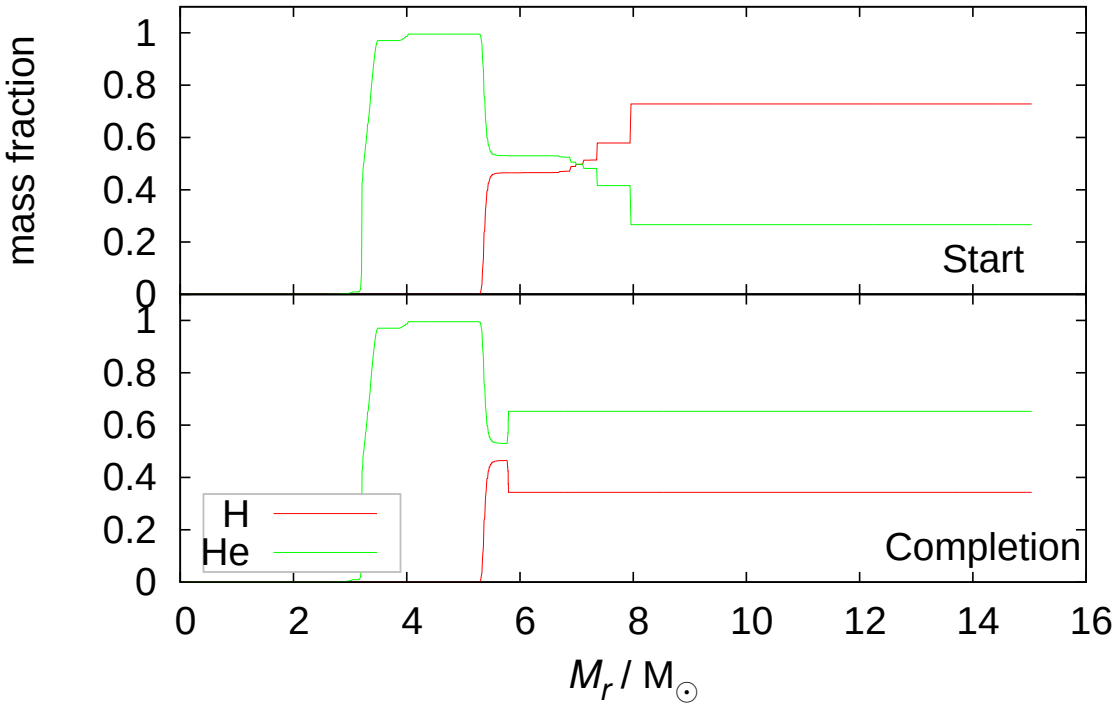

Figure 2.3. Profiles of hydrogen and helium in the helium enhancement model. The top panel is same as the top in Fig 2.2. The bottom is also same as the bottom in Fig 2.2, but at the end of the enhancement of helium. In this figure, the changed region is from $M_{\rm He,bottom} = 5.8$ M$_\odot$ to $M_{\rm surf}$ and $Y_{\rm He} = 0.625$.

the evolutionary one. Secondly, helium abundance in the envelope is altered according to the helium enhanced model. $Y_{\rm He}$ is set to be 0.38 – 0.55, which is changed in 10.0 yr. The calculation time and $M_{\rm He,bottom}$ are also same as the helium enhanced model.

The changed	$M_{\rm add}$ [M$_\odot$]	$Y_{\rm He}$
P16a	4.73 – 19.73	0.38 – 0.55

Table 2.4. Parameters in the combination model. M_2 and $Y_{\rm He}$ are same in the increasing mass and helium enhanced models.

2.4 Model for the slow merger

My model for the progenitor is based on the stellar merger scenario suggested by Podsiadlowski *et al.* (1992); Ivanova *et al.* (2002). The basic picture has already been described

in Introduction. The primaries are P14b, P15a, and P16b. To enter a common envelope phase, the secondary has to be a MS star because the radiative envelope is necessary for the unstable mass transfer, so the initial mass of the secondary is about 1.25 $M_\odot$ – about 10.0 $M_\odot$ for the mass range of the primary. Since the common envelope phase ceases within on the order of 10^2 yr, time-scale of the melting is shorter than of the evolution of the RSG. It is, however, much longer than the dynamical time-scale of the secondary (a few hours). In that sense, this type of merger is called a *slow merger*.

Here, I estimate the fate of a common envelope in my model. To do it, the energy formalism has been carried out in a standard way (Ivanova *et al.*, 2013). In the formalism, difference of the orbital energy between the initial and the common envelope, $\Delta E_{\rm orb}$, is used as measure of the fate;

$$\Delta E_{\rm orb} = E_{\rm orb,i} - E_{\rm orb,c} \tag{2.30}$$

$$= -\frac{GM_1M_2}{2a_{\rm i}} + \frac{GM_{1,c}M_2}{2a_{\rm c}} \tag{2.31}$$

where $E_{\rm orb,i}$ is the initial orbital energy, $E_{\rm orb,c}$ the final orbital energy, $a_{\rm i}$ the current separation between the core of the RSG and the secondary, $a_{\rm c}$ the current separation between them, and $M_{1,c}$ the current mass of the primary, respectively. When the secondary moves to an inner region, $\Delta E_{\rm orb}$ is added to the envelope. For the estimate, I assume that $M_{1,c}$ is always same as M_1 to keep simplicity although it is affected by the mass loss because of transfer of the angular momentum and the frictional heating.

The parameters $\{M_1,\ M_2,\ a_{\rm i}\} = \{15.0\ M_\odot,\ 7.0\ M_\odot,\ 1.0 \times 10^3\ R_\odot\}$ are set to be constant with the progenitor of SN 1987A, and variation of $\Delta E_{\rm orb}$ is then described in Fig 2.4. Since the secondary starts to melt at about 10.0 $R_\odot$ according to (1.5), $\Delta E_{\rm orb}$ becomes 1.973×10^{49} erg. The binding energy (the gravitational energy plus the internal one) for P14b is -1.574×10^{50} erg, so the envelope cannot be significantly affected even though all the $\Delta E_{\rm orb}$ is transfered to the internal energy.

2.4.1 Spiral motion in the common envelope

While the secondary is spiraling toward the center, its orbital angular momentum and frictional energy are transfered to the envelope until the secondary reaches at about 10.0 $R_\odot$. It is expected that transfers of the two physical quantities lead to enhancement of the mass loss because these generate repulsive force against the self-gravitation. Only transfer of the orbital angular momentum is, however, considered for this model, that is to say, the effect of the frictional heating is not included. The reason is to avoid complexity for the modeling and difficulty of the calculation, and is according to the analysis for the fate in the previous subsection. As mentioned above, the two effects contribute to the mass

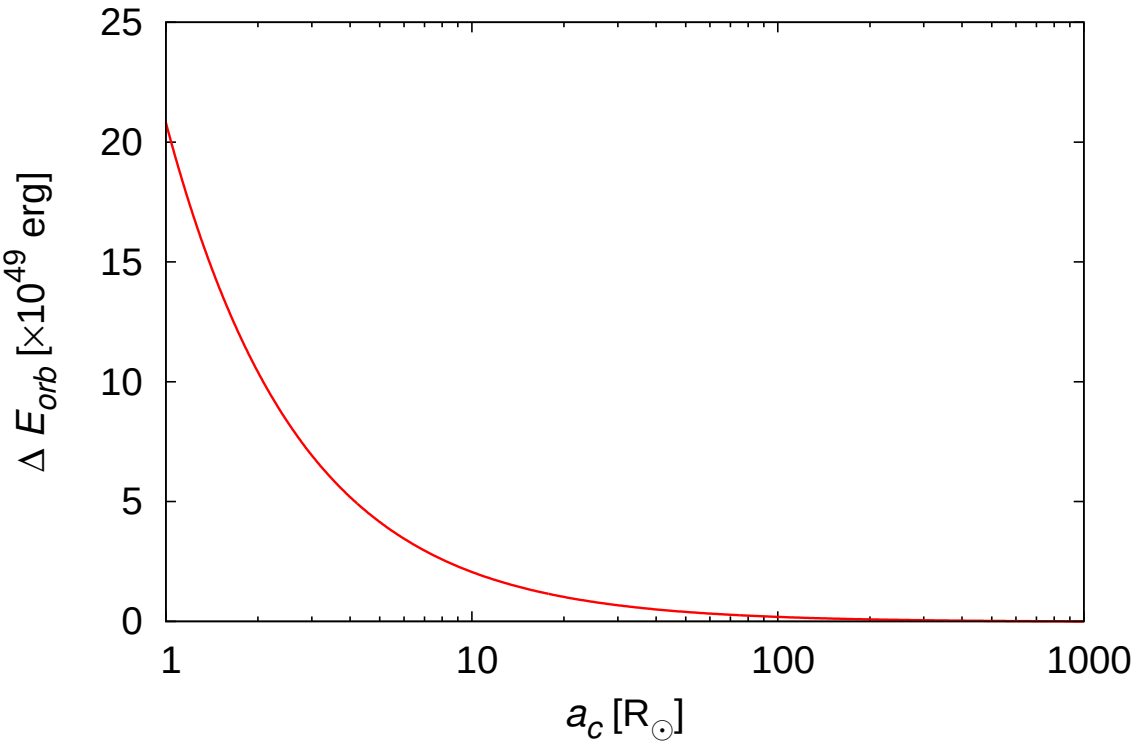

Figure 2.4. Energy difference for a binary system in my model. As a sample, $M_1 = 15.0$ $M_\odot$ and $M_2 = 7.0$ $M_\odot$ are adopted here. a_c represents the current separation between the core of the RSG and the secondary.

loss mainly, leading ejection of material of the rings. Here, the contribution is unified by one effect, which is transfer of the orbital angular momentum.

For the modeling of this phase, three parameters are introduced; The first is orbital angular momentum of the secondary star, $J_{\rm orb}$. If the secondary rotates around the surface of the envelope with Kepler motion, the typical value is on the order of 10^{54} erg sec estimated by

$$J_{\rm orb} = M_1 M_2 \sqrt{\frac{{\rm G} R_{\rm surf}}{M_1 + M_2}} \tag{2.32}$$

Since the stellar evolutionary code is described in one dimension, the spherical wind mass loss is assumed. However, it would be expected that the mass loss with efficient loss of angular momentum, such disk like mass loss, occurs. Therefore, I select the wide range 1.0×10^{53} – 3.0×10^{54} erg sec as $J_{\rm orb}$. The second is time of the transfer, $\tau_{\rm spin}$, whose value is determined by the friction. $\tau_{\rm spin}$ is fixed to be 1.0×10^2 yr, which is according to time-scale for the common envelope phase, in all the models. The third is a position which determines the added region, $R_{\rm bottom}$ or $M_{\rm bottom}$. These indicate the same position, so the

difference is whether the mass or radial coordinate. With it, the region can be determined from $R_{\rm bottom}$ to $R_{\rm surf}$. Of cause, the region from $M_{\rm bottom}$ to $M_{\rm surf}$ is the same. $J_{\rm orb}$ is added to the convective envelope. Therefore, the bottom of the region is set within the convective region. I adopt 1.0×10^2 $\rm R_\odot$ as $R_{\rm bottom}$ in all the models. The value corresponds to near the bottom of the convective region.

The equation of addition of the orbital angular momentum is

$$\frac{\partial j(M_r)}{\partial t} = \frac{j(M_r)}{\tau_{\rm spin}} \frac{J_{\rm orb}}{J_{\rm env}} \tag{2.33}$$

with

$$J_{\rm env} \equiv \int_{R_{\rm bottom}}^{R_{\rm surf}} j(M_r) {\rm d}M \tag{2.34}$$

where $j(M_r)$ is the specific angular momentum of the primary at the mass coordinate M_r and $J_{\rm env}$ the total angular momentum of the envelope of the primary. The right side is composed of the constant part times $j(M_r)$. Since the rigid rotation is established in the convective region, the angular momentum are transfered by (2.20) to keep the rotation law.

2.4.2 Melting of the secondary into the envelope

When the secondary starts to dissolve in the envelope, the matter flow, like a stream, moves to the core due to tidal force between them. The stream can affect chemical profiles between them because of orbital motion of the melting secondary. Besides, it can penetrate some degrees in the core under some conditions such as the initial entropy and angular momentum of the stream, the structure near the core, and the generated entropy due to interaction between the stream and the core (Ivanova *et al.*, 2002).

To model the melting, four parameters are introduced; The first is the mass of the secondary, M_2. The appropriated range is 1.25 $\rm M_\odot$ – 10.0 $\rm M_\odot$ as mentioned above, so I select 4.0 $\rm M_\odot$ – 10.0 $\rm M_\odot$ as M_2. The second is degree for the penetration of the stream, $M_{\rm in}$, whose value is designated by the mass coordinate. This parameter is set in the helium layer of the core. The third is a position of the secondary, $R_{\rm out}$, and the corresponding mass coordinate is $M_{\rm out}$. The value is set to be 10.0 $\rm R_\odot$ at which the secondary starts to melt, and is fixed in all the models. The fourth is time until the melt of the secondary is completed, $\tau_{\rm melt}$, which is set to be 1.0×10^2 yr in all the models.

Since the mass coordinate is used in the evolutionary code, the increasing mass due to the melt is represented by extension of difference between the proximate meshes. When the added mass in the every step, ΔM, increases, there are the three divisions as follows:

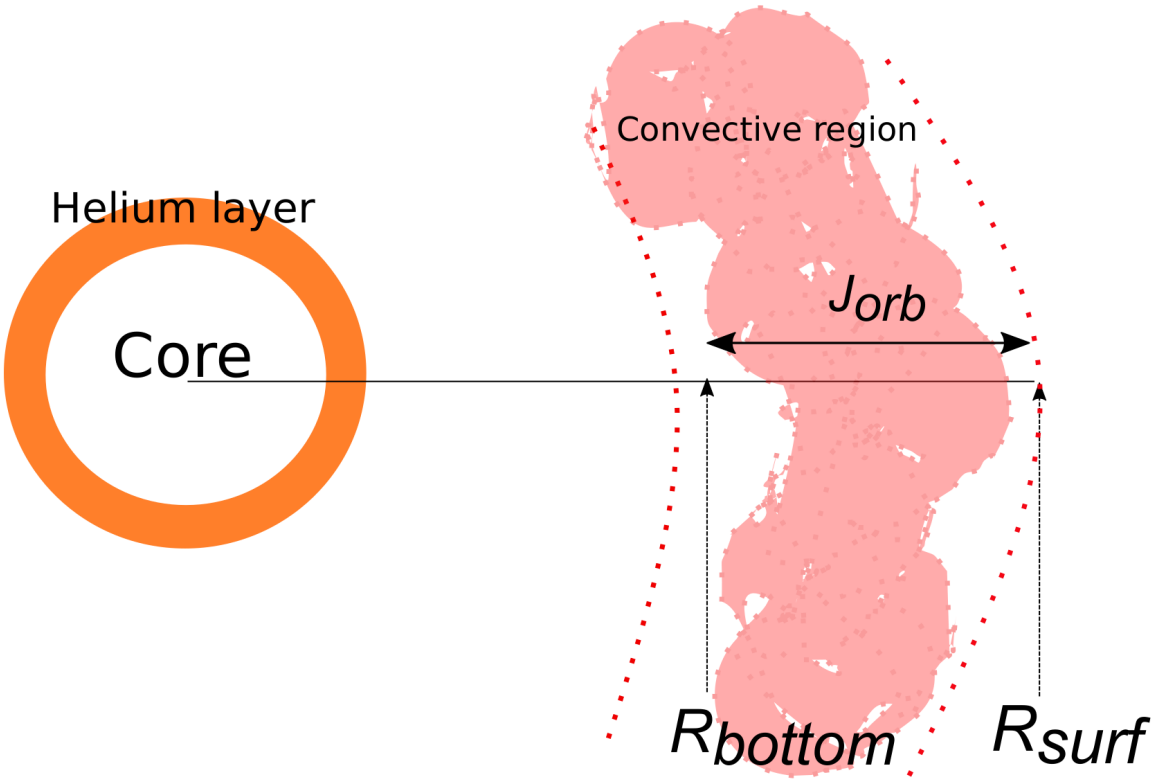

Figure 2.5. Schematic image for modeling an addition of the orbital angular momentum. The angular momentum are added to the convective region only.

$$M_j^{new} = \begin{cases} M_j^{\rm old} & (j < j_{\rm in}) \\ M_j^{\rm old} + \frac{M_j^{\rm old} - M_{\rm in}}{M_{\rm out} - M_{\rm in}} \Delta M & (j_{\rm in} \leq j \leq j_{\rm out}) \\ M_j^{\rm old} + \Delta M & (j_{\rm out} < j) \end{cases} \tag{2.35}$$

with

$$\Delta M \equiv dtime \times \frac{M_2}{\tau_{\rm melt}} \tag{2.36}$$

where j is the j-th mesh number, $M_j^{\rm new}$ the modified mass at j-th, $M_j^{\rm old}$ the previous mass at j-th, $j_{\rm in}$ the mesh number of $M_{\rm in}$, and $j_{\rm out}$ the mesh number of $M_{\rm out}$. The first division is the mass range from the center to $M_{\rm in}$. Even though ΔM increases, the meshes in this region do not extend (see (1) in Fig 2.6). Therefore, the mass of the core except for a part of the helium layer does not change. The second is the region from $M_{\rm out}$ to $M_{\rm surf}$. The mass meshes in this division are added ΔM, meaning that these are shifted ΔM outside (see (2) in Fig 2.6). The third division is the range from $M_{\rm in}$ to $M_{\rm out}$. The extension

is obeyed by the middle in (2.35) (see (3) in Fig 2.6). Clearly, the sum of the extension is ΔM. Difference between the original meshes in the region is set to be high-resonance for solving the equations. To avoid the unconvergence, the change has to be carried out gradually.

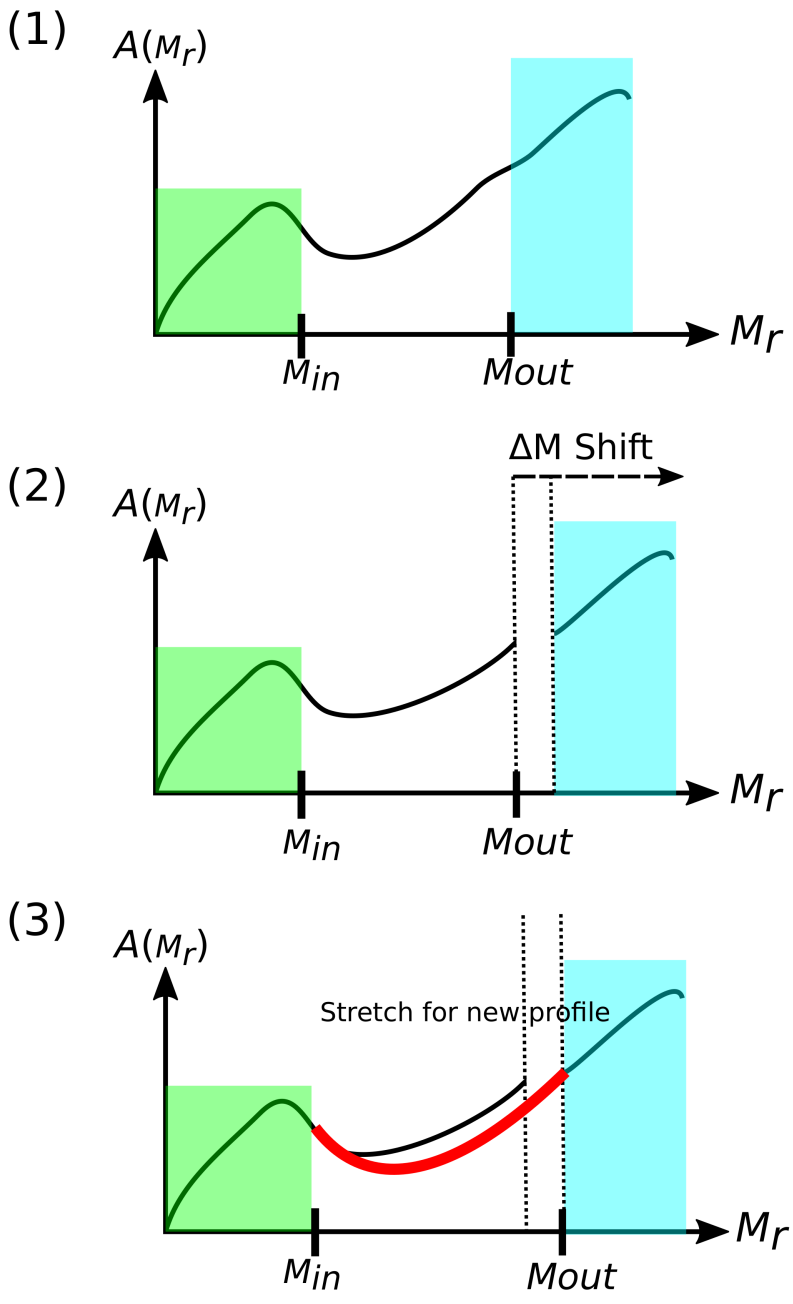

Figure 2.6. Schematic image for the stretch of the meshes and for the new profile of some physical quantities.

For modeling the effect for the motion of the stream on the chemical profiles, the new

compositions are uniformly changed by

$$X_i = \frac{\bar{X}_{i,b}(M_{\rm out} - M_{\rm in}) + X_{2,i}\Delta M}{M_{\rm out} + \Delta M - M_{\rm in}} \tag{2.37}$$

with

$$\bar{X}_{i,b} \equiv \int_{M_{\rm in}}^{M_{\rm out}} X_{i,b} {\rm d}M \tag{2.38}$$

where X_i is the mass fraction of the i-th isotope, $\bar{X}_{i,b}$ the mean mass fraction at the previous step, and $X_{2,i}$ the mass fraction of the i-th isotope of the secondary, respectively. As the compositions of the secondary, it is adopted that these of the 5.0 and 7.0 $M_\odot$ stars with $v_{\rm ini} = 102.7$ km sec^{-1} at time of the phase of P14b. If the mass of the secondary is less than 7.0 $M_\odot$, the compositions of 5.0 $M_\odot$ are used as these of the secondary. On the other hand, if the mass of the secondary is 7.0 $M_\odot$ or more, the compositions of 7.0 $M_\odot$ are adopted.

After the penetration, there is a possibility of occurrence of hydrodynamical phenomenon. I assume that a large scale mixing is induced by the hydrodynamics, and the mixing uniformly alters the chemical compositions in the region from $M_{\rm in}$ to $M_{\rm surf}$ as follows;

$$X_i^{\rm mix} = \frac{\int_{M_{\rm in}}^{M_{\rm surf}} X_i(m) {\rm d}m}{\int_{M_{\rm in}}^{M_{\rm surf}} {\rm d}m} \tag{2.39}$$

where $X_i^{\rm mix}$ is the modified mass fraction of i-th isotope due to the mixing. Whether the large scale mixing is included or not is given as a parameter although the mixing from $M_{\rm in}$ to $M_{\rm out}$ is included in all the models.

The schematic image for relation among the parameters in this phase is described in Fig 2.7.

2.4.3 Summary of the parameters

There are eight parameters in the merger model as seen above. These are summarized in Table 2.5. The parameters $\{\tau_{\rm spin}, R_{\rm bottom}, \tau_{\rm melt}, R_{\rm out}\} = \{1.0 \times 10^2$ yr, 1.0×10^2 $R_\odot$, 1.0×10^2 yr, 10.0 $R_\odot\}$ are fixed, the other are varied.

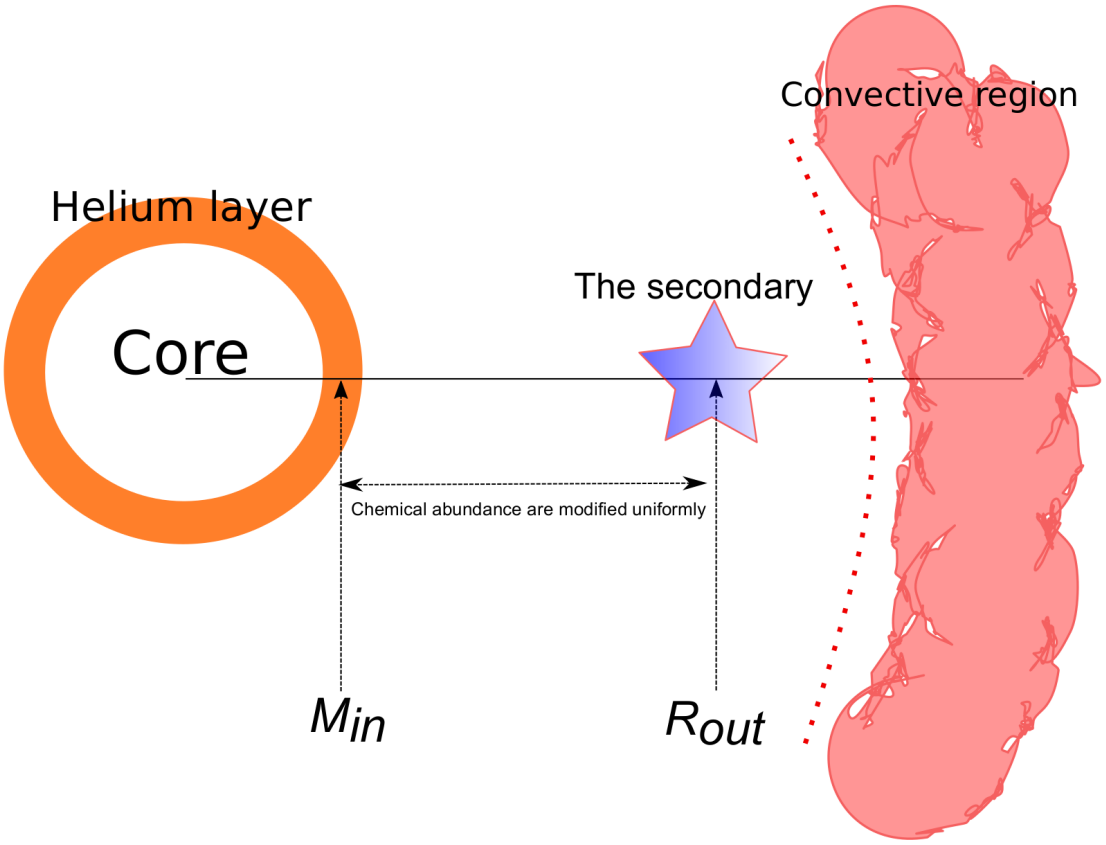

Figure 2.7. Schematic image for modeling the melt.

The spiral-in phase				
$J_{\rm orb}$	$\tau_{\rm spin}$	$R_{\rm bottom}$		
[$\times 10^{53}$erg sec]	[yr]	[$R_\odot$]		
1.0 – 30.0	1.0×10^2	1.0×10^2		
The melting phase				
M_2	$\tau_{\rm melt}$	$M_{\rm in}$	$R_{\rm out}$	Mixing
[$M_\odot$]	[yr]		[$R_\odot$]	
4.0 – 10.0	1.0×10^2	In He layer	10.0	Yes or No

Table 2.5. Parameters in the merger model.

Chapter 3

Results

In this chapter, I will present the results of all of the model, consisting of three verification and merger models.

3.1 Increasing mass

The results of the increasing mass model are summarized in Table 3.1. In the table, $M_{\rm fin}$ is the final mass and "Track" represents transition of the stellar color which is the rough evolutionary path. The evolutionary tracks for the models based on P14a in the HRD are described in the top panel of Fig 3.1 and these for the P14b are done in the bottom of Fig 3.1.

For the P14a, the RSG becomes a blue progenitor if $M_{\rm add}$ is 6.0 $M_\odot$ or more. Here, I use P14aM5 and P14aM7 to see the evolutionary properties. For P14aM5, the star begins to leave the Hayashi line and moves bluer while the matter is being added to the envelope. It first enters a phase of a BSG in 1.026×10^4 yr since the accretion, and continues to shrink further. Its effective temperature peaks at 1.3×10^5 yr after the first blue. After the peak, the star begins to expand toward the red region, returning to a RSG by 1.0×10^6 yr. P14aM7 is the case of a blue progenitor. The star takes 6.664×10^3 yr to first reach the blue region. In this phase, the whole convective envelope transitioned to a radiative state. It takes about 8.4×10^5 yr from the first blue to reach the peak. After this, the star moves redder, as with P14aM5, but has exploded as a BSG without returning to the red state. As a tendency, the more massive $M_{\rm add}$ is, the higher the luminosity and temperature of a progenitor are.

On the other hand, the RSG never become a blue star even though $M_{\rm add}$ is 12.0 $M_\odot$ for P14b. The star moves a little bluer, but it starts to rise along the Hayashi line soon. In M14bM9, the star takes 9.153×10^3 yr to reach the peak, and has exploded as a RSG. Comparing P14aM5 with P14bM9 or P14bM12, it is found that the evolutionary paths are quite different although the final state is a RSG.

The results are quite different, according to the structure of the changed star. The structure is determined by the chemical distribution inside a star. Since the difference between P14a and P14b is the region between the surface of the core and the bottom of the convective envelope, it would considerably affect the evolution.

If a binary scenario is considered for the progenitor of SN 1987A, the primary has to be P14b to meet the transition time (see Table 2.1). Since the mass of P14b is 12.01 $M_\odot$, the upper limit of the mass of its companion is less than 12.0 $M_\odot$. However, the progenitor for P14bM12 in which $M_{\rm add}$ is 12.0 $M_\odot$ is a RSG. Therefore, a blue progenitor is not produced in a realistic parameter.

P14a			
Name	$M_{\rm add}$ [$M_\odot$]	$M_{\rm fin}$ [$M_\odot$]	Track
P14aM5	5.0	17.4	R → B → R
P14aM6	6.0	18.4	R → B
P14aM7	7.0	19.5	R → B
P14b			
P14bM9	9.0	20.9	R → R
P14bM12	12.0	23.9	R → R

Table 3.1. The results of the increasing mass model. $M_{\rm fin}$ is the final mass of the progenitor. "Track" means the rough evolutionary track. R and B indicate a state of the RSG and BSG, respectively.

3.2 Helium enhancement

The results of the helium enhanced model are summarized in Fig 3.2. The final states of progenitors are red or blue. In $Y_{\rm He}$, the border between the two colors is located in the range $Y_{\rm He} = 0.6 \sim 0.625$, so the range permitted to the border is very narrow. Therefore, the transition occurs discontinuously. This indicates that thermal equilibrium for the envelope of a yellow or white supergiant (YSG or WSG) is considerably limited.

Time for thermal equilibrium of the envelope in the cases of $Y_{\rm He} = 0.55$ and 0.65 can be seen in Fig 3.3. Variation of the effective temperature ceases at about 2.0×10^4 yr in the both cases. After this, the constant effective temperature phase lasts until the end of this calculation, meaning that equilibrium was achieved. Since the changed star is P16a, a blue star is produced within constraints for the transition time.

There is, however, a problem. $Y_{\rm He} = 0.625$ is not a realistic parameter in a single star. Here, I show it with a rough estimate: I assume that the mass fractions of hydrogen and

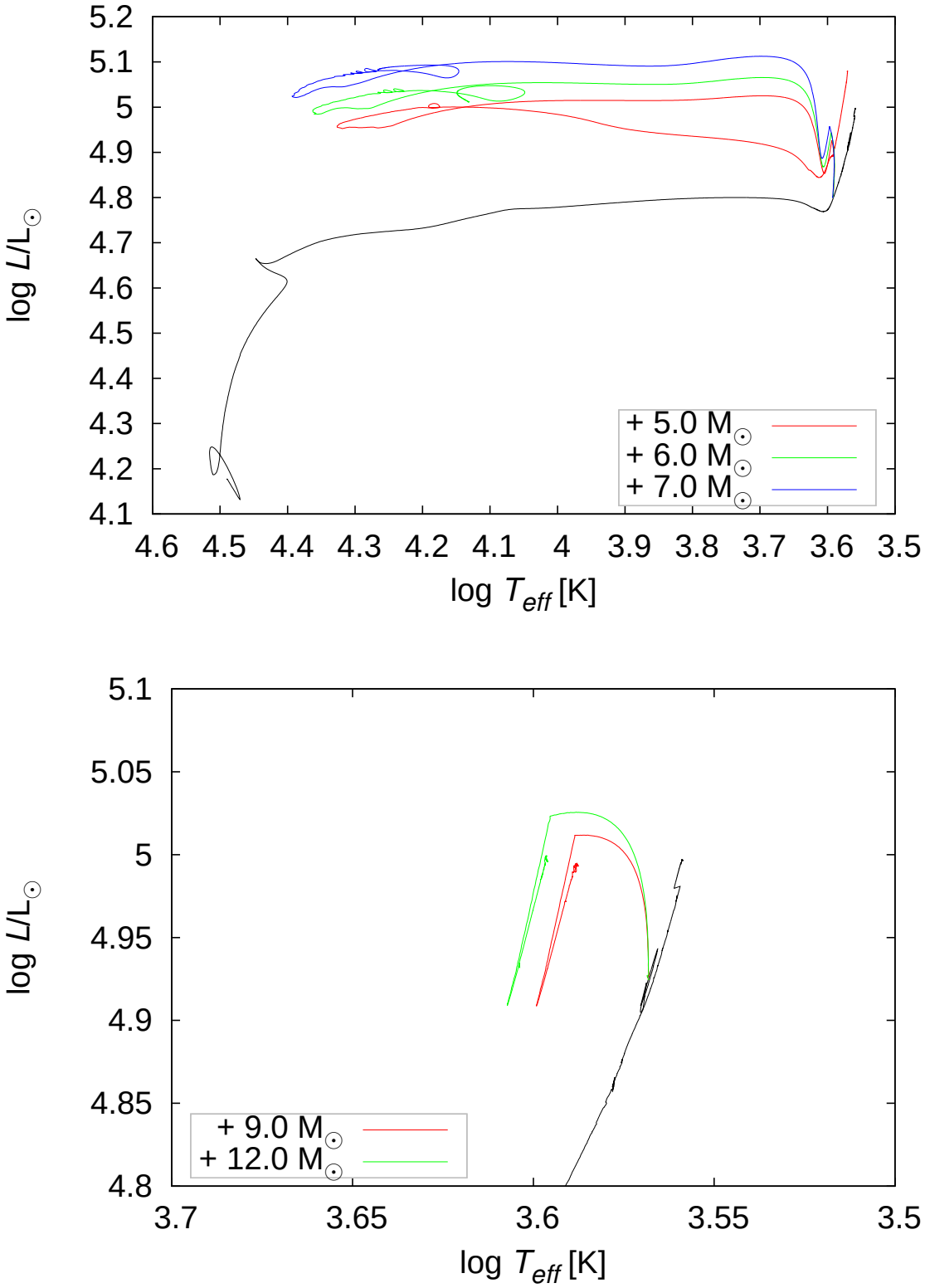

Figure 3.1. The top panel is the evolutionary tracks for the models based on P14a in the increasing mass model. The bottom is same as the top, but for the P14b model. The black line represents the track of P14.

helium are 0.7 and 0.3 for simplicity. Since the total mass of P16a is distinguished into the mass of the core 6.23 $M_\odot$ and of the envelope 6.28 $M_\odot$, the masses of hydrogen and helium ($M_{\rm H}$ and $M_{\rm He}$) are 4.4 $M_\odot$ and 1.88 $M_\odot$. If the helium layer is reduced due to the strong rotation, the reduced mass, $\Delta M_{\rm He}$, is converted to a part of the envelope. According to

$$0.625 = \frac{1.88 + \Delta M_{\rm He}}{6.28 + \Delta M_{\rm He}}, \tag{3.1}$$

$\Delta M_{\rm He}$ is 5.45 $M_\odot$ with the assumption that the compositions are mixed uniformly. Obviously, this amount is more massive than the mass of the helium layer.

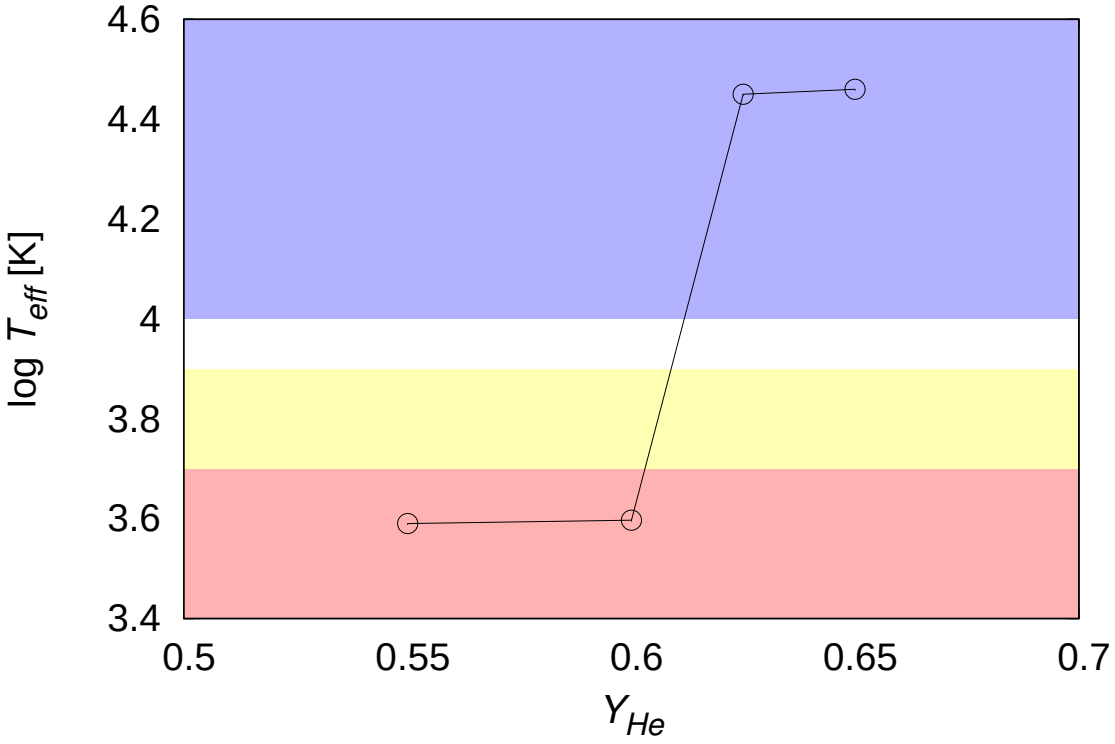

Figure 3.2. The results of the helium enhanced model. The plots represent the stellar colors (effective temperatures) at the end of the calculation against the given helium abundance $Y_{\rm He}$.

3.3 Combination of the two effects

The results of the combination model are plotted in Fig 3.4 in which a part of the results of the helium enhancement model is also shown. The border between the colors is very narrow, as the helium enhanced model. For $Y_{\rm He} = 0.38$ which is in a realistic parameter range, $M_{\rm add}$ has to be larger than 18.32 $M_\odot$ for the transition. If $M_{\rm add}$ is less than 12.0

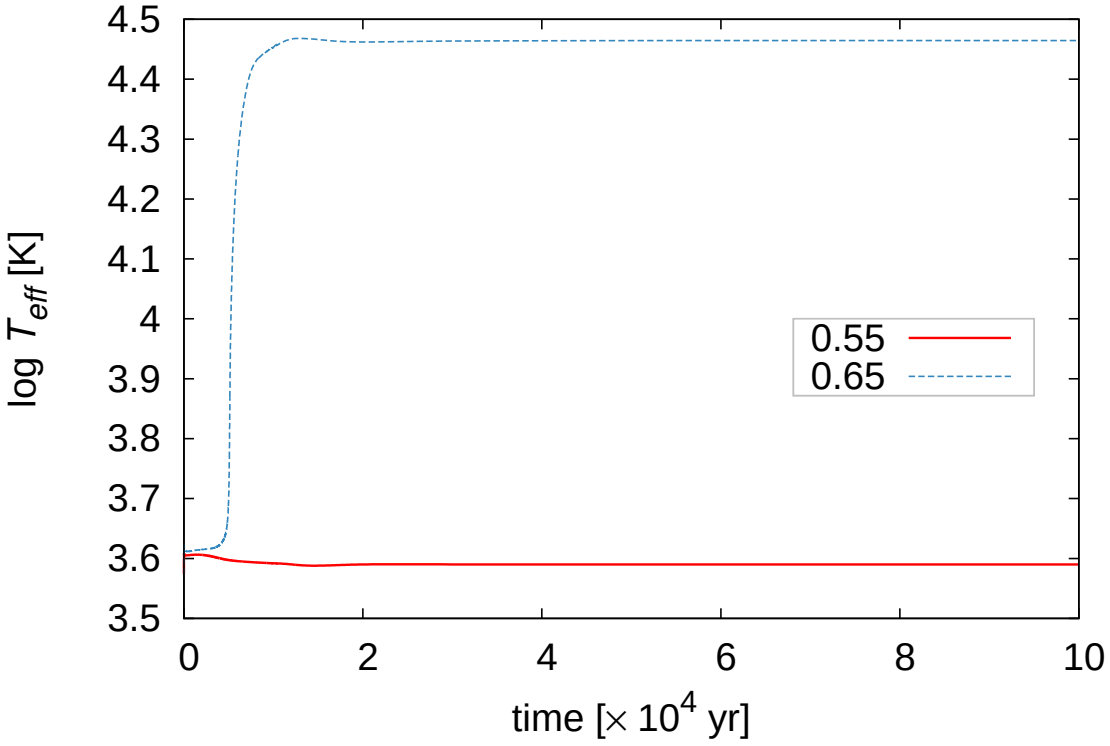

Figure 3.3. Time evolution of log $T_{\rm eff}$ for $Y_{\rm He} = 0.55$ and 0.65.

$M_\odot$, $Y_{\rm He}$ needs to be larger than about 0.5 to become blue. As a tendency, the higher $Y_{\rm He}$ is, the lower $M_{\rm add}$ is for the making the blue.

As with the increasing mass and helium enhanced models, a blue progenitor is not produced within realistic parameters. This can be represented as follows with the similar analysis used in the helium enhancement model: I assume that the mass fractions of hydrogen and helium in the added matter are $X_{\rm comb}$ and $Y_{\rm comb}$. If the matter consists of hydrogen and helium, $Y_{\rm comb} = 1.0 - X_{\rm comb}$. To produce $Y_{\rm He} = 0.5$ for $M_{\rm add}$ =12.0$M_\odot$, according to

$$0.5 = \frac{1.88 + 12.0 \times (1.0 - X_{\rm comb})}{6.28 + 12.0}, \tag{3.2}$$

$X_{\rm comb} = 0.395$ and $Y_{\rm comb} = 0.605$. Therefore, it is difficult to consider that the compositions of the added MS star are such, in reality.

3.4 The slow merger model

All results of the merger model are summarized as tables in Appendix C. In this section, I pick up some models to investigate properties of the evolution.

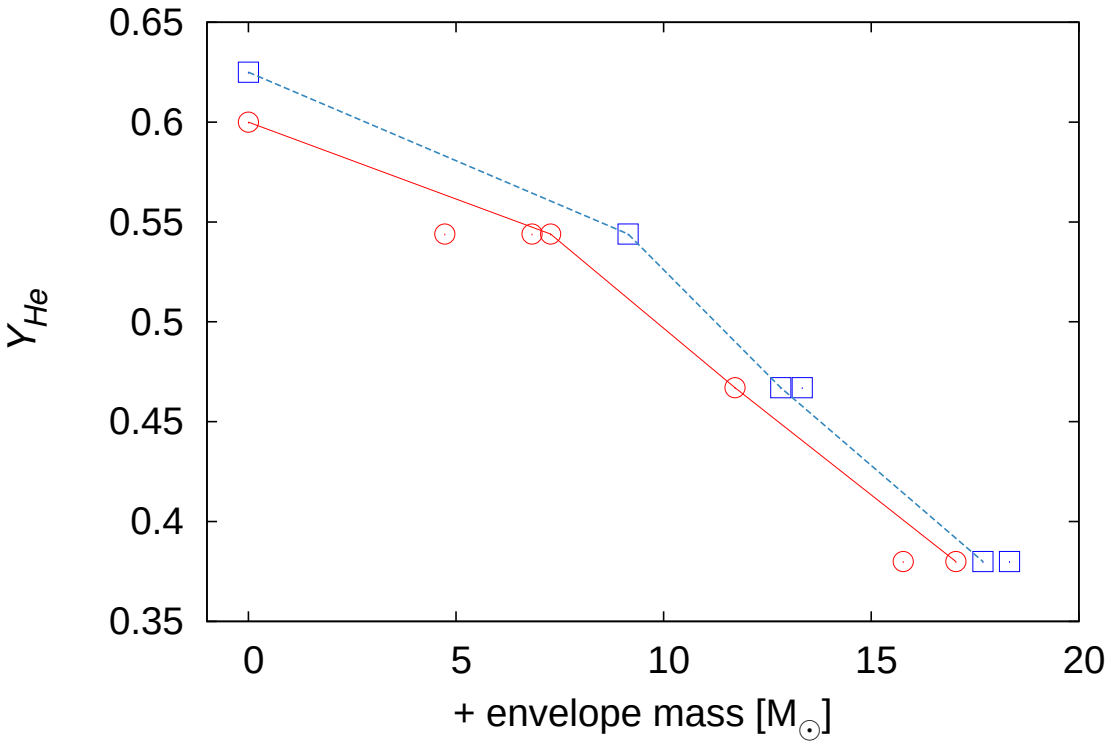

Figure 3.4. The results of the combination model. The colors at the end of the calculation are plotted. The red is a RSG and the blue a BSG.

3.4.1 History of the mass-loss since the begging of the merger

$J_{\rm orb}$ = 1.0, 3.0, 10.0, and 30.0 $\times 10^{53}$ erg sec is adopted for P14b, and history of the mass loss for the difference $J_{\rm orb}$ is investigated. The other common parameters are $\{M_{\rm in}$, M_2, Mixing$\}$ = $\{4.6$ M$_\odot$, 9.0 M$_\odot$, No$\}$.

The top panel in Fig 3.5 represents variation of the total stellar masses in the range from the beginning to the progenitor phase, and the bottom panel focuses on the early phase of the total evolutionary period (until 1.5×10^3 yr). The variation of the mass-loss rate at the initial phase is described in Fig 3.6. As these figures show, the variation of the total mass mainly occurs during the initial phase because the mass-loss rate is significantly enhanced due to injection of $J_{\rm orb}$.

According to the top panel in Fig 3.7, almost no mass loss occurs for $J_{\rm orb} = 1.0 \times 10^{53}$ erg sec before the melting, while about 2.0 M$_\odot$ is ejected for $J_{\rm orb} = 3.0 \times 10^{54}$ erg sec. Since $M_{\rm env}$ for P14b is 7.17 M$_\odot$, about 27 % of the envelope is ejected during the injection. In the middle and bottom panels in Fig 3.7, the mass loss for P15a and P16b at the early phase is plotted with the parameters $\{M_1$, $M_{\rm in}$, Mixing$\}$ = $\{$P15a, 5.2M$_\odot$, Yes$\}$, and

{P16b, 5.96$M_\odot$, Yes}. From this figure, it is found that the most important factor to determine the amount of mass loss is $J_{\rm orb}$.

The rate is a positive value, which means a mass gain, during the melting. In this phase, the mass loss affected by injection of $J_{\rm orb}$ is not involved in the computation, so only the added matter is purely considered for simplicity. Since the parameters $\{M_2, \tau_{\rm melt}\} = \{9.0$ $M_\odot$, $1.0 \times 10^2\}$ are set in Fig 3.5, all the rates become 9.0×10^{-2} $M_\odot$ $\sec^{-1}$.

After the melting is completed, the mass is lost more for higher $J_{\rm orb}$ since the rate of the mass loss becomes higher for higher $J_{\rm orb}$. The stored $J_{\rm orb}$ is extracted with the ejected matter, and the rate returns to the original within 1.0×10^3 yr from the beginning. The phase for the high rate ceases more quickly for larger $J_{\rm orb}$.

Amounts of the ejected matter after the melt for P14b are 0.75 $M_\odot$ for $J_{\rm orb} = 1.0 \times 10^{53}$ erg sec and 3.51 $M_\odot$for $J_{\rm orb} = 3.0 \times 10^{54}$ erg sec. Therefore, the total ejected mass is 0.75 $M_\odot$ – 5.3 $M_\odot$ (see Table 3.2 in which the primary is P14b). In the cases of the models for P15a and P16b, the amount is almost same for same $J_{\rm orb}$.

Total ejected mass in the models based on P14b	
$J_{\rm orb}$	$M_{\rm ejecta}$
[$\times 10^{53}$erg sec]	[$M_\odot$]
1.0	0.75
3.0	1.98
10.0	4.17
30.0	5.32

Table 3.2. Total ejected mass, $M_{\rm ejecta}$, for $J_{\rm orb}$ until just before core-collapse from the beginning of a common envelope phase. The primary is P14b with the other parameters $\{M_{\rm in}$, M_2, Mixing$\}$ = {4.6 $M_\odot$, 9.0 $M_\odot$, No}.

3.4.2 The chemical anomalies at the surface

He/H, N/C, and N/O at the surface in all of the merger models are plotted against the final effective temperature in Fig 3.8 – 3.13. In these figures, the blue cover represents the observational constraints from Lundqvist & Fransson (1996), the yellow these from Mattila *et al.* (2010), and the green the common region showed by the both researches.

Fig 3.8, 3.10, and 3.12 are the ratios based on P14b, P15a, and P16b with no-mixing. For the models based on P14b in the no-mixing case, He/H is 0.1 – 0.12 and N/O is 0.65 – 0.8 in blue progenitors. The values are near the lower limits. Obviously, N/C is, however, lower than the lower limit of the observation. Although there are some models in which all the ratios are enhanced for red progenitors, the ratios are almost the same as the surface of the primary. As seen Fig 3.10 and 3.12, tendencies for the ratios are the

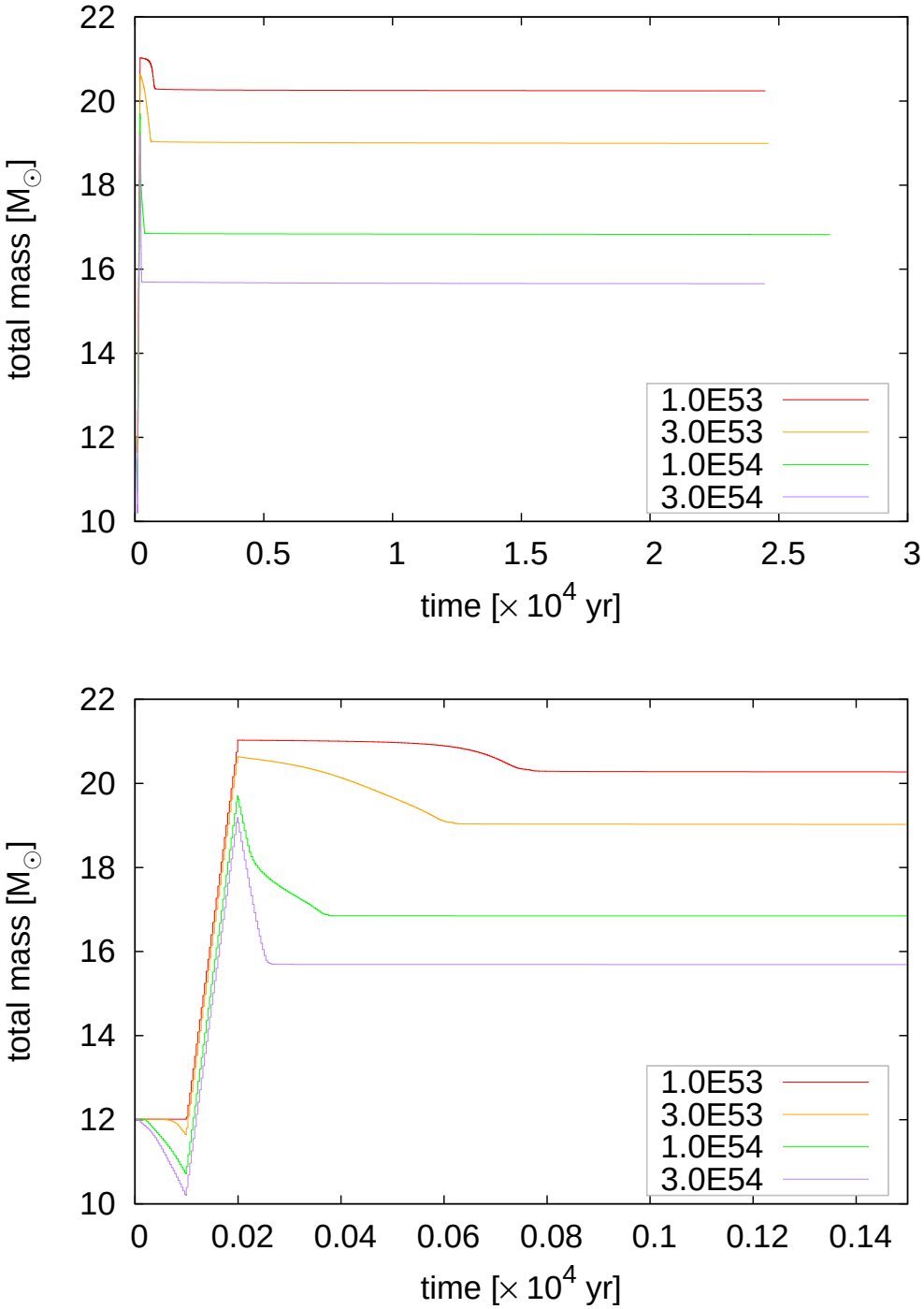

Figure 3.5. History of the mass loss in the merger model. 1.0E53, 3.0E53, 1.0E54, and 3.0E54 represent $J_{orb} = 1.0 \times 10^{53}$, 3.0×10^{53}, 1.0×10^{54}, and 3.0×10^{54} erg sec, respectively. The common parameters are $\{M_{\rm in}$, M_2, Mixing$\}$ = {4.6 $M_\odot$, 9.0 $M_\odot$, No}. The top pane is the history until just before core-collapse. The bottom is same as the top, but until 1.5×10^3 yr.

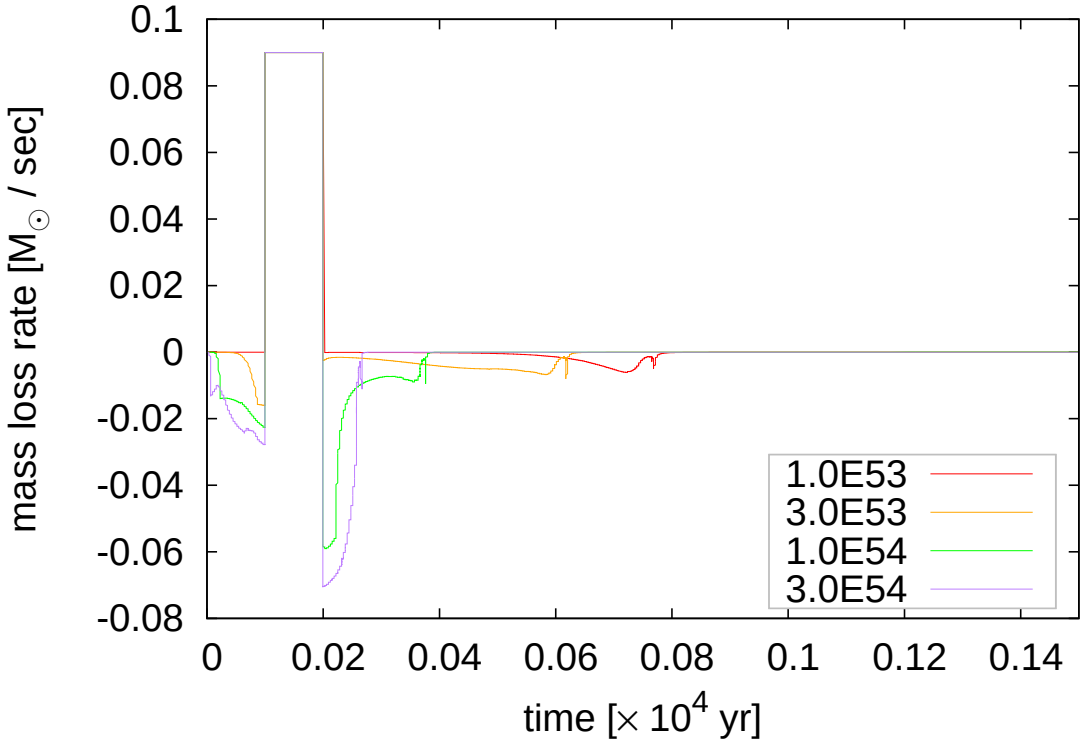

Figure 3.6. History of a rate of the mass loss from the beginning of a common envelope phase to 1.5×10^3 yr. The positive represents a mass gain and the negative does a mass loss. 1.0E53, 3.0E53, 1.0E54, and 3.0E54 represent $J_{orb} = 1.0 \times 10^{53}$, 3.0×10^{53}, 1.0×10^{54}, and 3.0×10^{54} erg sec, respectively. The common parameters are $\{M_{\rm in}$, M_2, Mixing$\}$ = {4.6 M$_\odot$, 9.0 M$_\odot$, No}.

same. Since the initial velocity of P16 is about 1.6 times as fast as those of P14 and P15, the rotational mixing works more. As a result, He/H and N/O in the models for P16b match the constraints.

On the other hand, all the ratios in blue are within the observations for the models with the mixing (see Fig 3.9, 3.11, and 3.13). As same as the no-mixing models, there are some models in which N/C is enhanced in red progenitors. Since the heaver elements are dredged up due to the large scale mixing, the ratios become high relative to the no-mixing cases.

3.4.3 The best model for the progenitor of SN 1987A

Parameters of the model which are in best agreement with the observations are $\{M_1$, $J_{\rm orb}$, $M_{\rm in}$, M_2, Mixing$\}$ = {P14b, 3.0×10^{53} erg sec, 4.6 M$_\odot$, 7.7M$_\odot$, Yes}. Its HRD is described in Fig 3.14 and time variations of log $T_{\rm eff}$, log L/L$_\odot$, log R/R$_\odot$, J, and $M_{\rm tot}$

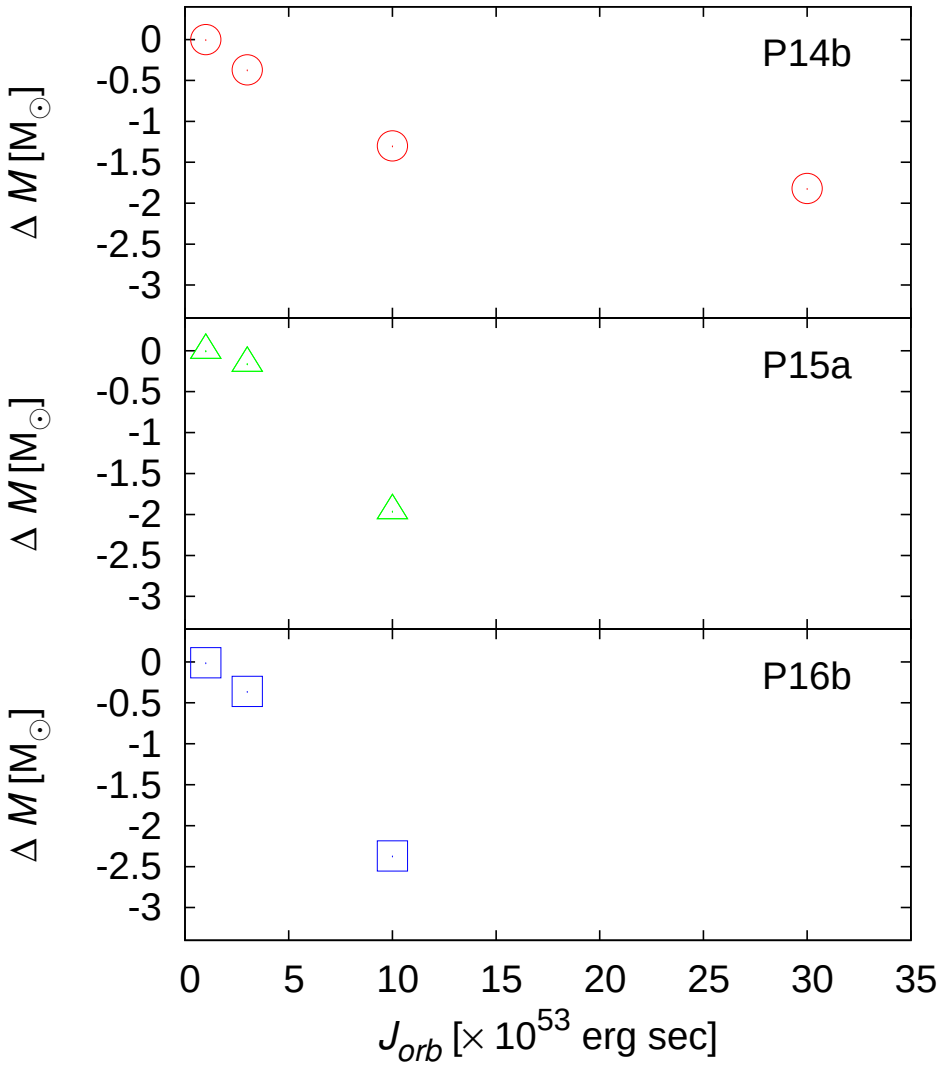

Figure 3.7. Ejected mass during injection of $J_{\rm orb}$ with the parameters $\{M_1, M_{\rm in}, \text{Mixing}\}$ = {P14b, 4.6 $M_\odot$, Yes}, {P15a, 5.2 $M_\odot$, Yes}, and {P16b, 5.96 $M_\odot$, Yes}.

since the beginning of the common envelope phase are plotted in Fig 3.15.

During injection of $J_{\rm orb}$, the star moves right direction in the HRD. This motion has lasted until the end of the injection. 0.37 $M_\odot$ of the envelope is ejected. Next, the system enters into the melting phase. The luminosity and temperature starts to rise during this phase in which the energy source is the gravitational contraction of the radiative region just under the bottom of the convective one. However, since the convective region expands, the stellar radius becomes larger. The surface states are log $L/L_\odot$ = 5.256 and log $T_{\rm eff}$ = 3.567 at the end of the melting phase. While the star is expanding, the luminosity has achieved its peak (log $L/L_\odot$ = 5.358) for 2.54×10^2 yr from the common envelope phase.

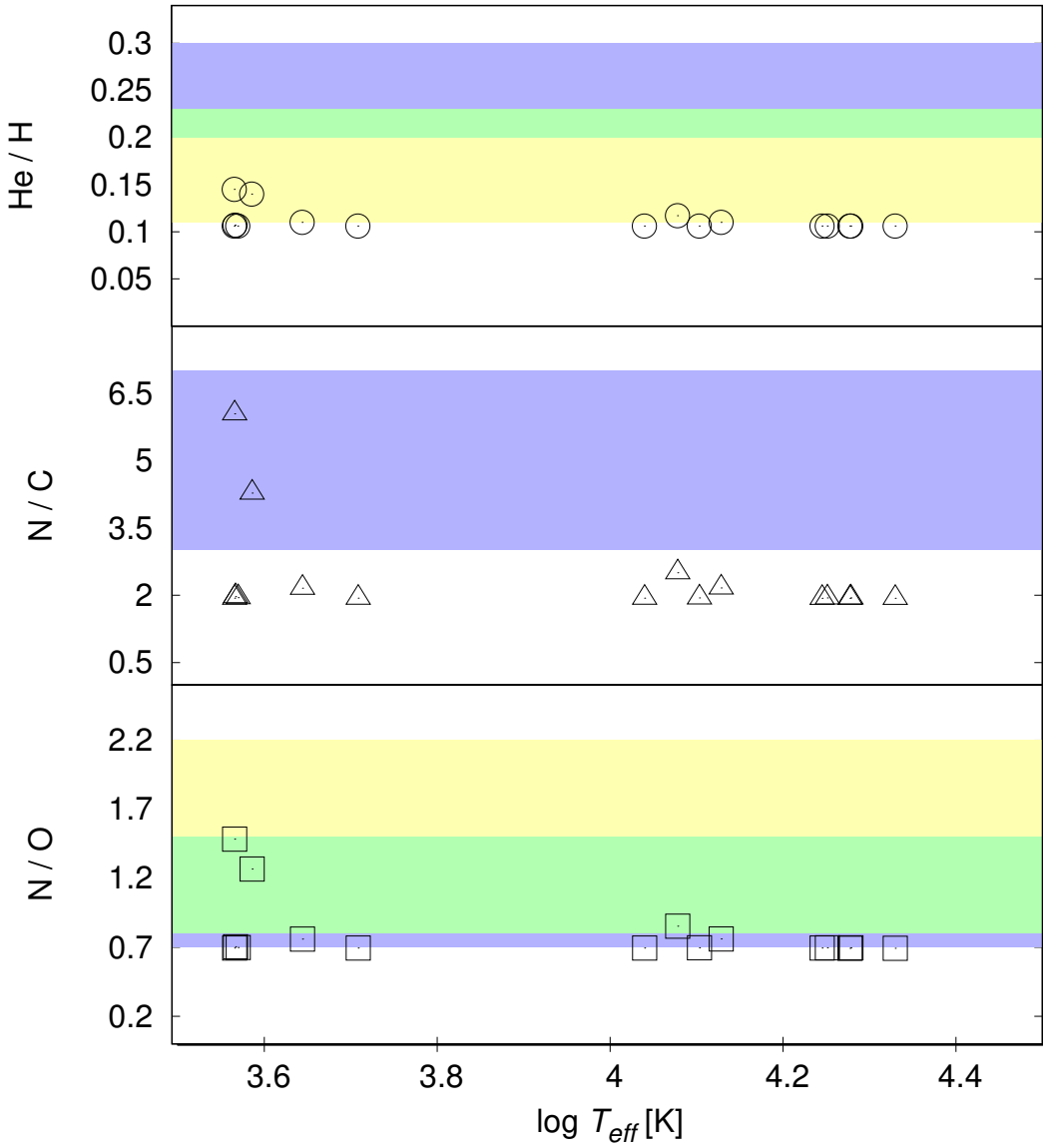

Figure 3.8. The chemical abundances in the models with the no-mixing based on P14b.

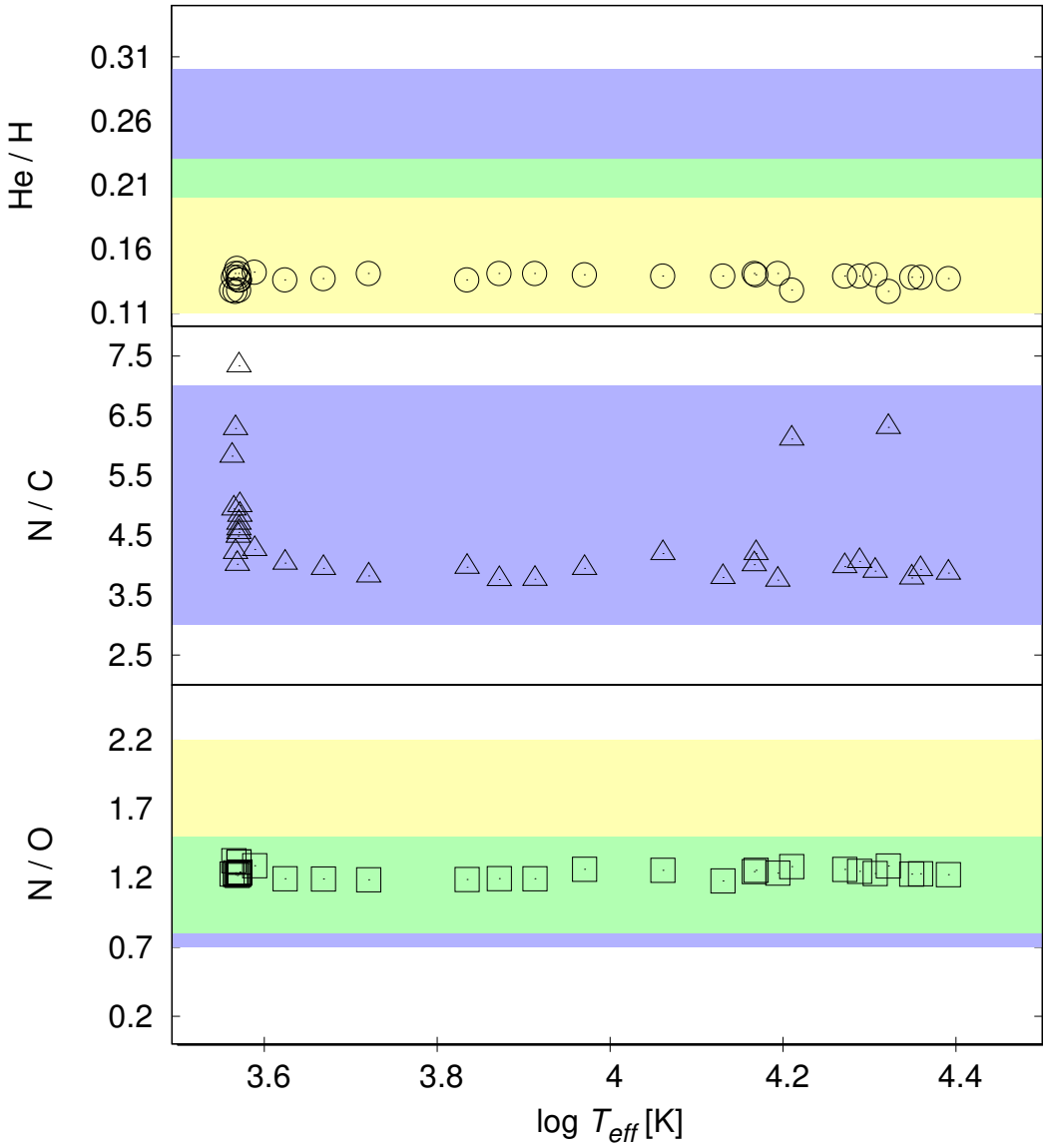

Figure 3.9. Same as 3.8, but with the mixing.

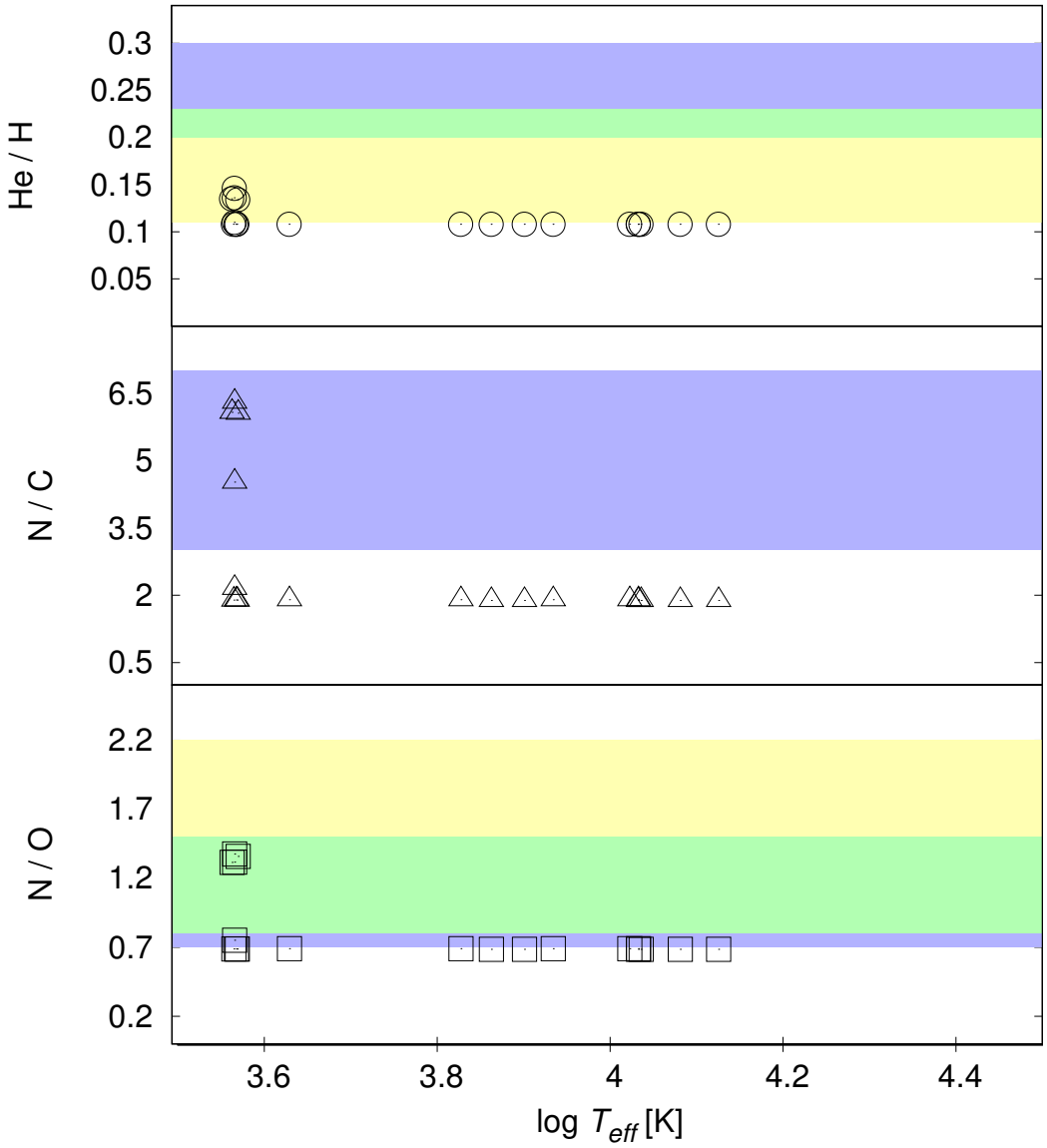

Figure 3.10. Same as 3.8, but based on P15a.

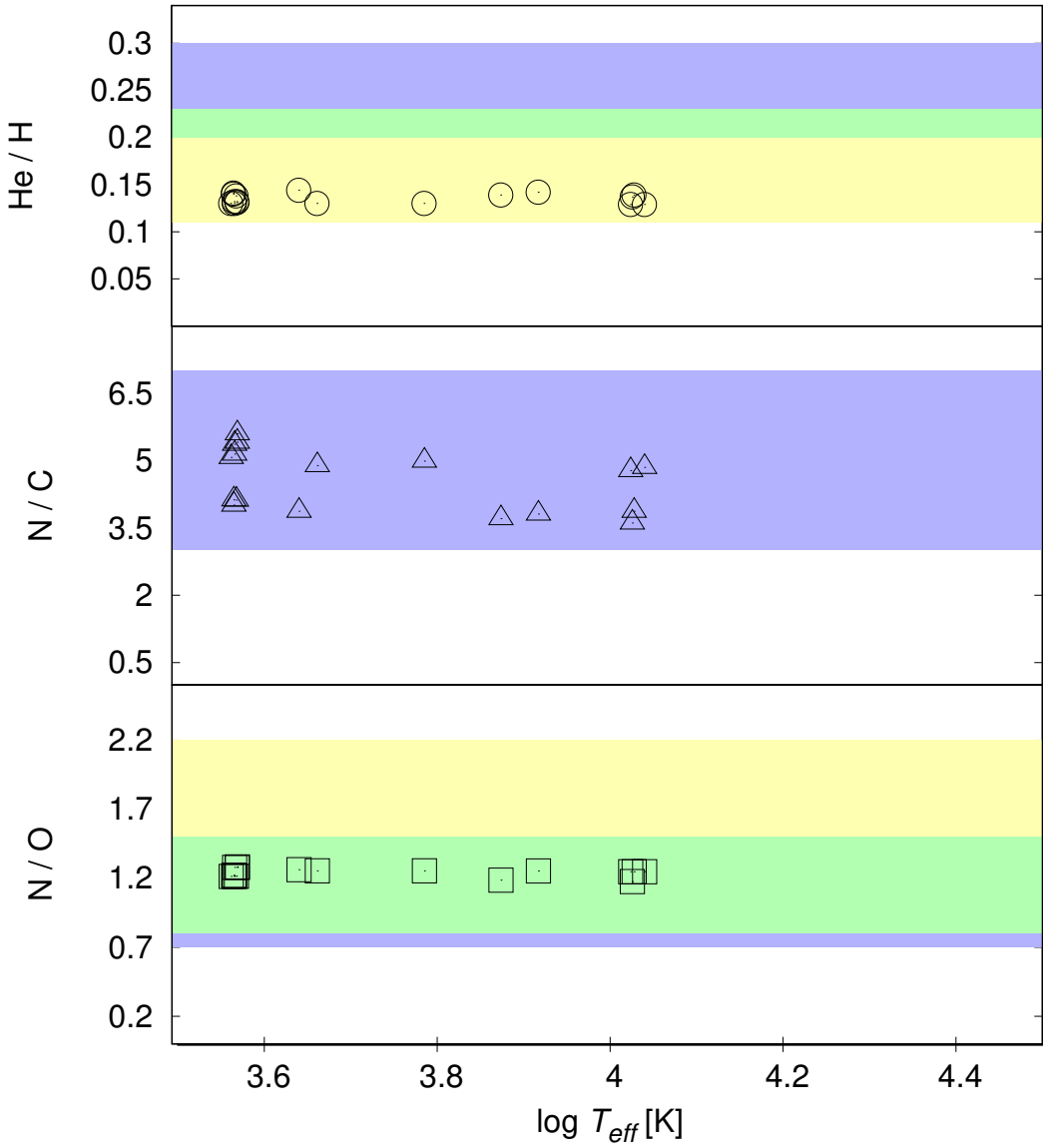

Figure 3.11. Same as 3.10, but with the mixing.

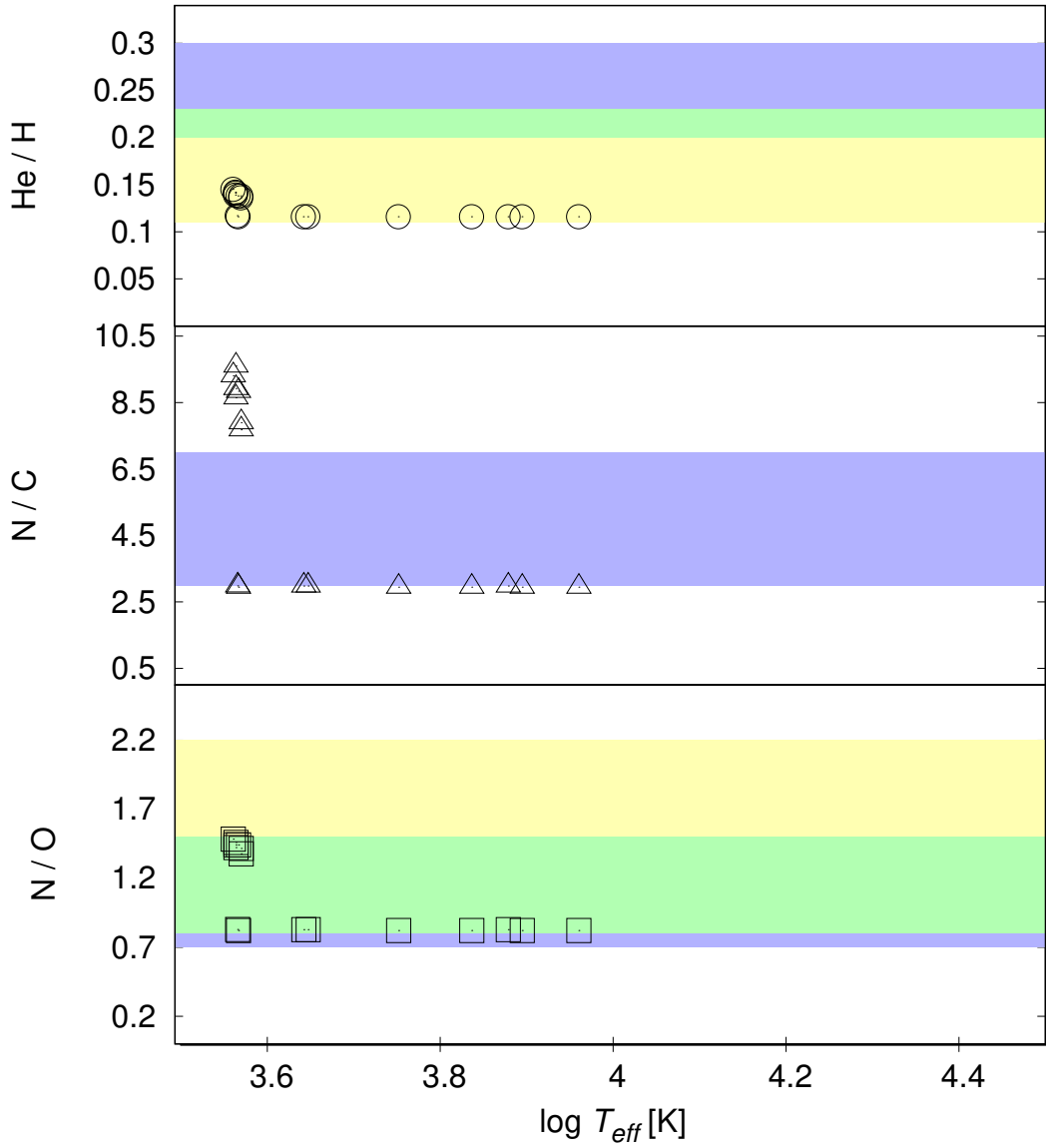

Figure 3.12. Same as 3.8, but based on P16b.

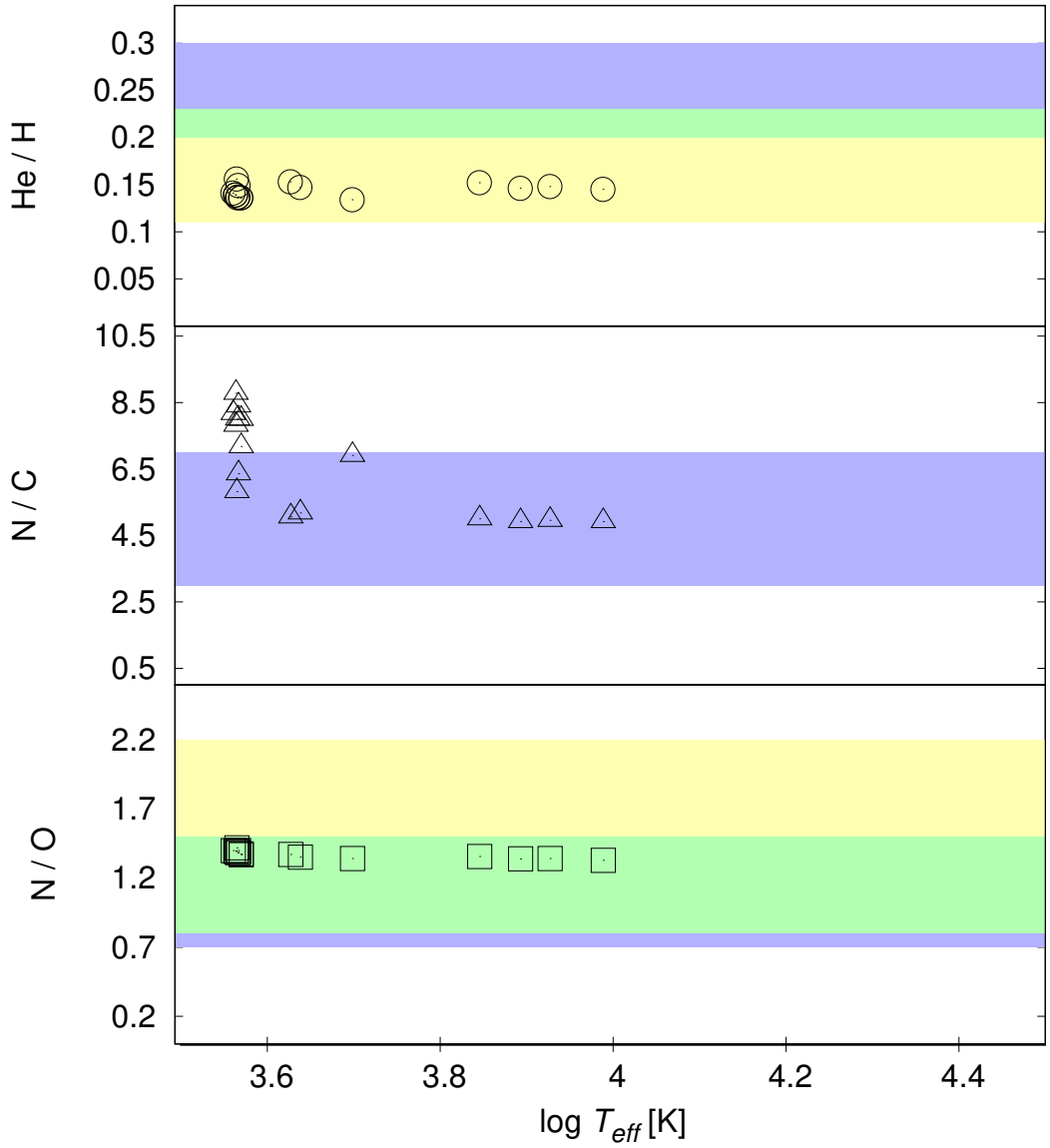

Figure 3.13. Same as 3.12, but with the mixing.

After the peak, the star moves in the lower-left direction in the HRD while the convective envelope is changing to a radiative one. Due to the injection of $J_{\rm orb}$, the mass loss is enhanced a lot and the rate is about -10^{-3} $M_\odot$ sec^{-1} then. The ejected mass eventually reaches about 2.0 $M_\odot$ in total for about 5.0×10^2 yr from the beginning. In addition, most of $J_{\rm orb}$ are excluded accompanied with the ejecta. The star takes 6.07×10^2 yr since the beginning to enter the first blue phase ($\log T_{\rm eff} > 4.0$) in which the envelope has changed to the radiative completely. At this time, the stellar radius is 1.235×10^2 $R_\odot$, which is yet a bit larger than the observational constraint. The star has continued to shrink and to increase in temperature since the first blue phase. When 1.802×10^4 yr passes, the temperature has reached its peak ($\log T_{\rm eff} = 4.293$) in which the radius is 25.0 $R_\odot$. In the next sequence, the star starts to expand because the carbon burning is established in the central region although the energy source is helium shell burning, moving that the star in the right direction on the HRD. This motion ceases when ν-cooling dominates over energy generation. After the carbon burning, time-scale of nucleosynthesis is much shorter than the Kelvin-Helmholtz one. Therefore, the star enters the pre-core-collapse phase with little change since the carbon burning in the HRD. The internal change cannot affect stellar surface due to the difference in time-scales. In the best model, the progenitor stays in the observational region of the HRD and the stellar radius is 38.0 $R_\odot$ at its end.

The profiles of abundances, pressure, density, temperature, angular velocity of the progenitor are described in Fig 3.16, 3.17, 3.18, 3.19, and 3.20, respectively. Properties in the final phase are summarized in Table 3.3. As seen in the table, the best model explains all the observational constraints quantitatively.

Properties in the final phase in the best model							
$M_{\rm fin}$ [$M_\odot$]	$M_{\rm core}$ [$M_\odot$]	$M_{\rm env}$ [$M_\odot$]	$\log T_{\rm eff}$ [K]	$\log L/L_\odot$	He/H	N/C	N/O
17.45	4.24	13.21	4.196	4.903	0.141	3.789	1.237
The constraints							
		10.0±5.0^{*1}	4.22±0.04^{*2}	5.09±0.19^{*2}	0.17±0.06^{*3}	5.0±2.0^{*4}	1.5±0.7^{*3}

Table 3.3. The top: states of the progenitor in the best model. The bottom: the observational constraints. ∗1 refers to Woosley *et al.* (1997), ∗2 Arnett *et al.* (1989), ∗3 Lundqvist & Fransson (1996), and ∗4 Mattila *et al.* (2010), respectively.

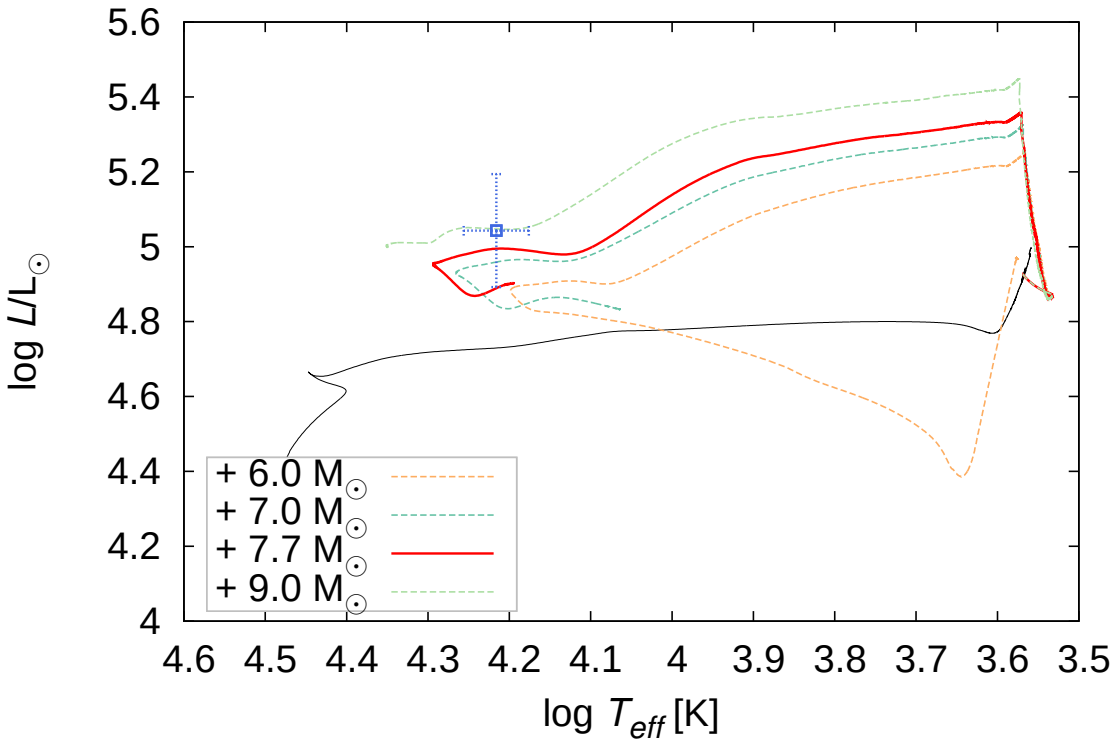

Figure 3.14. The evolutionary tracks of the models based on P14b. The common parameters are $\{M_1, J_{\rm orb}, M_{\rm in}, \text{Mixing}\} = \{\text{P14b}, 3.0\times10^{53}$ erg sec, 4.6 $\mathrm{M}_\odot$, Yes$\}$. The values of M_2 are 6.0 $\mathrm{M}_\odot$, 7.0 $\mathrm{M}_\odot$, 7.7 $\mathrm{M}_\odot$, and 9.0 $\mathrm{M}_\odot$. M_2 in the best model is 7.7 $\mathrm{M}_\odot$. The cross lines represent the observational constraints in the final phase.

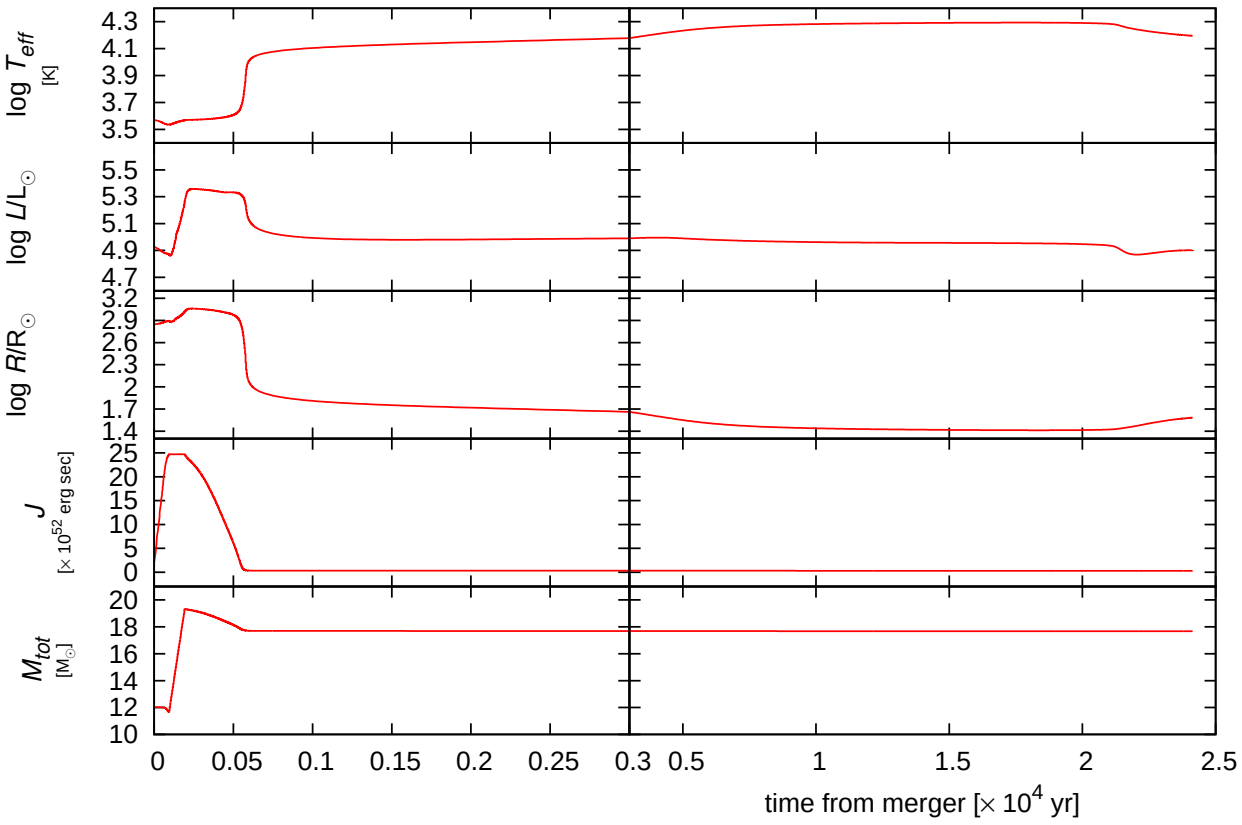

Figure 3.15. Time evolutions of log $T_{\rm eff}$, log $L/{\rm L}_\odot$, log $R/{\rm R}_\odot$, J, and $M_{\rm tot}$ from the beginning of a common envelope phase to the final phase in the best model whose parameters $\{M_1,\, J_{\rm orb},\, M_{\rm in},\, M_2,\, \text{Mixing}\} = \{\text{P14b},\, 3.0\times10^{53}$ erg sec, 4.6 M$_\odot$, 7.7M$_\odot$, Yes$\}$.

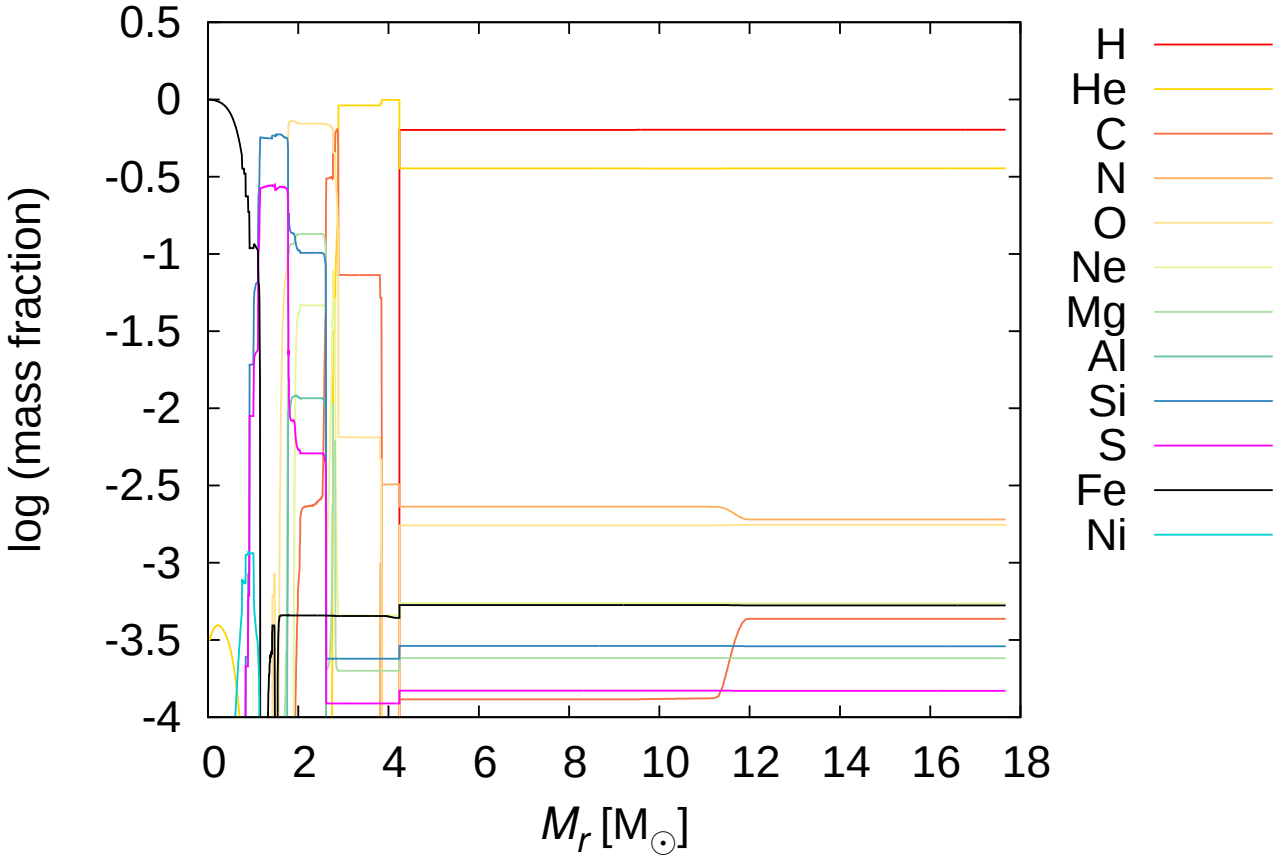

Figure 3.16. Chemical profiles in the final phase in the best model. Here, 12 isotopes are described although 49 isotopes are involved in the model (see Table A.1).

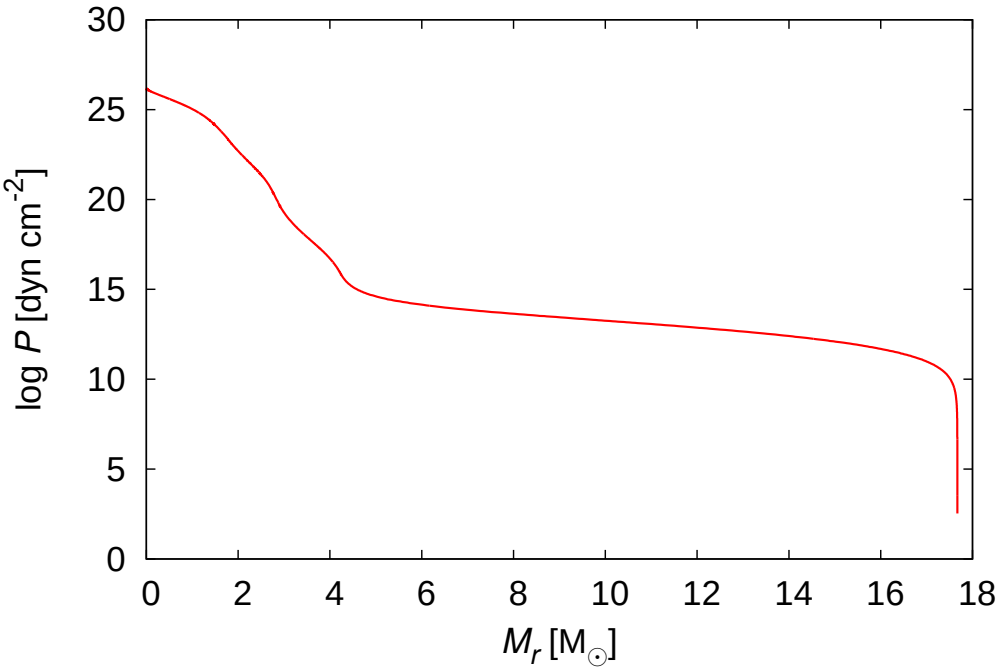

Figure 3.17. Pressure distribution in the final phase in the best model.

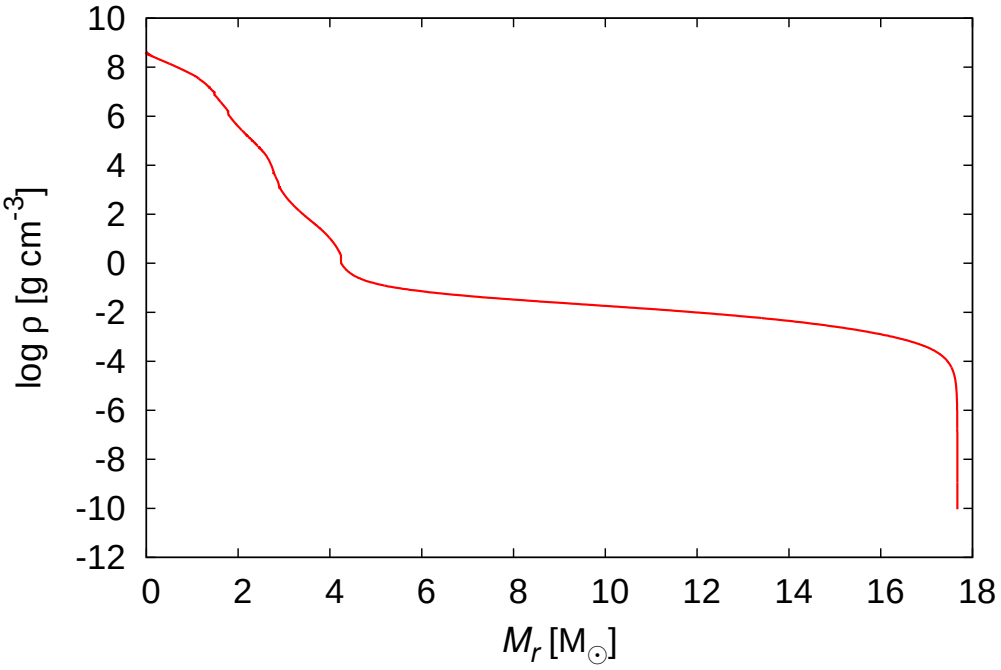

Figure 3.18. Density distribution in the final phase in the best model.

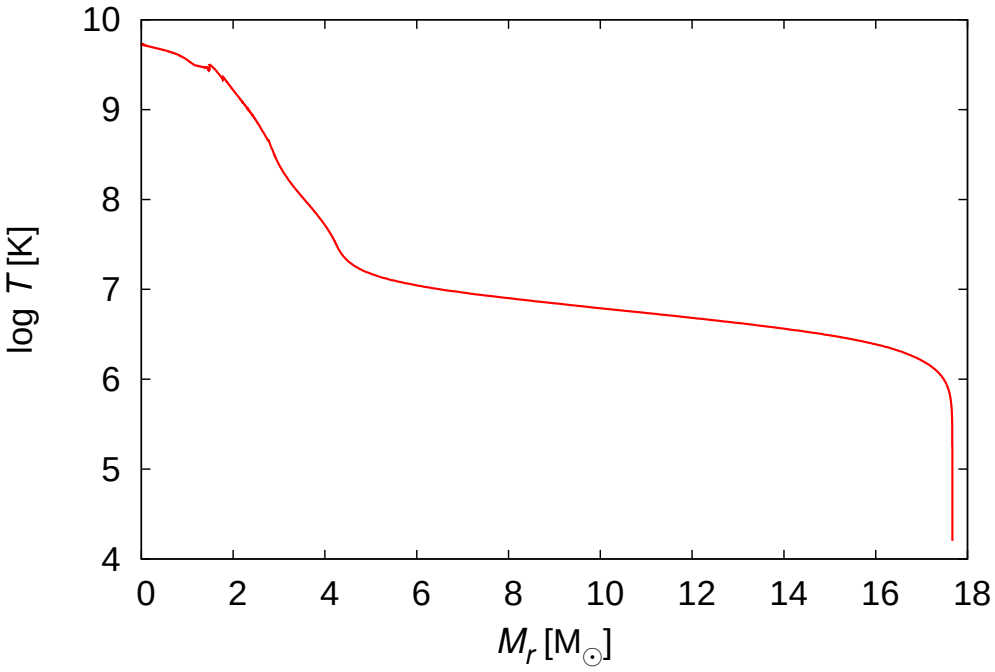

Figure 3.19. Temperature distribution in the final phase in the best model.

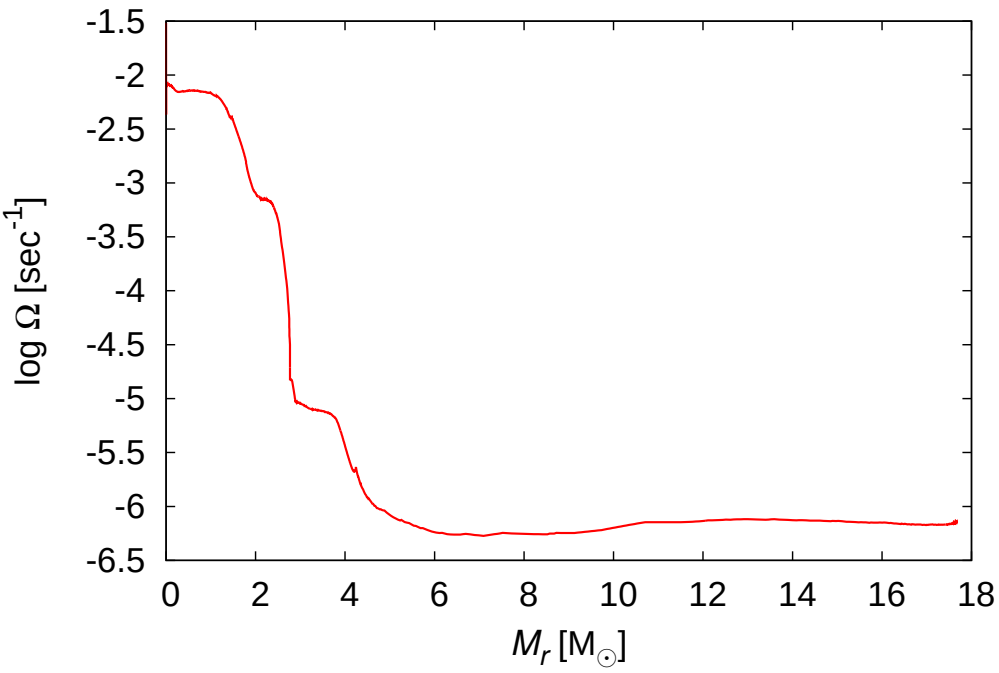

Figure 3.20. Angular velocity distribution in the final phase in the best model.

Chapter 4

Discussion

4.1 Parameter dependence on the surface's color

There are eight parameters, of which four are varied, in my merger model. In this section, one of the parameters $\{M_1, J_{\rm orb}, M_{\rm in}, \text{Mixing}\}$ and M_2 are varied to discuss the effects of each parameter on the surface's color.

4.1.1 Orbital angular momentum: $J_{\rm orb}$

Here, the varied parameter is $J_{\rm orb}$. The final temperature (color) of a progenitor is plotted with the common parameters $\{M_1, M_{\rm in}, \text{Mixing}\}$ = {P14b, 4.6 $M_\odot$, No} in the top panel of Fig 4.1 and with $\{M_1, M_{\rm in}, \text{Mixing}\}$ = {P16b, 5.96 $M_\odot$, No} in the bottom panel.

As shown in the top panel, the primary can become a blue progenitor for M_2 = 6.0 $M_\odot$ or more although there are only red progenitors for M_2 =5.0 $M_\odot$and less. Looking at $J_{\rm orb} = 1.0 \times 10^{53}$, 3.0×10^{53}, and 1.0×10^{54} erg sec, it is found that a blue progenitor is produced for more massive M_2. For M_2 = 9.0 $M_\odot$, only the star for $J_{\rm orb} = 3.0 \times 10^{54}$ erg sec becomes a red progenitor. Therefore, the stellar mass after the mass loss is important factor for understanding the red to blue evolution.

In the bottom panel, there are no blue progenitors even if M_2 = 10.0 $M_\odot$ is added. For M_2 = 10.0 $M_\odot$ and $J_{\rm orb} = 1.0 \times 10^{53}$ erg sec, the mass of the progenitor is 21.6 $M_\odot$. If a similar mass could have been produced in the model based on P14b, the star becomes a blue progenitor. As seen in 2.1, since the main difference between P14b and P16b is the mass of the core, q for the P16b case is larger that that for the P14b for the same total mass case. This indicates that a smaller q seems to be a better indicator for the red to blue evolution than the total mass. Because $J_{\rm orb}$ is enable to significantly affect q, its value is important to determine the color.

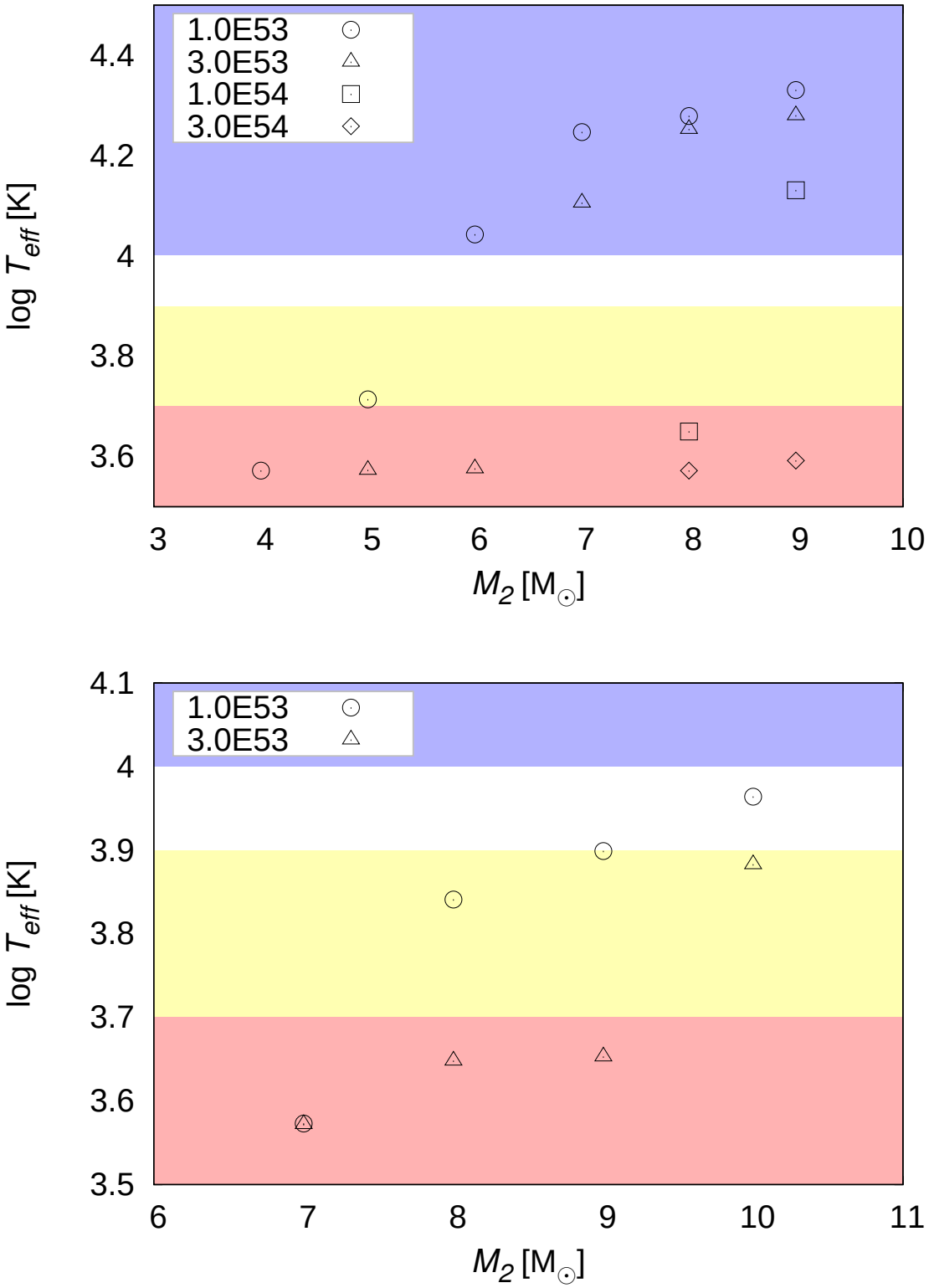

Figure 4.1. The top panel shows results for different values of $J_{\rm orb}$ with varying M_2. The circle represents $J_{\rm orb} = 1.0 \times 10^{53}$ erg sec, the triangle 3.0×10^{53} erg sec, the square 1.0×10^{54} erg sec, and the diamond 3.0×10^{54} erg sec, respectively. The common parameters are $\{M_1,\ M_{\rm in},\ \text{Mixing}\} = \{\text{P14b, 4.6 M}_\odot, \text{No}\}$. The bottom is same as the top, but with the common parameters $\{M_1,\ M_{\rm in},\ \text{Mixing}\} = \{\text{P16b, 5.96 M}_\odot, \text{No}\}$.

4.1.2 Large scale mixing

Here, the varied parameter is whether large scale mixing occurs or not. The temperature of a progenitor for this case is plotted in Fig 4.2 in which the common parameters are $\{M_1, M_{\rm in}, J_{\rm orb}\} = \{$P14b, 4.6 $M_\odot$, 3.0×10^{53} erg sec$\}$.

For same values of M_2 which is 7.0 $M_\odot$ or more, it is found that progenitors are BSGs and their temperatures are almost the same whether large scale mixing is included or not. On the other hand, the star becomes a YSG for M_2 = 6.1 $M_\odot$ and a WSG for M_2 = 6.2 $M_\odot$ in the mixing case. Their evolutionary tracks are that the stars return to be RSGs after they have become BSGs, but they enters progenitor phases before they have returned to their original colors. The track is very sensitive to M_2 as seen in the helium and combination models in these colors. Since number of calculations for M_2 = 6.0 $M_\odot$ – 7.0 $M_\odot$ for the no-mixing case is insufficient, I cannot conclude the effect on the evolution completely. However, I think that the presence/absence would not significantly affect the evolution from the results in which M_2 is 7.0 $M_\odot$ or more.

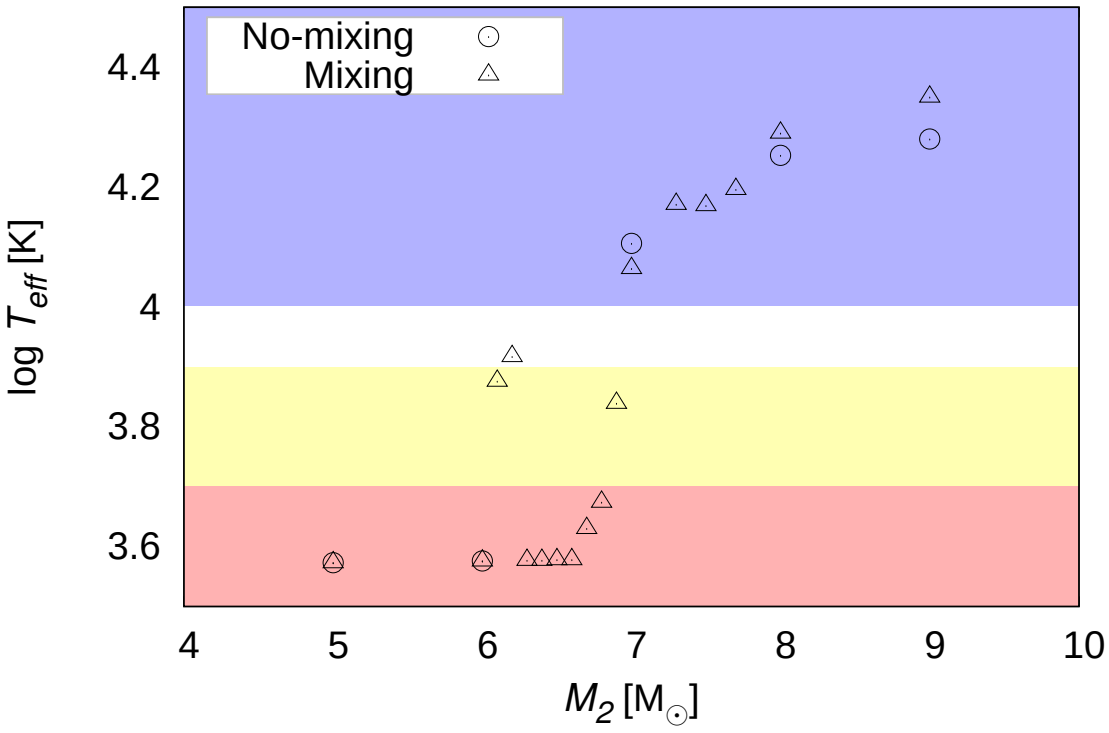

Figure 4.2. Results for mixing and no-mixing cases. The circle is for the no-mixing case and the triangle for the mixing. The common parameters are $\{M_1, M_{\rm in}, J_{\rm orb}\} = \{$P14b, 4.6 $M_\odot$, 3.0×10^{53} erg sec$\}$.

4.1.3 Degree of erosion: $M_{\rm in}$

The final varied parameter is $M_{\rm in}$. The temperature of a progenitor is plotted in the top panel of Fig 4.3 with the common parameters $\{M_1,\ J_{\rm orb},\ \text{Mixing}\} = \{\text{P14b},\ 3.0 \times 10^{53}$ erg sec, No$\}$ and in the bottom panel with $\{M_1,\ J_{\rm orb},\ \text{Mixing}\} = \{\text{P16b},\ 3.0 \times 10^{53}$ erg sec, No$\}$.

As seen in the top panel, $M_{\rm in}$ seems not to affect the evolution. Since the difference between $M_{\rm in} = 4.6$ M$_\odot$ and 4.8 M$_\odot$ is 0.2 M$_\odot$ and $J_{\rm orb}$ is the same, q and the total mass are almost the same. Therefore, there is little difference with respect to the physical structure, meaning no effect on the evolution.

In the bottom panel, since the difference between $M_{\rm in} = 5.96$ M$_\odot$ and 6.21 M$_\odot$ is 0.15 M$_\odot$, the physical structures are also little changes, leading to the same conclusion mentioned above.

4.1.4 The most important factor for making a BSG from a RSG in the merger model

In Sec 4.1.1, 4.1.2, and 4.1.3, I investigated the parameter dependence and obtained that the smallness of q would be more important than the total mass for the color. Concerning the mass relation (the mass ratio q and the total mass), I assess which is the most important factor with all of the merger models quantitatively as follows.

Fig 4.4 shows the final effective temperature against the total mass. There are few blue progenitors in the region of less than about 17.0 M$_\odot$. If $M_{\rm fin}$ is larger than this value, many blue progenitors are produced. What is important, however, is that there are a lot of red progenitors in the same region. As seen in this figure, there is obviously no correlation between the color and $M_{\rm fin}$. On the other hand, Fig 4.5 shows the final temperature against the mass ratio q. It is found that there is a clear negative correlation. If q is less than about 0.27, a RSG with a CO core becomes a BSG in the final state. Therefore, the most important factor is q. Since q is significantly affected by a value of $J_{\rm orb}$, it is also important.

Note that the effect of helium enhancement in the envelope is not confirmed from Sec 3.4.2 although it has been expected that the abundance is important in the helium and combination models.

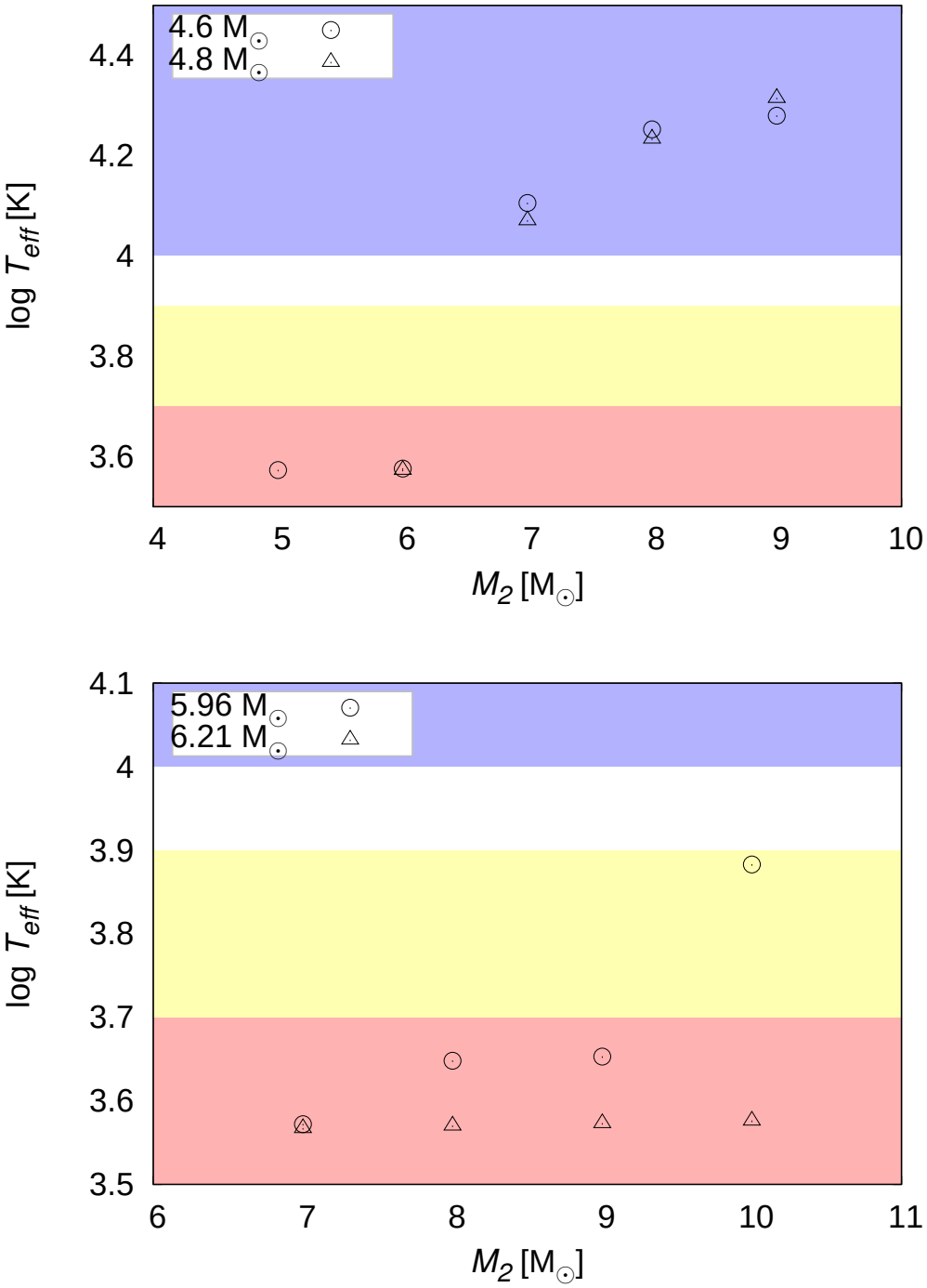

Figure 4.3. The top panel represents result for different values of $M_{\rm in}$ with varying M_2. The common parameters are $\{M_1,\ J_{\rm orb},\ \text{Mixing}\} = \{\text{P14b},\ 3.0 \times 10^{53}\ \text{erg sec},\ \text{No}\}$. The circle represents results with $M_{\rm in} = 4.6\ \mathrm{M}_\odot$, and the triangle with $M_{\rm in} = 4.8\ \mathrm{M}_\odot$. The bottom is same as the top, but with the common parameters $\{M_1,\ J_{\rm orb},\ \text{Mixing}\} = \{\text{P16b},\ 3.0 \times 10^{53}\ \text{erg sec},\ \text{No}\}$. The circle represents results with $M_{\rm in} = 5.96\ \mathrm{M}_\odot$, the triangle with $M_{\rm in} = 6.21\ \mathrm{M}_\odot$.

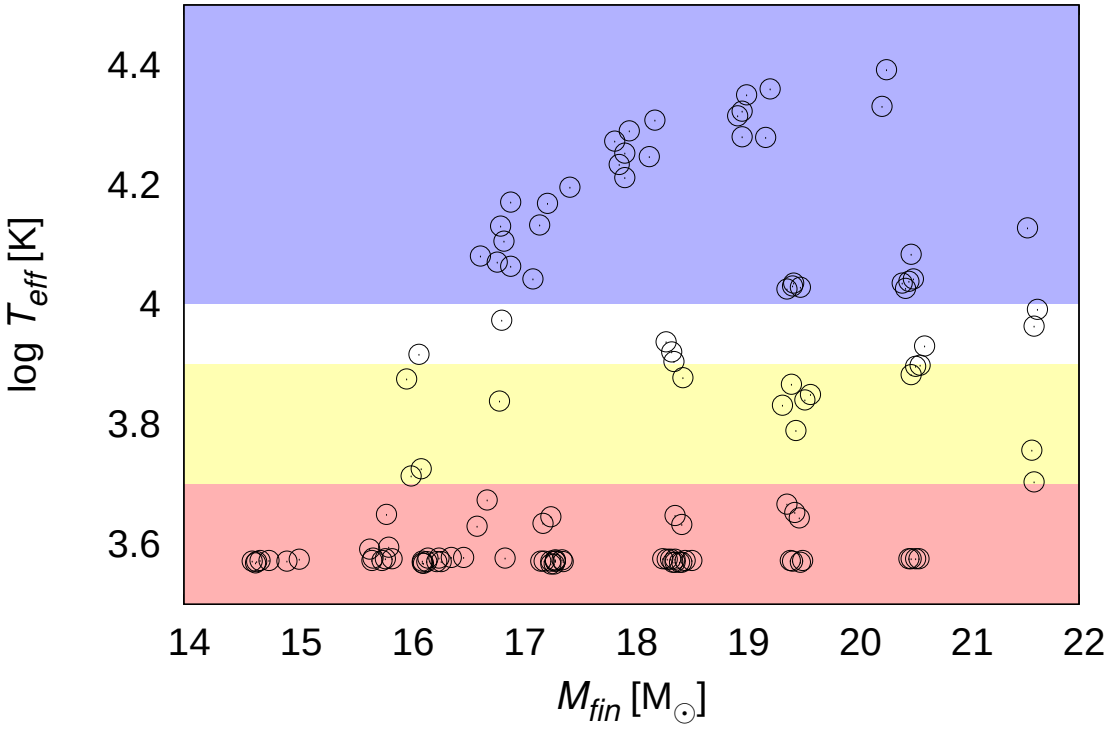

Figure 4.4. The final effective temperature against $M_{\rm fin}$ in all models.

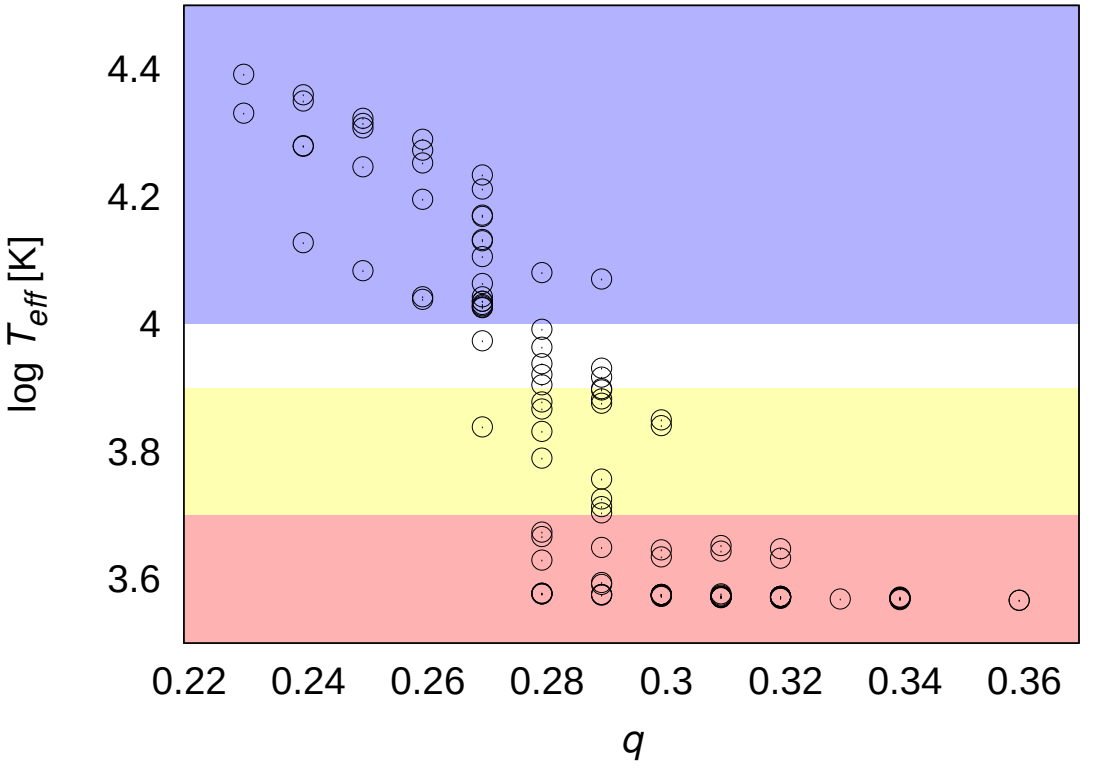

Figure 4.5. The final effective temperature against q in all models.

4.2 Importances of the physical quantities of the primary and secondary for the red to blue evolution

In the increasing mass model, P14b never moves to the blue phase even if q decreases due to the increasing mass of the envelope. On the other hand, P14a becomes a blue progenitor easily if $M_{\rm add}$ is 6.0 $M_\odot$ or more. Since the structure of the added matter is similar in both models in which the surface structure is used, the main difference between these models is the structure of the primary. As seen Table 2.1, P14a is a RSG with a He core in which the central helium is burning and P14b a RSG with a CO core in which the shell helium is burning.

Comparing the merger model with the increasing mass models for P14b, we find that the radiative region in the merger model is more massive than in the mass increasing one. This could be a hint to reveal the important factor except for q has been obtained. Unfortunately, I have not found what physical quantities are important because there are many physical quantities in a star and probably multiple candidates for the factor. Namely, the influence of each physical quantity on the transition has to be investigated. To specify it, more types of parametric models would be required, which is a future task.

4.3 Disk-like mass ejection

Since the typical $J_{\rm orb}$ is on the order of 10^{54} erg sec in this system (see Sec 2.4.1), a reasonable value should be adopted in the merger model is 1.0×10^{54} and 3.0×10^{54} erg sec. As seen in Sec 3.4.1, the ejected masses in total are about 4.0 $M_\odot$ for $J_{\rm orb} = 1.0 \times 10^{54}$ erg sec and about 5.0 $M_\odot$ for $J_{\rm orb} = 3.0 \times 10^{54}$ erg sec, which are almost the same in spite of the models of the primary. If the ejecta is converted to the rings, the amount is too massive according to Table 1.1. Besides, there are no blue progenitors for the models based on P15a and P16b for $J_{\rm orb} \geq 10^{54}$ erg sec.

To match the observation, $J_{\rm orb}$ has to be 1.0 – 3.0 $\times 10^{53}$ erg sec, indicating that there is a contradiction between this value and the typical one. Therefore, the mass loss with more efficient loss of angular momentum, such as a disk-like mass ejection, is necessary instead of the wind mass loss which is assumed in the calculation code. In this case, an efficiency about 10.0 times higher than the wind mass loss case is required.

4.4 Large scale mixing for the chemical anomalies

For the no-mixing case, the chemical abundances are basically determined by the surface velocity of the primary, $v_{\rm ini}$. In my models of the primary, the initial velocity of P16b, which is taken as 20.0 % of the Kepler one, is the fastest. As pointed out in Sec 3.4.2, the abundance ratios except for N/C in the models based on P16b for the no-mixing case are consistent with observations and the N/C is near the lowest value, implying that the chemical anomalies can be explained by the higher $v_{\rm ini}$ even if large scale mixing does not occur.

There is, however, a certain problem. Since the higher $v_{\rm ini}$ leads to decreasing the mass of the envelope during a MS phase, q becomes larger at the red phase. This prevents a RSG from undergoing the red to blue evolution as shown in Sec 4.1.4. Therefore, I conclude that large scale mixing, by which most stellar matter in the envelope is homogenized, is induced by interaction between the helium layer and the stream originating from the secondary from the point of view of producing the red to blue evolution.

4.5 Condition for making a yellow or white progenitor

SN 20011dh in Messier 51, which is located at about 2.6×10^7 light yr, was observed on March 31st 2011. As with SN 1987A, the progenitor of this SN has been identified by the HST (Van Dyk *et al.*, 2011) and is a YSG. In addition, Bersten *et al.* (2012) revealed properties of the progenitor with hydrodynamical calculation for its LCs; the mass of the helium core of 3.0 $M_\odot$ – 4.0 $M_\odot$ from which the stellar mass in a MS phase was about 12.0 – 15.0 $M_\odot$, the mass of the envelope at the progenitor phase was about 0.1 $M_\odot$, and the radius was about 2.0×10^2 $R_\odot$ which was consistent with the typical value of a YSG to reproduce the LCs in the early phase. Therefore, the fact that the progenitor was a YSG was confirmed by observation and theory. To produce the thin envelope, it was considered that the envelope of the progenitor was robbed by its companion star in a binary system. This scenario was confirmed because the candidate companion star was observed near the explosion position.

YSGs are also produced as progenitors of CCSNe in the merger model. There is, however, a serious difference between YSGs in the merger model and the progenitor of SN2011dh. Obviously, it is the mass of the envelope. In my models, the mass is lager than 10.0 $M_\odot$ for YSGs, so yellow progenitors have a H-rich envelope. On the other hand, the progenitor of SN 2011dh had a thin envelope as mentioned above. This difference affects the LCs of SNe. When YSGs in the merger model explode, their LCs will become Type II-P although those of SN 2011dh are classified Type IIn.

In addition, WSGs are also produced in the merger model. Although that white progenitors explode has not been detected until now, it would be expected to detect white progenitors in future. Since the produced white progenitors have a H-rich envelope, their LCs will be observed as Type II-P.

When the parameters are $\{M_1,\ J_{\rm orb},\ M_{\rm in},\ \text{Mixing}\} = \{14.0\ \mathrm{M}_\odot,\ 3.0\times10^{53}\ \text{erg sec},\ 4.6\ \mathrm{M}_\odot,\ \text{Yes}\}$, the condition for making a yellow or white progenitor are as follows:

$$\begin{cases} 6.0M_\odot < M_2 < 6.3M_\odot & \text{(for a YSG)} \\ 6.8M_\odot < M_2 < 7.0M_\odot & \text{(for a WSG)} \end{cases} \tag{4.1}$$

This ranges do not almost depend on the others $\{M_1,\ J_{\rm orb},\ M_{\rm in},\ \text{Mixing}\}$. Thus, yellow and white progenitors with a H-rich envelope are rare objects.

Chapter 5

Conclusion

5.1 Summary and conclusion

I construct three parametric models, which are the increasing mass, the helium enhancement, and the combination of both effects, to verify a mechanism for the rad to blue evolution suggested by previous studies. I also construct a stellar merger model to explain the evolutionary history of the progenitor of SN 1987A. The merger model is based on the slow merger scenario (Podsiadlowski *et al.*, 1992; Ivanova *et al.*, 2002). The binary system is composed of $\{M_1, M_2\} = \{14.0\ \mathrm{M}_\odot - 16.0\ \mathrm{M}_\odot, 1.25\ \mathrm{M}_\odot - 10.0\ \mathrm{M}_\odot\}$. This model can be described with two phases; injection of the orbital angular momentum and melting of the secondary. My model first includes the former effect. Therefore, I can discuss the mass loss enhanced by injection of J_{orb} and investigate the effect on the evolution.

From the three parametric models, I obtained the following results and conclusions:

- Important factors for the red to blue evolution suggested by the previous studies are to decrease q and to increase helium abundance in the envelope. The increasing mass model shows that the former factor is identified for P14a, which has a He core, and that q should be less than 0.23 in this case. However, the model with P14b, which has a CO core, does not produce a blue progenitor even if $q < 0.18$. These imply that not only q but also the structure of the primary is important to explain the property. The helium enhanced model shows that blue progenitors are produced although the model of the primary is P16a, having a CO core. Then, a helium abundance in the envelope of more than at least 0.625, by mass fraction, is necessary. This example shows that the helium effect is useful. However, in order to produce such a large value, 5.45 $\mathrm{M}_\odot$ of helium must be provided from the helium layer. This is actually not possible because the mass of the helium layer is only about 2.0 $\mathrm{M}_\odot$. The combination model decreases the required helium abundance to produce a blue progenitor. For example, Y_{He} is 0.5 for $M_{\mathrm{add}} = 12.0\ \mathrm{M}_\odot$ for making

the blue envelope. However, hydrogen and helium abundances of the added matter have to be 0.395 and 0.605 to meet the condition with the assumption. Therefore, the smallness of q and helium enhancement can explain the red to blue evolution but not with realistic parameter values in my parametric models.

Next, I obtained the following results and conclusions with the merger model:

- I investigate the effect of $J_{\rm orb}$, mixing, and $M_{\rm in}$ on the evolution. Injection of $J_{\rm orb}$ promotes the mass loss, leading to an increase in q and a decrease in $M_{\rm tot}$. The other parameters enhance helium abundance in the envelope but the enhancement would not affect the evolution. This reinforces that q is one of the important factors for the red to blue evolution.

- All of progenitors experienced moving bluer. On the other hand, the RSG for case C, in the increasing mass model, never move bluer even if considerable mass is added to the envelope. The difference between the merger and the increasing mass models is the structure of the envelope of the merged object while/after the mass is added, according to the different ways of the mass enhancement.

- The typical value of $J_{\rm orb}$ is on the order of 10^{54} erg sec in the binary system. It is, however, difficult to produce a blue progenitor if the typical value is adopted. The mass loss for $J_{\rm orb} = 3.0\times10^{54}$ is about 5.0 $M_\odot$ in total, leading to a considerable increase of q. To explain the red to blue evolution and mass of the ring system, the good value is 1.0 – 3.0 $\times10^{53}$ erg sec. This implies that the mass loss with more efficient loss of angular momentum, such as disk-like mass ejection, is required instead of the wind mass loss assumed in the code. This is compatible the history of mass loss suggested by observations.

- Large scale mixing induced by erosion is important to match the chemical anomalies although it would not affect the final state as seen above. I compare the calculation results with the observations suggested by Lundqvist & Fransson (1996) and Mattila *et al.* (2010). None of the models based on any of the non-mixing primaries explain the anomalies. Especially, N/C is difficult. On the other hand, the mixing models can match with observations. I conclude that it is necessary that heavy metals in the inner region are dredged up to the surface due to large scale mixing.

- YSGs and WSGs are produced naturally. For example, conditions for M_2 with the parameters $\{M_1,\ J_{\rm orb},\ M_{\rm in},\ \text{Mixing}\} = \{\text{P14b},\ 3.0\times10^{53}\ \text{erg sec},\ 4.6\ M_\odot,\ \text{Yes}\}$ is $6.0\ M_\odot < M_2 < 6.3\ M_\odot$ for a yellow progenitor or $6.8\ M_\odot < M_2 < 7.0\ M_\odot$ for a WSG. The progenitor of SN 2011dh is identified as a YSG. The difference between the progenitor of SN 2011dh and my yellow progenitor is the mass of the envelope.

The LCs of SN 2011dh are classified as Type IIn. This type shows that hydrogen lines emerge but soon disappear. Thus, this indicates that the envelope is very thin. On the other hand, my progenitors have a massive envelope because at least several $M_{\odot}$ of H-rich matter is added. Therefore, it is expected that the LCs of these are observed as Type II-P

- My merger model succeeds in explaining the position on the HRD, the mass of the envelope of the progenitor, the mass of the ring system, the chemical anomalies in the rings, and the time from the transition to the explosion (see Table 5.1). Comparing the merger model with previous studies, this work is the best evolutionary model.

Models for the progenitor				
	SA88 Rotation	PO92 Merger	ME17 Merger	This work Merger
The HRD	Yes	Yes	Yes	Yes
Envelope mass	Yes	Yes	Yes	Yes
Ring mass	?	?	?	Yes
Chemical anomalies	?	?	Yes or No	Yes
Lifetime	Yes	Yes	Yes or No	Yes

Table 5.1: The previous studies and this work.

5.2 Future works

Enhancements of s-process elements in the early-time spectrum of SN 1987A was identified (Mazzali *et al.*, 1992; Mazzali & Chugai, 1995). I do not investigate this enhancement although He/H, N/C, and N/O are considered. 49 isotopes are involved in my models (see Table A.1 in details). As seen in the table, s-process elements are not considered in the models to reduce the cost of the calculation: I primarily have tried to investigate a mechanism for the red to blue evolution. Since the mechanism has been confirmed, I will construct the models involving s-process elements to study their enhancement.

From the increasing mass and merger models, the physical quantities of the added matter considerably affect evolution In my models, treatment of the structure depends on that of the primary. Therefore, it is required to introduce a realistic structure. This can alter the mass ranges of the primary and secondary to produce a blue progenitor.

In the modeling of spiral-in phase, matter heating due to friction between the secondary and the envelope is not included in the merger model for simplicity. Since the heating

contributes to the mass loss, this effect has to be included for the refined model. Using this model, I will discuss a more detailed mass loss and evolutionary history.

Appendix A

Isotopes in the calculations

Name	A	Name	A
n	1	P	31
H	1–3	Si	32
He	3–4	Cl	35
Li	6–7	Ar	36
Be	7,9	K	39
B	8,10–11	Ca	40
C	12–13	Sc	43
N	13–15	Ti	44
O	15–18	V	47
F	17–19	Cr	48
Ne	20	Mn	51
Na	23	Fe	52–56
Mg	24	Co	55–56
Al	27	Ni	56
Si	28		

Table A.1. 49 isotopes are involved in the calculations.

Appendix B

Evolution of massive stars

Stars (about 0.75 $M_\odot \leq M$) are factories which create heavier elements by nuclear reaction, and are complex physical systems supported by balance of the inner forces and self-gravitation. Properties of the evolution of stars depend on its mass mainly. For about 8.0 $M_\odot \leq M \leq$ about 25.0 $M_\odot$, stars, which are near galaxies, have a dramatic fate.

Stars at ZAMS consist of mostly hydrogen, which is burning in the center. In this phase, four hydrogens are synthesized to a helium in two ways; the *pp* chain reaction and CNO cycle. Which reaction dominates depends on temperature. The *pp* chain reaction is distinguished into three kinds of processes. As its first reaction, the *pp* reaction occurs:

$$^1\mathrm{H} + ^1\mathrm{H} \rightarrow ^2\mathrm{H} + e^+ + \nu \tag{B.1}$$

$$^2\mathrm{H} + ^1\mathrm{H} \rightarrow ^3\mathrm{He} + \gamma \tag{B.2}$$

^{3}He, which is created in the above reaction, have an important role for the following two reactions. The first is two ^{3}He nuclei are synthesized:

$$^3\mathrm{He} + ^3\mathrm{He} \rightarrow ^4\mathrm{He} + 2^1\mathrm{H} \tag{B.3}$$

It is called the *pp*1. The other requires ^{4}He which already exists since the birth or is created with the *pp*1:

$$^3\mathrm{He} + ^4\mathrm{He} \rightarrow ^7\mathrm{Be} + \gamma \tag{B.4}$$

^{7}Be leads to the others for ^{4}He:

$$^7\mathrm{Be} + e^- \rightarrow ^7\mathrm{Li} + \nu \tag{B.5}$$

$$^7\mathrm{Li} + ^1\mathrm{H} \rightarrow ^4\mathrm{He} + ^4\mathrm{He} \tag{B.6}$$

and

$$^{7}\mathrm{Be} +^{1} \mathrm{H} \rightarrow^{8} \mathrm{Be} + \gamma \tag{B.7}$$

$$^{8}\mathrm{B} \rightarrow^{8} \mathrm{Be} + e^{+} + \nu \tag{B.8}$$

$$^{8}\mathrm{Be} \rightarrow^{4} \mathrm{He} +^{4} \mathrm{He} \tag{B.9}$$

The first is called the *pp*2 and the second the *pp*3. The energy carrier is different in each reaction, so the released energy to the stellar matter differs. The energies are 26.2 MeV with the *pp*1, 25.67 MeV with the *pp*2, and 19.2 MeV with the *pp*3 per ^{4}He. The *pp*3 cannot contribute to the energy generation, but the neutrino flux from this is high, so it is important for the observation of solar neutrino.

The CNO cycle is also an important reaction for ^{4}He. The basic concept is that hydrogen is captured into carbon, nitrogen, and oxygen and synthesized to helium. The cycle has two branches; the CN and NO cycles. The main cycle can be represented as follows:

$$^{12}\mathrm{C} +^{1} \mathrm{H} \rightarrow^{13} \mathrm{N} + \gamma \tag{B.10}$$

$$^{13}\mathrm{N} \rightarrow^{13} \mathrm{C} + e^{+} + \nu \tag{B.11}$$

$$^{13}\mathrm{C} +^{1} \mathrm{H} \rightarrow^{14} \mathrm{N} + \gamma \tag{B.12}$$

$$^{14}\mathrm{N} +^{1} \mathrm{H} \rightarrow^{15} \mathrm{O} + \gamma \tag{B.13}$$

$$^{15}\mathrm{O} \rightarrow^{15} \mathrm{N} + e^{+} + \nu \tag{B.14}$$

$$^{15}\mathrm{N} +^{1} \mathrm{H} \rightarrow^{12} \mathrm{C} +^{4} \mathrm{He} \tag{B.15}$$

^{12}C is consumed at first, but it is reproduced by (B.15). Therefore the reproduced ^{12}C returns to (B.10), meaning *cycle*.

The lowest reaction takes part in a secondary cycle. It can be represented as follows:

$$^{15}\mathrm{N} +^{1} \mathrm{H} \rightarrow^{16} \mathrm{O} + \gamma \tag{B.16}$$

$$^{16}\mathrm{O} +^{1} \mathrm{H} \rightarrow^{17} \mathrm{F} + \gamma \tag{B.17}$$

$$^{17}\mathrm{F} \rightarrow^{17} \mathrm{O} + e^{+} + \nu \tag{B.18}$$

$$^{17}\mathrm{O} +^{1} \mathrm{H} \rightarrow^{14} \mathrm{N} +^{4} \mathrm{He} \tag{B.19}$$

$$^{14}\mathrm{N} +^{1} \mathrm{H} \rightarrow^{15} \mathrm{O} + \gamma \tag{B.20}$$

(B.20) is same as (B.13). This shows that the secondary cycle connects with the main one. The duration of ^{14}N + ^{1}H is longest in the cycle, leading to enhancement of ^{14}N in a star. The CNO cycle is important in middle-massive stars. On the other hand, the

pp chain is important in low mass stars. The difference is due to the temperature in the center.

What time massive stars have been staying on the main sequence phase can be estimated as a function of stellar mass and luminosity:

$$\tau_{ms} \approx 10^{10} \frac{M/\mathrm{M}_\odot}{L/\mathrm{L}_\odot} [\mathrm{yr}] \tag{B.21}$$

Since the luminosity is proportional to $M^{1<\alpha\leq 5}$, this duration is determined as an approximation of $M^{1-\alpha}$. Therefore, the higher the stellar mass is, the shorter the duration is.

After hydrogen is exhausted via the above reactions in the central region, the inner force decreases, promoting contraction of the central region due to collapse of the equilibrium between forces. As a result, gravitational energy is released to the stellar matter, so temperature near the region increases. When temperature at some positions from the center achieves that needed for hydrogen burning, the hydrogen layer on the helium core burns via the CNO cycle, which is called shell burning. This is the main source of stellar luminosity in this phase. On the other hand, the collapse proceeds alongside shell burning, and pressure near the core becomes high. As a result, pressure gradient near the region where the shell burning occurs becomes very sharp. Since the balance between the forces is changed, the core pushes the shell and envelope outside. Stars enter into a RSG phase after this has ceased, so the envelope extends to be about 10^{2-3} $\mathrm{R}_\odot$, which depends on the metalicity and so on.

In the following reactions, a star with $M >$ about 12.0 $\mathrm{M}_\odot$ have always a core which is more massive than the Chandrasekhar mass M_{ch}, so this state is a gravitational thermodynamics catastrophe. Energy is lost due to radiation of photons and neutrinos in a star. In this state, temperature of the core increases with the lost energy. Therefore, some reactions are induced, and the core does not enter degeneracy.

When the temperature reaches about 10^8 K, three nuclei of helium are fused into a nucleus of carbon. This is called the triple α reaction, which is represented by

$$^4\mathrm{He} + ^4\mathrm{He} \rightleftharpoons ^8\mathrm{Be} \tag{B.22}$$

$$^8\mathrm{Be} + ^4\mathrm{He} \rightarrow ^{12}\mathrm{C} + \gamma \tag{B.23}$$

A part of ^{12}C , which is created in the above reaction, is used by the reaction with ^{4}He:

$$^{12}\mathrm{C} + ^4\mathrm{He} \rightarrow ^{16}\mathrm{O} + \gamma \tag{B.24}$$

Therefore, the main composition in the core becomes carbon and oxygen after it has been completed.

For carbon burning, it also depends on temperature, so about 5.0×10^8 K. At first, two ^{12}C are fused into a nucleus of ^{23}Mg. There are a lot of different channels as in following reactions:

$$^{12}\mathrm{C} + ^{12}\mathrm{C} \rightarrow ^{24}\mathrm{Mg} + \gamma \tag{B.25}$$
$$\rightarrow ^{23}\mathrm{Mg} + n \tag{B.26}$$
$$\rightarrow ^{23}\mathrm{Na} + p \tag{B.27}$$
$$\rightarrow ^{20}\mathrm{Ne} + \alpha \tag{B.28}$$
$$\rightarrow ^{16}\mathrm{O} + 2\alpha \tag{B.29}$$

The most probable reactions are (B.27) and (B.28). the α particle originating from (B.28) is captured by ^{22}Ne and ^{18}O, which emits a neutron. Such neutrons are also absorbed into another neutron-rich nuclei, producing ^{23}Na, ^{25}Mg, and ^{27}Al. Because of these channels, the main constituents of the core are ^{16}O, ^{20}Ne, and ^{24}Mg.

The next reaction occurs when the temperature reaches about 3.0×10^9 K which breaks the high Coulomb barrier:

$$^{16}\mathrm{O} + ^{16}\mathrm{O} \rightarrow ^{32}\mathrm{S} + \gamma \tag{B.30}$$
$$\rightarrow ^{31}\mathrm{P} + p \tag{B.31}$$
$$\rightarrow ^{31}\mathrm{S} + n \tag{B.32}$$
$$\rightarrow ^{28}\mathrm{Si} + \alpha \tag{B.33}$$
$$\rightarrow ^{24}\mathrm{Mg} + 2\alpha \tag{B.34}$$

α nuclei produced by (B.33) is captured into ^{28}Si, leading formations of ^{32}S, ^{36}Ar, and ^{40}Ca.

For silicon burning, the required temperature is more about 4.0×10^9 K. Iron group elements are synthesized in this reaction. If the temperature does not exceed 5.0×10^9 K, the reaction is incomplete. Mos silicons are left in the core, and a part of these capture α nuclei, producing nickel, calcium, chrome, and manganese. This nickel is ^{56}Ni, so it becomes ^{56}Co and ^{56}Fe because of β-decay. On the other hand, the reaction is completed if temperature can exceed 5.0×10^9 K. ^{56}Ni is the most produced nuclei in this reaction.

After silicon burning, the main composition of the core is ^{56}Fe. Nuclear fusion ceases because ^{56}Fe has the lowest binding energy. On the other hand, neutrinos carry energy away. As a result, the collapse of the core is promoted, leading to an increase of density and temperature in the region. Then, two instabilities are induced; the electron capture and photodisintegration. The former occurs when the central density reaches about 10^{10} g cm^{-3}:

$$\mathrm{p} + \mathrm{e}^- \rightarrow \mathrm{n} + \nu_\mathrm{e} \tag{B.35}$$

$$\mathrm{n} \rightarrow \mathrm{p} + \mathrm{e}^- + \bar{\nu_\mathrm{e}} \tag{B.36}$$

p is a proton, e^- an electron, n a neutron, ν_e an electron neutrino, and $\bar{\nu_\mathrm{e}}$ an anti-electron neutrino, respectively. The rest mass of the neutron is bigger than the total rest mass of the proton and electron, so the excess energy is carried by an anti-electron neutrino. This causes instability in the central region, and the collapse progresses. The later occurs when the temperature reaches about 10^{10} K. In this state, the energy of a photon is so high that the iron resolves to helium, proton, and neutron. This is an endothermic reaction, leading to an instability.

These instabilities lead to the collapse of the core more and more. Since neutron abundance has been enhanced according to (B.35), the core becomes neutralized. As a result, it is left as a neutron star in its final phase. Matter above the core falls to the surface of the core, and bounces back in a shockwave. Part of the kinetic energy of the shock is transfered to inner material. These scatter electrons, emitting photons. It is observed as a supernova.

Appendix C

Results of the merger model

P14b												
$J_{\rm orb}$	$M_{\rm in}$	Reduce	M_2	Mixing	$M_{\rm fin}$	q	log $T_{\rm eff}$	Color	log $L/{\rm L}_\odot$	He/H	N/C	N/O
[$\times 10^{53}$ erg sec]	[$M_\odot$]	[%]	[$M_\odot$]	-	[$M_\odot$]	-	[K]	-	[erg$\times$sec^{-1}]	-	-	-
1	4.6	95	4	No	14.92	0.31	3.572	R	4.957	0.106	1.935	0.694
1	4.6	95	5	No	16.03	0.29	3.714	Y	4.619	0.106	1.935	0.694
1	4.6	95	6	No	17.12	0.27	4.043	B	4.872	0.106	1.934	0.694
1	4.6	95	7	No	18.16	0.25	4.247	B	4.885	0.106	1.933	0.694
1	4.6	95	8	No	19.2	0.24	4.279	B	4.904	0.106	1.933	0.693
1	4.6	95	9	No	20.24	0.23	4.331	B	4.990	0.106	1.932	0.693
1	4.6	95	4	Yes	15.03	0.31	3.575	R	4.960	0.145	4.018	1.220
1	4.6	95	5	Yes	16.12	0.29	3.726	Y	4.562	0.141	3.824	1.189
1	4.6	95	6	Yes	17.18	0.27	4.133	B	4.866	0.139	3.797	1.181
1	4.6	95	7	Yes	18.21	0.25	4.308	B	4.953	0.140	3.902	1.234
1	4.6	95	8	Yes	19.24	0.24	4.360	B	5.010	0.138	3.930	1.232
1	4.6	95	9	Yes	20.28	0.23	4.392	B	5.051	0.137	3.871	1.226
3	4.6	95	5	No	14.68	0.31	3.573	R	4.966	0.107	1.969	0.704
3	4.6	95	6	No	15.8	0.29	3.576	R	4.969	0.106	1.947	0.698
3	4.6	95	7	No	16.86	0.27	4.106	B	4.889	0.106	1.940	0.696
3	4.6	95	8	No	17.94	0.26	4.253	B	4.923	0.106	1.940	0.696
3	4.6	95	9	No	18.99	0.24	4.280	B	4.898	0.106	1.940	0.696
3	4.6	95	5	Yes	14.76	0.31	3.573	R	4.964	0.141	4.217	1.227
3	4.6	95	6	Yes	15.86	0.29	3.576	R	4.969	0.138	4.489	1.230
3	4.6	95	6.1	Yes	15.99	0.29	3.876	Y	4.675	0.141	3.763	1.197
3	4.6	95	6.2	Yes	16.1	0.29	3.917	W	4.708	0.141	3.767	1.196
3	4.6	95	6.3	Yes	16.18	0.28	3.577	R	4.970	0.136	4.611	1.229
3	4.6	95	6.4	Yes	16.28	0.28	3.577	R	4.967	0.136	4.707	1.233

3	4.6	95	6.5	Yes	16.39	0.28	3.578	R	4.969	0.136	4.839	1.238
3	4.6	95	6.6	Yes	16.5	0.28	3.578	R	4.969	0.136	4.998	1.245
3	4.6	95	6.7	Yes	16.62	0.28	3.630	R	4.457	0.136	4.037	1.196
3	4.6	95	6.8	Yes	16.71	0.28	3.674	R	4.507	0.137	3.950	1.194
3	4.6	95	6.9	Yes	16.82	0.27	3.839	Y	4.684	0.136	3.969	1.191
3	4.6	95	7	Yes	16.92	0.27	4.064	B	4.833	0.139	4.198	1.257
3	4.6	95	7.3	Yes	16.92	0.27	4.171	B	4.886	0.140	4.198	1.257
3	4.6	95	7.5	Yes	17.25	0.27	4.169	B	4.890	0.141	4.012	1.248
3	4.6	95	7.7	Yes	17.45	0.26	4.196	B	4.903	0.141	3.753	1.237
3	4.6	95	8	Yes	17.98	0.26	4.290	B	4.941	0.139	4.064	1.250
3	4.6	95	9	Yes	19.03	0.24	4.350	B	4.999	0.138	3.789	1.230
3	4.8	99	6	No	15.68	0.31	3.573	R	4.993	0.131	7.225	1.331
3	4.8	99	7	No	16.8	0.29	4.071	B	4.872	0.106	1.940	0.696
3	4.8	99	8	No	17.89	0.27	4.234	B	4.955	0.106	1.940	0.696
3	4.8	99	9	No	18.95	0.25	4.315	B	5.010	0.106	1.940	0.696
3	4.8	99	5	Yes	14.64	0.33	3.569	R	4.993	0.128	5.826	1.231
3	4.8	99	6	Yes	15.77	0.3	3.573	R	4.993	0.127	6.288	1.239
3	4.8	99	7	Yes	16.87	0.28	3.577	R	4.994	0.128	7.338	1.316
3	4.8	99	8	Yes	17.94	0.27	4.212	B	4.934	0.128	6.113	1.284
3	4.8	99	9	Yes	18.99	0.25	4.323	B	4.998	0.127	6.308	1.289
10	4.6	95	8	No	15.81	0.29	3.650	R	4.420	0.110	2.158	0.759
10	4.6	95	9	No	16.83	0.27	4.131	B	4.875	0.110	2.163	0.760
10	4.6	95	8	Yes	15.83	0.29	3.595	R	4.785	0.142	4.266	1.291
10	4.6	95	9	Yes	16.84	0.27	3.974	W	4.778	0.140	3.949	1.265
10	4.6	95	10	Yes	17.85	0.26	4.273	B	4.926	0.139	3.979	1.264
30	4.6	95	8	No	14.61	0.31	3.572	R	4.976	0.145	6.046	1.483
30	4.6	95	9	No	15.66	0.29	3.592	R	4.816	0.140	4.278	1.267

30	4.6	95	10	No	16.65	0.28	4.081	B	4.832	0.117	2.501	0.853
30	4.6	95	8	Yes	14.65	0.31	3.571	R	4.975	0.138	4.944	1.327
30	4.6	95	9	Yes	15.69	0.29	3.577	R	4.960	0.141	4.549	1.319

Table C.1: Results in the merger model based on P14b. "Reduce" represents reduction of the core due to the penetration. "Color" indicates the color of the progenitor. Values of the chemical ratio are described by number.

P15a												
$J_{\rm orb}$ [$\times 10^{53}$ erg sec]	$M_{\rm in}$ [$M_\odot$]	Reduce [%]	M_2 [$M_\odot$]	Mixing -	$M_{\rm fin}$ [$M_\odot$]	q -	log $T_{\rm eff}$ [K]	Color -	log $L/L_\odot$ [erg$\times$sec^{-1}]	He/H -	N/C -	N/O -
1	5.2	95	5	No	16.26	0.32	3.571	R	5.065	0.108	1.893	0.688
1	5.2	95	6	No	17.32	0.3	3.574	R	5.065	0.108	1.894	0.688
1	5.2	95	7	No	18.38	0.28	3.905	W	4.900	0.108	1.884	0.685
1	5.2	95	8	No	19.45	0.27	4.036	B	4.986	0.108	1.884	0.685
1	5.2	95	9	No	20.5	0.25	4.084	B	5.055	0.108	1.884	0.685
1	5.2	95	10	No	21.54	0.24	4.128	B	5.096	0.108	1.884	0.685
1	5.2	95	5	Yes	16.3	0.32	3.571	R	5.064	0.141	4.126	1.222
1	5.2	95	6	Yes	17.38	0.3	3.574	R	5.065	0.138	4.122	1.215
1	5.2	95	7	Yes	18.46	0.28	3.878	Y	4.848	0.139	3.708	1.186
1	5.2	95	8	Yes	19.51	0.27	4.029	B	4.960	0.137	3.612	1.176
1	5.42	99	6	No	17.28	0.31	3.572	R	5.084	0.110	2.156	0.751
1	5.42	99	7	No	18.35	0.3	3.575	R	5.086	0.108	1.892	0.687
1	5.42	99	8	No	19.43	0.28	3.867	Y	4.931	0.108	1.884	0.685
1	5.42	99	9	No	20.48	0.26	4.039	B	5.037	0.108	1.884	0.685
1	5.42	99	6	Yes	17.32	0.31	3.572	R	5.084	0.130	5.148	1.214
1	5.42	99	7	Yes	18.39	0.29	3.575	R	5.084	0.132	5.600	1.282
1	5.42	99	8	Yes	19.47	0.28	3.790	Y	4.854	0.130	4.990	1.254
1	5.42	99	9	Yes	20.52	0.26	4.043	B	5.015	0.129	4.852	1.247
3	5.2	95	6	No	16.13	0.32	3.572	R	5.063	0.146	4.523	1.317
3	5.2	95	7	No	17.21	0.3	3.635	R	4.549	0.108	1.902	0.690
3	5.2	95	8	No	18.31	0.28	3.938	W	4.898	0.108	1.902	0.690
3	5.2	95	9	No	19.39	0.27	4.026	B	4.975	0.108	1.902	0.690
3	5.2	95	6	Yes	16.17	0.32	3.571	R	5.062	0.140	4.010	1.215

3	5.2	95	7	Yes	17.28	0.3	3.646	R	4.526	0.144	3.874	1.262
3	5.2	95	8	Yes	18.36	0.28	3.921	W	4.874	0.142	3.811	1.253
3	5.2	95	9	Yes	19.44	0.27	4.031	B	4.965	0.139	3.873	1.247
3	5.42	99	6	No	16.13	0.34	3.569	R	5.084	0.135	6.080	1.315
3	5.42	99	7	No	17.19	0.32	3.572	R	5.085	0.136	6.305	1.376
3	5.42	99	8	No	18.28	0.3	3.576	R	5.085	0.134	6.060	1.358
3	5.42	99	9	No	19.35	0.28	3.832	Y	4.896	0.108	1.902	0.690
3	5.42	99	10	No	20.42	0.27	4.036	B	5.028	0.108	1.902	0.690
3	5.42	99	6	Yes	16.14	0.34	3.568	R	5.083	0.130	5.074	1.213
3	5.42	99	7	Yes	17.22	0.31	3.572	R	5.084	0.132	5.366	1.279
3	5.42	99	8	Yes	18.32	0.3	3.575	R	5.084	0.131	5.413	1.278
3	5.42	99	9	Yes	19.39	0.28	3.667	R	4.710	0.130	4.890	1.254
3	5.42	99	10	Yes	20.45	0.27	4.027	B	5.005	0.129	4.780	1.247
10	5.2	95	9	Yes	17.46	0.3	3.574	R	5.061	0.142	4.384	1.328
10	5.2	95	10	Yes	18.21	0.29	3.924	W	4.869	0.144	3.893	1.298

Table C.2: Results in the merger model based on P15a.

P16b												
$J_{\rm orb}$	$M_{\rm in}$	Reduce	M_2	Mixing	$M_{\rm fin}$	q	log $T_{\rm eff}$	Color	log $L/{\rm L}_\odot$	He/H	N/C	N/O
[$\times 10^{53}$ erg sec]	[$M_\odot$]	[%]	[$M_\odot$]	-	[$M_\odot$]	-	[K]	-	[erg$\times$sec^{-1}]	-	-	-
1	5.96	95	7	No	18.48	0.32	3.573	R	5.159	0.116	2.944	0.821
1	5.96	95	8	No	19.55	0.3	3.841	Y	4.984	0.116	2.943	0.821
1	5.96	95	9	No	20.58	0.29	3.899	Y	5.035	0.116	2.943	0.821
1	5.96	95	10	No	21.6	0.28	3.964	W	5.084	0.116	2.943	0.821
1	5.96	95	7	Yes	18.54	0.32	3.573	R	5.159	0.149	6.356	1.401
1	5.96	95	8	Yes	19.6	0.3	3.850	Y	4.937	0.152	5.003	1.357
1	5.96	95	9	Yes	20.62	0.29	3.931	W	5.013	0.148	4.955	1.343
1	5.96	95	10	Yes	21.63	0.28	3.992	W	5.068	0.145	4.918	1.330
1	6.21	99	7	No	18.43	0.34	3.570	R	5.181	0.141	9.601	1.442
1	6.21	99	8	No	19.51	0.32	3.57	R	5.181	0.139	8.921	1.422
1	6.21	99	9	No	20.54	0.3	3.576	R	5.180	0.136	7.897	1.377
1	6.21	99	10	No	21.58	0.29	3.757	Y	4.983	0.116	2.943	0.821
1	6.21	99	7	Yes	18.45	0.34	3.570	R	5.180	0.139	8.780	1.397
1	6.21	99	8	Yes	19.53	0.32	3.573	R	5.181	0.137	8.400	1.386
1	6.21	99	9	Yes	20.57	0.3	3.576	R	5.180	0.136	7.995	1.376
1	6.21	99	10	Yes	21.6	0.29	3.704	Y	4.914	0.134	6.911	1.343
3	5.96	95	7	No	17.32	0.34	3.572	R	5.144	0.117	2.983	0.829
3	5.96	95	8	No	18.39	0.32	3.648	R	4.727	0.116	2.977	0.828
3	5.96	95	9	No	19.46	0.31	3.653	R	4.767	0.116	2.977	0.828
3	5.96	95	10	No	20.5	0.29	3.883	Y	5.010	0.116	2.977	0.828
3	5.96	95	7	Yes	17.39	0.34	3.571	R	5.144	0.156	5.822	1.420
3	5.96	95	8	Yes	18.45	0.32	3.633	R	4.632	0.153	5.058	1.372
3	5.96	95	9	Yes	19.5	0.31	3.644	R	4.681	0.147	5.178	1.353

3	5.96	95	10	Yes	20.54	0.29	3.897	Y	4.990	0.146	4.916	1.341
3	6.21	99	7	No	17.28	0.36	3.567	R	5.176	0.145	9.307	1.483
3	6.21	99	8	No	18.37	0.34	3.570	R	5.176	0.142	8.643	1.459
3	6.21	99	9	No	19.42	0.32	3.573	R	5.180	0.138	8.836	1.442
3	6.21	99	10	No	20.48	0.3	3.576	R	5.176	0.138	7.679	1.416
3	6.21	99	7	Yes	17.31	0.36	3.567	R	5.176	0.141	8.171	1.400
3	6.21	99	8	Yes	18.39	0.34	3.570	R	5.176	0.139	7.819	1.394
3	6.21	99	9	Yes	19.44	0.32	3.572	R	5.180	0.136	8.005	1.385
3	6.21	99	10	Yes	20.5	0.3	3.576	R	5.176	0.136	7.176	1.370
10	5.96	95	9	Yes	17.42	0.34	3.571	R	5.146	0.155	5.729	1.457
10	5.96	95	10	Yes	18.45	0.32	3.575	R	5.134	0.152	5.469	1.430

Table C.3: Results in the merger model based on P16b.

Acknowledgments

Firstly, I express gratitude to members of Umeda's research group. I would like to thank my supervisor, Hideyuki Umeda for his great aids. I have belonged to the research group since the doctor course. Since then, he has educated me kindly and strictly. I would like to thank the collaborators, Koh Takahashi and Takashi Yoshida. I used the numerical code described by them for my research. In addition, their advice and discussion has helped my study greatly.

Secondly, I express gratitude to my family for kindness, aid, and encouragement. They have always supported me deeply. My study could not be completed without their support.

Thirdly, I express gratitude to my friends. I encountered some difficulties originating from my study, beating my mind. Then, they helped me with recreation. I would like to thank: Bell Aaron Christopher, Ryota Kawamata, Taku Okamura, Koh Takahashi, and Kentaro Wada.

Bibliography

Arnett, W. D., Bahcall, J. N., Kirshner, R. P. & Woosley, S. E. (1989). *Supernova 1987A.* Annual Review of Astronomy & Astrophysics, **27**, 629–700.

Bersten, M. C., Benvenuto, O. G., Nomoto, K., Ergon, M., Folatelli, G., Sollerman, J., Benetti, S., Botticella, M. T., Fraser, M., Kotak, R., Maeda, K., Ochner, P. & Tomasella, L. (2012). *The Type IIb Supernova 2011dh from a Supergiant Progenitor.* The Astrophysical Journal, **757**, 31.

Blondin, J. M. & Lundqvist, P. (1993). *Formation of the circumstellar shell around SN 1987A.* The Astrophysical Journal, **405**, 337–352.

Böhm-Vitense, E. (1958). *Über die Wasserstoffkonvektionszone in Sternen verschiedener Effektivtemperaturen und Leuchtkräfte. Mit 5 Textabbildungen.* Zeitschrift fuer Astrophysik, **46**, 108.

Brunish, W. M. & Truran, J. W. (1982). *The evolution of massive stars. II - The influence of initial composition and mass loss.* The Astrophysical Journal, Supplement, **49**, 447–468.

Burrows, C. J., Krist, J., Hester, J. J., Sahai, R., Trauger, J. T., Stapelfeldt, K. R., Gallagher, J. S., III, Ballester, G. E., Casertano, S., Clarke, J. T., Crisp, D., Evans, R. W., Griffiths, R. E., Hoessel, J. G., Holtzman, J. A., Mould, J. R., Scowen, P. A., Watson, A. M. & Westphal, J. A. (1995). *Hubble Space Telescope Observations of the SN 1987A Triple Ring Nebula.* The Astrophysical Journal, **452**, 680.

Crotts, A. P. & Heathcote, S. R. (1991). *Velocity structure of the ring nebula around supernova 1987A.* Nature, **350**, 683–685.

Crotts, A. P. S., Kunkel, W. E. & McCarthy, P. J. (1989). *Light echoes and transient luminescence near SN 1987A.* The Astrophysical Journal, Letters, **347**, L61–L64.

de Jager, C., Nieuwenhuijzen, H. & van der Hucht, K. A. (1988). *Mass loss rates in the Hertzsprung-Russell diagram.* Astronomy & Astrophysics Supplement Series, **72**, 259–289.

Denissenkov, P. A. & VandenBerg, D. A. (2003). *Thermal Stability of Rotating Low-Mass Subgiants and Red Giants.* The Astrophysical Journal, **598**, 1246–1254.

Fransson, C., Cassatella, A., Gilmozzi, R., Kirshner, R. P., Panagia, N., Sonneborn, G. & Wamsteker, W. (1989). *Narrow ultraviolet emission lines from SN 1987A - Evidence for CNO processing in the progenitor.* The Astrophysical Journal, **336**, 429–441.

Heger, A., Langer, N. & Woosley, S. E. (2000). *Presupernova Evolution of Rotating Massive Stars. I. Numerical Method and Evolution of the Internal Stellar Structure.* The Astrophysical Journal, **528**, 368–396.

Hirata, K., Kajita, T., Koshiba, M., Nakahata, M. & Oyama, Y. (1987). *Observation of a neutrino burst from the supernova SN1987A.* Physical Review Letters **58**, 1490–1493.

Ivanova, N., Justham, S., Chen, X., De Marco, O., Fryer, C. L., Gaburov, E., Ge, H., Glebbeek, E., Han, Z., Li, X.-D., Lu, G., Marsh, T., Podsiadlowski, P., Potter, A., Soker, N., Taam, R., Tauris, T. M., van den Heuvel, E. P. J. & Webbink, R. F. (2013). *Common envelope evolution: where we stand and how we can move forward.* The Astronomy & Astrophysics Review, **21**, 59.

Ivanova, N., Podsiadlowski, P. & Spruit, H. (2002). *Hydrodynamical simulations of the stream-core interaction in the slow merger of massive stars.* Monthly Notices of the Royal Astronomical Society, **334**, 819–832.

Langer, N. (1998). *Coupled mass and angular momentum loss of massive main sequence stars.* Astronomy & Astrophysics, **329**, 551–558.

Lundqvist, P. & Fransson, C. (1996). *The Line Emission from the Circumstellar Gas around SN 1987A.* The Astrophysical Journal, **464**, 924.

Luo, D. & McCray, R. (1991). *The circumstellar shell of SN 1987A.* The Astrophysical Journal, **379**, 659–662.

Maran, S. P., Sonneborn, G., Pun, C. S. J., Lundqvist, P., Iping, R. C. & Gull, T. R. (2000). *Physical Conditions in Circumstellar Gas Surrounding SN 1987A 12 Years after Outburst.* The Astrophysical Journal, **545**, 390–398.

Mattila, S., Lundqvist, P., Gröningsson, P., Meikle, P., Stathakis, R., Fransson, C. & Cannon, R. (2010). *Abundances and Density Structure of the Inner Circumstellar Ring Around SN 1987A.* The Astrophysical Journal, **717**, 1140–1156.

Mazzali, P. A. & Chugai, N. N. (1995). *Barium in SN 1987A and SNe II-P.* Astronomy & Astrophysics, **303**, 118.

Mazzali, P. A., Lucy, L. B. & Butler, K. (1992). *Barium and other s-process elements in the early-time spectrum of SN 1987A.* Astronomy & Astrophysics, **258**, 399–411.

Menon, A. & Heger, A. (2017). *The quest for blue supergiants: binary merger models for the evolution of the progenitor of SN 1987A.* Monthly Notices of the Royal Astronomical Society, **469**, 4649–4664.

Meyer, F. (1997). *Formation of the outer rings of Supernova 1987A.* Monthly Notices of the Royal Astronomical Society, **285**, L11–L14.

Meyer, F. & Meyer-Hofmeister, E. (1979). *Formation of cataclysmic binaries through common envelope evolution.* Astronomy & Astrophysics, **78**, 167–176.

Morris, T. & Podsiadlowski, P. (2006). *Anisotropic mass ejection in binary mergers.* Monthly Notices of the Royal Astronomical Society, **365**, 2–10.

Morris, T. & Podsiadlowski, P. (2007). *The Triple-Ring Nebula Around SN 1987A: Fingerprint of a Binary Merger.* Science **315**, 1103.

Panagia, N., Scuderi, S., Gilmozzi, R., Challis, P. M., Garnavich, P. M. & Kirshner, R. P. (1996). *On the Nature of the Outer Rings around SN 1987A.* The Astrophysical Journal, Letters, **459**, L17.

Podsiadlowski, P. (2001). Common-Envelope Evolution and Stellar Mergers. In: *Evolution of Binary and Multiple Star Systems* (Podsiadlowski, P., Rappaport, S., King, A. R., D'Antona, F. & Burderi, L., eds.), vol. 229 of *Astronomical Society of the Pacific Conference Series.*

Podsiadlowski, P., Joss, P. C. & Hsu, J. J. L. (1992). *Presupernova evolution in massive interacting binaries.* The Astrophysical Journal, **391**, 246–264.

Saio, H., Nomoto, K. & Kato, M. (1988a). *Nitrogen and helium enhancement in the progenitor of supernova 1987A.* Nature, **334**, 508–510.

Saio, H., Nomoto, K. & Kato, M. (1988b). *Why did the progenitor of SN 1987A undergo the blue-red-blue evolution?* The Astrophysical Journal, **331**, 388–393.

Shigeyama, T. & Nomoto, K. (1990). *Theoretical light curve of SN 1987A and mixing of hydrogen and nickel in the ejecta.* The Astrophysical Journal, **360**, 242–256.

Shigeyama, T., Nomoto, K. & Hashimoto, M. (1988). *Hydrodynamical models and the light curve of Supernova 1987A in the Large Magellanic Cloud.* Astronomy & Astrophysics, **196**, 141–151.

Shigeyama, T., Nomoto, K., Hashimoto, M. & Sugimoto, D. (1987). *Light-curve models for supernova SN1987A in the Large Magellanic Cloud.* Nature, **328**, 320–323.

Sugerman, B. E. K., Crotts, A. P. S., Kunkel, W. E., Heathcote, S. R. & Lawrence, S. S. (2005). *The Three-dimensional Circumstellar Environment of SN 1987A.* The Astrophysical Journal, Supplement, **159**, 60–99.

Takahashi, K., Umeda, H. & Yoshida, T. (2014). *Stellar Yields of Rotating First Stars. I. Yields of Weak Supernovae and Abundances of Carbon-enhanced Hyper-metal-poor Stars.* The Astrophysical Journal, **794**, 40.

Urushibata, T., Takahashi, K., Umeda, H. & Yoshida, T. (2017). A Progenitor Model of SN 1987A; Spiral-in Merger Including Rotational Effects. In: *14th International Symposium on Nuclei in the Cosmos (NIC2016)* (Kubono, S., Kajino, T., Nishimura, S., Isobe, T., Nagataki, S., Shima, T. & Takeda, Y., eds.).

Urushibata, T., Takahashi, K., Umeda, H. & Yoshida, T. (2018). *A progenitor model of SN 1987A based on the slow-merger scenario.* Monthly Notices of the Royal Astronomical Society, **473**, L101–L105.

Van Dyk, S. D., Li, W., Cenko, S. B., Kasliwal, M. M., Horesh, A., Ofek, E. O., Kraus, A. L., Silverman, J. M., Arcavi, I., Filippenko, A. V., Gal-Yam, A., Quimby, R. M., Kulkarni, S. R., Yaron, O. & Polishook, D. (2011). *The Progenitor of Supernova 2011dh/PTF11eon in Messier 51.* The Astrophysical Journal, Letters, **741**, L28.

Wampler, E. J. & Richichi, A. (1989). *Observations of nebular emission lines towards SN 1987A.* Astronomy & Astrophysics, **217**, 31–34.

Wampler, E. J., Wang, L., Baade, D., Banse, K., D'Odorico, S., Gouiffes, C. & Tarenghi, M. (1990). *Observations of the nebulosities near SN 1987A.* The Astrophysical Journal, Letters, **362**, L13–L16.

Woosley, S. E. (1988). *SN 1987A - After the peak.* The Astrophysical Journal, **330**, 218–253.

Woosley, S. E., Heger, A., Weaver, T. A. & Langer, N. (1997). *SN 1987A - Presupernova Evolution and the Progenitor Star.* ArXiv Astrophysics e-prints .

Zahn, J.-P. (1992). *Circulation and turbulence in rotating stars.* Astronomy & Astrophysics, **265**, 115–132.